THE CONTROL OF MICROSTRUCTURAL AND CRYSTALLOGRAPHIC ORIENTATION VIA CERAMIC FORMING METHODS FOR IMPROVED SINTERED TRANSPARENCY

by

William James Costakis Jr.

A Dissertation

Submitted to the Faculty of Purdue University

In Partial Fulfillment of the Requirements for the degree of

Doctor of Philosophy

School of Materials Engineering

West Lafayette, Indiana

May 2020

THE PURDUE UNIVERSITY GRADUATE SCHOOL
STATEMENT OF COMMITTEE APPROVAL

Dr. Rodney Trice, Co-Chair

School of Materials Engineering

Dr. Jeffrey Youngblood, Co-Chair

School of Materials Engineering

Dr. Elliott Slamovich

School of Materials Engineering

Dr. Kevin Trumble

School of Materials Engineering

Approved by:

Dr. David Bahr

To the people closest to me, my family that gave me encouragement and constant support

ACKNOWLEDGMENTS

TABLE OF CONTENTS

LIST OF TABLES

LIST OF FIGURES

ABSTRACT

Transparent alumina is a candidate material for ballistic applications where visible or infrared wavelength transmission is required. However, the transparency of polycrystalline alumina can be limited due to the rhombohedral crystal structure being inherently birefringent. Birefringence causes light scattering at grain boundaries and is detrimental to the transparency. It has been shown experimentally that the application of a high magnetic field during processing can lead to crystallographic alignment and the reduction of birefringent light scattering. This alignment method is effective but is limited in terms of scalability. This research addresses these limitations through the use of simple and cost-effective shear and elongational forming processes such as uniaxial warm pressing and direct ink writing (DIW) for the improvement of final sintered transparency. To further support the improvement of these processes as alternatives and to evaluate the possibility of using powder ratios to improve the alignment, this research will also investigate the sintering behavior during hot-pressing of equiaxed and platelet powders.

Platelet ceramic-filled thermoplastic blends were developed and formed into sheets through uniaxial warm pressing. The solids loading (30 – 40 vol.%) and platelet diameter (1.2 and 11µm) were varied to compare effects on viscosity, percent reduction, and final alignment. All ceramic-filled thermoplastic polymer blends exhibited pseudoplastic behavior. Crystallographic alignment of green body samples was quantified by the orientation parameter (r) and grain misalignment angle (full width at half maximum, FWHM) obtained from rocking curve analysis. Blends with 11µm diameter platelets displayed a higher temperature sensitivity constant, better flow properties, and higher alignment compared to blends with 1.2µm diameter platelets. Optimal samples produced with blends containing 30 vol.% of 11µm diameter platelets demonstrated an alignment of $r = 0.251 \pm 0.017$; FWHM $= 11.16^{\circ} \pm 1.16^{\circ}$. A sample with optimal alignment was hot-pressed to transparency and obtained an in-line transmission of 70.0% at 645nm. The final alignment of this pre-aligned hot-pressed sample ($r = 0.254 \pm 0.008$; FWHM $= 11.38^{\circ} \pm 0.54^{\circ}$) improved when compared to a non-pre-aligned sample ($r = 0.283 \pm 0.005$; FWHM $= 13.40^{\circ} \pm 0.38^{\circ}$).

Additionally, the use of direct ink writing, an additive manufacturing technique, as a viable alignment process for producing transparent alumina was investigated. Highly loaded (> 54 vol.%)

equiaxed alumina suspensions were developed with platelet additions ranging from 0-20vol.% of the total solids loading. An increase in the amount of platelet powders from 5-20vol.% increased the dynamic yield stress from 104Pa to 169Pa and decreased in the equilibrium storage modulus from 17,036Pa to 13,816Pa. It was found that the DIW process significantly increased the alignment in one orientation when compared to samples cast from the same suspensions and this behavior may be connected to the rheological properties. Lastly, an optical analysis showed that sample developed with 5vol.% platelet suspensions had higher in-line transmission values across the visible spectrum when compared to samples developed with 20vol.% suspensions. A sample cast from a 5vol.% platelet suspensions had the lowest grain alignment but possessed an in-line transmission of 42.8% at 645nm, which was the highest of the samples produced in this study. An optical loss analysis showed, that this sample has the lowest backwards scattering losses due to residual porosity and this result was supported by the density data. It is suggested that the alignment of the DIW samples is more complex and a more advanced texture analysis will need to be conducted to properly characterize the grain alignment.

Lastly, the densification behavior of equiaxed and platelet powder ratios with no intentional pre-alignment was investigated. An initial sintering investigation identified the optimum maximum pressure selected for the hot-pressing process as 20MPa. Under the selected hot-pressing parameters, the effects of 0, 25, 50, 75, and 100wt.% equiaxed powder additions on the sintering behavior, optical properties, and grain alignment was investigated. The data showed that an increase in the amount of equiaxed powders decreased the initial powder compact displacements rate. Additionally, an increase in the wt.% equiaxed powders from 0wt% to 75wt% decreases the in-line transmission from 70.9% to 40.2%, respectively at 645nm. Lastly, an increase in the wt.% equiaxed powders from 0wt% to 75wt decreased the alignment from ($r = 0.321 \pm 0.005$; FWHM $= 16.26^{\circ} \pm 0.40^{\circ}$) to ($r = 0.509 \pm 0.022$; FWHM $= 34.63^{\circ} \pm 2.61^{\circ}$), respectively.

1. INTRODUCTION AND BACKGROUND

Willy's contribution to this collaborative effort includes project design, sample development and processing, rheology testing and analysis, binder burnout analysis, and sintered specimen analysis, rocking curve testing and analysis, optical analysis, and writing of the manuscript.

1.1 Transparent Alumina

Transparent alumina is an ideal material for ballistic protection applications where visible or infrared wavelength transmission is required.[1–3] However, to achieve these favorable properties, alumina must be sintered to high densities (>99.99%TD) to eliminate light scattering due to porosity.[4] Even at high densities, the transparency of alumina is limited due to the rhombohedral crystal structure being inherently birefringent.[5] Birefringence causes light scattering at misaligned grain boundaries due to differences in refractive index and is detrimental to the transparency of polycrystalline alumina.[1, 5–7] Fundamental equations developed by Apetz et al.[7] related the transparency of alumina to the refractive index difference and grain size. It has been shown experimentally that the crystallographic alignment of equiaxed alumina powders with a high magnetic field prior to densification reduces birefringent light scattering.[5, 6, 8] However, from a manufacturing stand point this method may be limited in terms of scalability. Ultimately, there is a need to develop forming methods that will allow for large scale and cost-effective production of transparent alumina with high crystallographic alignment.

1.2 Processing of Textured Ceramics

Textured or oriented polycrystalline ceramics have increasingly gained interest due to the enhanced properties they offer in magnetic, structural, piezoelectric, and optical materials.[6, 9–13] As a result of the demand for highly-oriented polycrystalline ceramics several methods have been

used to develop textured ceramics. Initial investigations on sintering techniques such as hot working (compression or tensile)[14–16] led to the development of general texture in electronic and structural materials. Following these initial investigations more advanced techniques such as shear[17–20] or elongational[21] fluid flow-based processes, electrophoretic deposition[22], gravitational sedimentation[23], and high magnetic field[24] were developed and used to achieve ceramic particle alignment in polycrystalline ceramics.

One of the most commonly used ceramic processing methods to fabricate highly-textured technical ceramics is templated grain growth (TGG).[9–11, 25–27] Typically, this process disperses 1-15 vol.% (of the total solids content) of morphologically anisotropic powders (seeding particles) in an equiaxed submicron powder matrix.[9–11, 25–27] Shear forming alignment techniques such as dry forming,[25] screen printing,[9] and slip or tape casting[9, 26–28] are used to physically align the anisotropic powders within the matrix. During the pressureless sintering process, the anisotropic single crystal powders grow and develop a high-volume fraction of crystallographic texture. This process, when paired with tape casting, is able to obtain highly textured (FWHM $\leq 10°$) alumina samples.[9, 29, 30] However, as promising as this process is, TGG is not a feasible alternative processing method for transparent alumina due to the liquid phase formers (typically alumniosilicates) required to promote anisotropic grain growth and preserve particle anisotropy.[9–11, 25, 27] The addition of these sintering aids causes the formation of secondary phases that result in degradation of the optical transmission.[7] Due to these issues with secondary phases, other ceramic processing methods that can achieve highly aligned polycrystalline structures with no sintering additives will need to be investigated for the development of transparent alumina.

A portion of this work proposes using forming process that utilizes shear and elongational stresses to align platelet alumina such that after subsequent hot pressing, a dense, highly textured sample with improved optical properties is obtained. Before the selected processes are discussed simple models developed on shear and elongation fluid flow particle alignment are provided.

1.2.1 Fluid Flow Alignment

High aspect-ratio particles dispersed in a fluid medium will align when subjected to flow fields due to developed velocity gradients. In the field of ceramics processing the most commonly discussed flow stresses in regard to alignment are either shear or elongational flow. Shear and elongational flow stresses evoke different responses leading to different velocity profiles and

particle orientation dynamics. Flow behavior analysis based on the principles of fluid dynamics were described for shear and elongational flow by Chou et al.[31] and McCrum et al.[32] respectively. The following sections will discuss these models and the corresponding velocity gradients to form a basis for particle orientation dynamics.

1.2.1.1 Shear Flow

Typically, systems experiencing shear flow can be described by the separate elementary flow patterns: Capillary or Couette flow. In fluid dynamics, capillary flow is modeled as the pressure-driven flow of a high-viscosity/low-velocity Newtonian fluid through a parallel, non-moving channel, which is shown schematically in Figure 1.1. Chou et al. used this model to explain the stress profiles developed in tape casting and showed that by solving for the Navier-Stokes equations, the velocity profile of capillary flow ($v_{x,Cap}$) can be expressed by Equation 1:

$$v_{x,Cap} = \frac{h_0^2 \Delta P}{2\eta L} \frac{y}{h_0} (1 - \frac{y}{h_0}) \qquad\qquad 1$$

Where x is the direction of flow, h_0 is the height between the plates, ΔP is the pressure exerted on the fluid along the x-direction, y is the incremental distance between the plates, η is the viscosity of the fluid, and L is the length of the plates. The following boundary conditions are applied to the model: velocity is zero at the surfaces, pressure is at a maximum at $x = 0$, and pressure is at a minimum at x $= L$. With these boundary conditions, the velocity profile demonstrates a parabolically behavior increasing from zero at the edges to a maximum at the midpoint as shown in Figure 1.1.
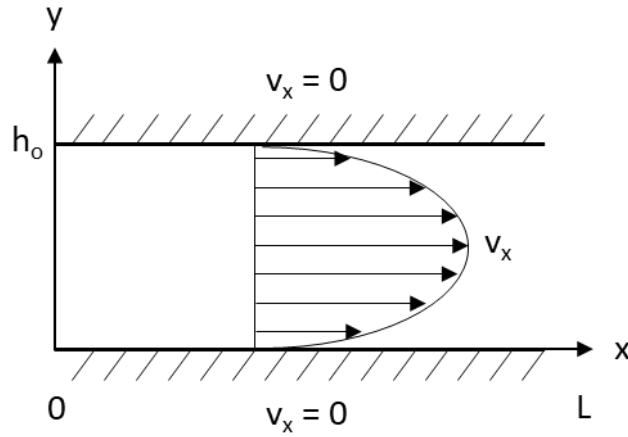
Figure 1.1. Velocity profile of capillary flow. Figure adapted from Chou et al.[31]

The other main type of elementary shear flow pattern is Couette flow. Couette flow is typically modeled as a high-viscosity/low-velocity Newtonian fluid between parallel plates, were one plate (the bottom) moves relative to the other at a constant velocity *V,* while the other (top plate) remains stationary. This process is shown schematically in Figure 1.2. Similar to the capillary flow model, the velocity profile of Couette flow, ($v_{x,Cou}$), is obtained by solving the Navier-Stokes equations with the following boundary conditions. The velocity of the fluid at the plate is equal to the velocity of that plate ($v_{x,s} = V$ at $y = 0$, and $v_{x,s} = 0$ at $y = h_0$), and the pressure is zero throughout the entire system. Applying these boundary conditions gives the velocity behavior expressed in Equation 2.

$$v_{x,Cou} = V(1 - \frac{y}{h_0}) \qquad\qquad 2$$

Where the velocity profile is minimum at the stationary plate surface and increases linearly to a max at the moving plate surface.[31]
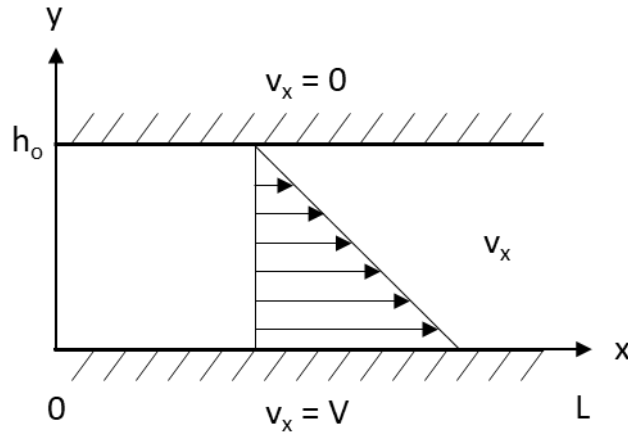
Figure 1.2. Velocity profile of Couette flow. Figure adapted from Chou et al.[31]

1.2.1.2 Elongational Flow

There are three types of pure elongation flow behaviors: uniaxial, biaxial, and planar.[33] The first, uniaxial flow, is described by a unit cube of material being stretched in one direction and contracted in the two normal directions. The second, biaxial flow, is described by a unit cube of material being stretched in two directions and contracted in the normal plane. The third, planar flow, is described by a unit cube of material being stretched in one direction and contracted in only one of the normal directions. The three pure elongational behaviors are demonstrated in Figure 1.3.
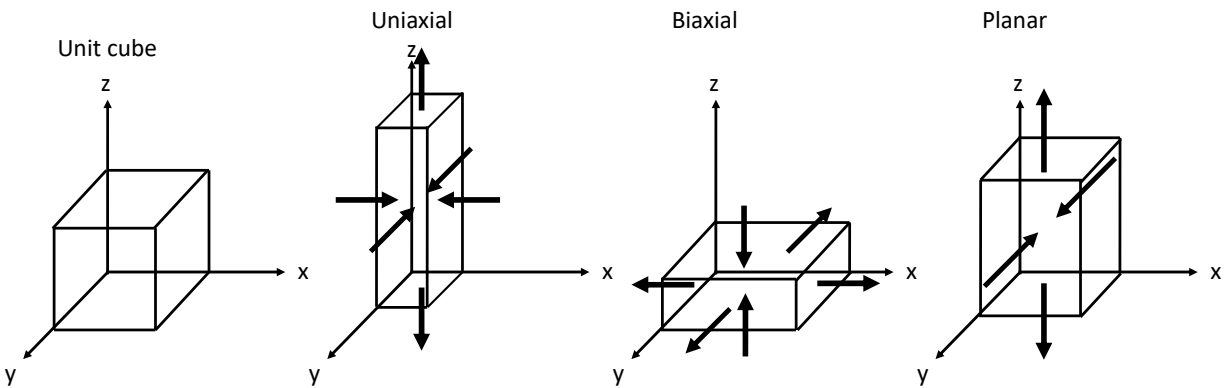
Figure 1.3. A schematic of the three pure elongational flow behaviors: uniaxial, biaxial, and planar elongational flow. Figure modified from Singh et al.[33]

For the three separate cases, the flow behaviors are similar for the stretching components. Due to this the simple uniaxial flow model will be used to describe the velocity profile obtained

from elongational flow. McCrum et al.[32] described uniaxial elongational flow as a change in the cross-sectional area of a polymer melt were the volumetric flow rate is conserved. To conserve the volumetric flow rate as the cross-sectional area decreases a velocity gradient (dv/dt) is formed. This velocity gradient can be related to the change in strain per unit time ($d\varepsilon_t/dt$). In doing so this gives a relationship where the velocity profile is dependent on the elongational viscosity (λ), volumetric flow rate (Q), and the force used to draw the polymer melt (F) giving in Equation 3.[32]

$$\frac{dv}{dz} = \frac{d\varepsilon_t}{dt} = \frac{1}{\lambda}\frac{Fv}{Q} \qquad\qquad 3$$

Thus, the characteristic feature of elongational flow is a change in the cross-sectional area of the fluid as a function of distance along the direction of flow. A more details explanation an examples of this behavior is described in the literature.[34]

1.2.1.3 Particle Orientation Dynamics

Now that a simple understanding of the developed velocity profiles has been given for shear and elongational flow, the orientation dynamics of high aspect-ratio particles will be discussed. Jeffery et al.[35] was the first to perform an analysis of the orientation dynamics of short fibers. This analysis is considered to be the basis for this phenomenon and cited throughout the literature. A description of Jeffery's analysis is provided by Tucker et al.,[36] and a simplified version of this analysis will be provided as an understanding of particle orientation dynamics.

Figure 1.4 models the orientation state of a single fiber with respect to the x, y and z axes which is defined by two angles, φ and θ, respectively.
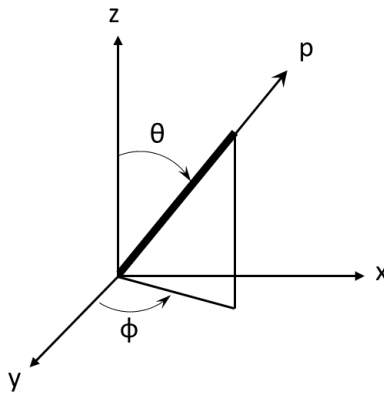
Figure 1.4. The orientation of a single fiber described by two angles: θ and φ (figure modified from Tucker et al.[36])

19

A single fiber in a dilute solution experiencing in-plane Couette flow ($v_1 = Gx_2$, $v_2 = v_3 = 0$, G is the shear rate), will rotate periodically in a skipping-like motion. This periodic rotation is explained by the difference in the moment-arms exerted on each end of the fiber during its rotation. This moment arm difference originates from the velocity gradient exhibited in-plane Couette flow and the rotation of the fiber can be defined by Equation 4 and Equation 5.[36]

$$tan\theta = \frac{Cr_e}{\sqrt{cos^2\phi + r_e^2 sin^2\phi}}$$

4

$$cot\phi = r_e tan\left(\frac{2\pi t}{T} + \kappa\right)$$

5

Where C is the orbit constant, κ is the phase and from this the period of rotation (T) is defined by Equation 6.

$$T = \frac{2\pi}{G}\left(r_e + \frac{1}{r_e}\right)$$

6

Where G is the shear rate and r_e is the equivalent ellipsoidal axis ratio (a/b) with a being the length and b the diameter of the fiber. If a disk-shape particle is desired, then a would simply be less than b. The motions of a fiber described by these equations are defined as Jeffery orbits, and the average orientation of the fiber during the Jeffery orbit is what dictates the direction of preferred alignment. Tucker et al.[36] showed that by plotting orientation angle as a function of time for one rotation period (t/T), that for the majority of the orbit a particle is at $\phi = 0°$ and $\theta = 90°$. Meaning that the fiber rotates rapidly when it is oriented perpendicular to the direction of flow, and rotates slowly when oriented parallel to the direction of flow.[37]If the fiber in Figure 1.4 were experiencing in-plane Couette flow in the y-axis, then this shear flow would align the fiber parallel to the y-axis. The same behavior would be observed for disk-shaped particles, although it is the diameter of the disk that will be aligned parallel to the direction of flow.

The orientation dynamics of elongational flow is similar to Couette flow. A fiber will also experience a periodic rotation for uniaxial elongational flow ($v_x = -(\varepsilon/2)x$, $v_y = \varepsilon y$, and $v_z = -(\varepsilon/2)z$, ε is the strain).[36] This behavior is modeled by Equation 7.[36]

$$tan\theta = tan\theta_0 \exp\left(-\frac{3}{2}\lambda\varepsilon t\right)$$
7

Since the flow is one dimensional, φ is constant for this situation, ε is the strain, and λ is a constant that defines the shape of the particle and is given by Equation 8.[36]

$$\lambda = \frac{\left(\frac{a}{b}\right)^2 - 1}{\left(\frac{a}{b}\right)^2 + 1}$$
8

As mentioned earlier, *a* is greater than *b* for fibers, and *b* is greater than *a* for disk-shaped particles. In the described case, the fluid is extending along the y-axis and therefore the velocity of the fluid is increasing with increasing distance along the y-axis. This will cause the fiber to rotate parallel to the y-axis such that θ tends towards zero. Thus, similar to the shear flows, in can be concluded that elongational flows align fibers in the direction of the elongation.[36]

From Jeffery's equations, it is clear that high aspect ratio particles in shear and/or elongational flows will preferentially align parallel to the direction of flow. In relation to ceramic processing, there are multiple processes that experience these types of flows. Most notably, these include tape-casting, and co-extrusion, and a variant of biaxial extensional flow. Examples of these types of processing and their viability for the alignment of transparent ceramics are explored in the following sections.

1.2.2 Shear and Elongational Forming Processes

1.2.2.1 Tape Casting

Tape casting is one of the most frequently used and successful shear forming processes for obtaining microstructural and crystallographic texture.[17–20, 26, 31, 38–44] This process could be a possible candidate for the development of texture in transparent alumina. However, a bulk of the literature focuses on seeding an equiaxed matrix with a small amount of aligned anisotropic powders. Unfortunately, few articles report on the fabrication of tape cast samples consisting of entirely platelet morphology powders.[20, 39, 44]

Watanabe et al.[20] successfully tape cast slurries with solids loading ranging from 15 to 33vol.% $BiTiO_3$ (4µm-diameter) platelets. This study performed a combination of XRD and SEM texture analysis to characterize their green body and sintered samples. They obtained a maximum orientation degree (f) of roughly 0.9.[20] The methods that were used to characterize these samples

are considered semi-quantitative at best and have been known to inflate the data when $f \geq 0.9$.[11, 29, 30] Therefore, it is difficult to compare this data to values of strong texture and to assess the extent of texture. Other studies performed by Fu et al.[39] on the tape casting of alumina produced green body samples of 20 vol.% platelets (8.7µm). However, they did not report the quantitative alignment of the samples since the primary focus was on binder burnout defects. A more recent study by Wonisch et al.[44] tape cast 28 vol.% alumina platelets (2.2µm) to compare experimental and simulated data. They used image analysis software on optical micrographs of cross-sections to determine an orientation angle with respect to the casting direction. Their results showed that anisotropic particles showed a higher degree of particle orientation when compared to equiaxed. However, the highest value reported was roughly 32°, with 0° being the maximum aligned state in the casting direction.[44] Even though this study was able to obtain a relatively high solids loading for the tape casting process, the orientation values that they calculated were low when compared to other shear forming processes.[9, 11, 25] At the current moment, it is not clear if tape casting is capable of processing highly aligned samples from entirely platelet alumina powders while maintaining a suitable solids loading (>30 vol.%).

1.2.2.2   Processing of Ceramic-filled Thermoplastic Polymer Blends

Ceramic-filled thermoplastic polymer blends have been used by the fibrous monolith and co-extrusion community for some time.[12, 13, 45–53] Many of these processes have taken advantage of the shear and elongational stresses developed during forming to align anisotropic powders. One study by Trice et al.[13] used a simple process termed warm pressing to develop qualitative alignment in systems consisting of a 50 vol.% hexagonal boron nitride and polymer additives mixture. They found that warm pressing the ceramic-filled polymer blends before hot pressing led to a qualitative increase in the grain alignment, which contributed to an increase in crack deflection during flexure testing.[13] This warm pressing technique was also used to fabricate silicon carbide and oriented boron nitride multi-layered composites to investigate crack deflection and propagation mechanisms.[54] In both of these studies they did not quantitively characterize the alignment of the sample but argued that other studies showed highly textured samples through similar processes.[55] Other studies on the co-extrusion of silicon nitride and boron nitride fibrous monoliths claimed that the shear stresses developed during the co-extrusion process lead to the alignment of anisotropically shaped boron nitride and β-silicon nitride powders.[55] However, the alignment

developed in these studies is also not fully understood as only a simple qualitative XRD texture analysis was performed instead of a pole figure analysis due to limitations associated with boron nitride basal plane intensities. Regardless, it is apparent that the shear and elongational stresses produced during processing influence the alignment of the final microstructure, yet investigation on the texture development is needed to determine if methods such as warm pressing or co-extrusion can obtain highly aligned microstructures.

1.2.2.3   Uniaxial Warm Pressing of Ceramic-filled Thermoplastic Polymers

What is apparent from the literature on ceramic-filled thermoplastic processing, is that warm pressing may be ideal for the axisymmetric alignment of platelet alumina powders for improved transparency. This simple process uses heated platens to apply a compressive load to a ceramic-filled thermoplastic blend. Upon compression, the blend flows and elongates in the non-constrained directions. It is expected that this flow behavior will induce elongational stresses via biaxial extensional flow[33, 56] as well as shear stresses via pressure drive flow.[20, 37, 57] A simplified schematic of these process with the possible velocity profiles developed in Section 1.2.1.1 and 1.2.1.2 is shown in Figure 1.5.
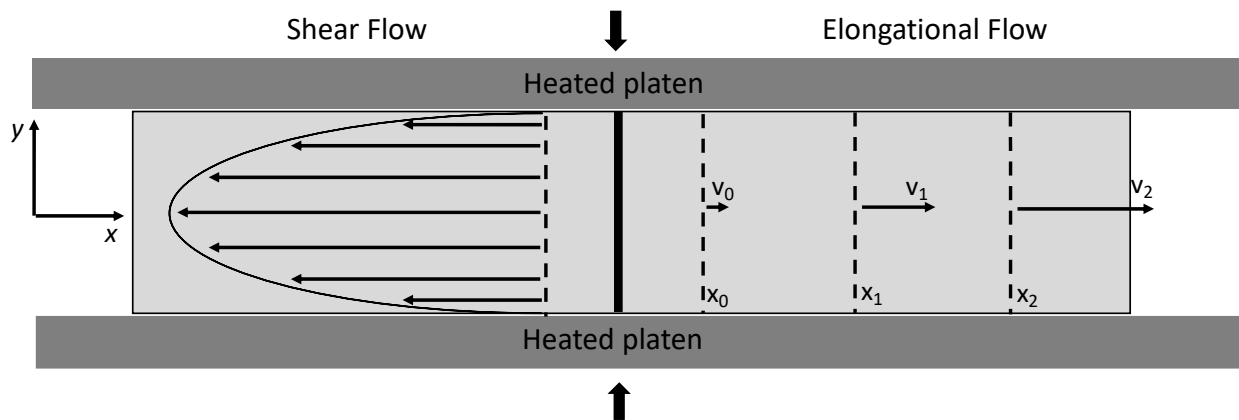
Figure 1.5. A simplified schematic of the warm pressing process illustrating the possible velocity gradients formed due to shear and elongational flows.

As explained earlier, these flow stresses should lead to velocity gradients that can preferentially align high aspect ratio platelets parallel to the direction of flow.[35, 37] Pre-aligned alumina brown bodies produced via warm pressing of a well-developed rheological blend will yield increased particle alignment and hence increase the in-line transmission when compared to

23

previous studies on hot pressed platelet alumina.[58] This method will be a strong candidate for producing large sheets of textured alumina over magnetic alignment methods.[5, 6, 8]

The work discussed in Section 3 will aim to produce axisymmetric-aligned platelet alumina in ceramic-filled thermoplastic polymer sheets via uniaxial warm pressing. The developed blends were modified from compositions of poly(ethylene-co-ethyl acrylate) (EEA) found in the literature.[45, 53] This was done via plasticizer additions and acrylate reductions, resulting in desirable flow properties and greater formability. The developed blends have a platelet alumina loading ranging from 30-40 vol.%, a constant amount of polymer additives, with a balance of base polymer (EEA). This study assesses the effects of alumina platelet diameter and solids loading on the rheological properties, percent reduction in thickness, and final platelet orientation of ceramic-filled polymer sheets produced via warm pressing. Additionally, a sample with the best pre-alignment conditions was hot-pressed to transparency and compared to a non-pre-aligned sample hot-pressed under the same conditions.

1.2.2.4 Direct Ink Writing aqueous-based suspension with alumina platelet additions

Another process that could possibly lead to the alignment of platelet powders prior to sintering is additive manufacturing. Additive manufacturing techniques have gained interest among the ceramics processing community due to the ability to form complex shapes that cannot be created through casting or machining in a cost-effective manner.[59–63] Direct ink writing (DIW) is a type of additive manufacturing process that uses an axis controlled syringe to deposited or extrude ceramic suspension in a controlled manner. This forming process can be divided into two main categories which is droplet or filament based. Of these types of DIW, filament-based processes use extrusion to deposit inks or colloidal suspensions in a continuous manner, which leads to the development of shear and elongational stresses.[63–65] Previous work focused on the developed of a filament-based DIW process with aqueous-based ceramic suspensions for multiple material systems.[65, 66] Further background and more details of this process can be found in the literature.[62–66] The current work will focus on the use of this filament-based DIW technique for the development of transparent alumina due to the shear and elongational stresses formed during extrusion and the ability to alignment high aspect ratio particles.[32]

DIW has allowed for the production of complex-shaped parts of many different ceramic systems such as mullite, alumina, stabilized zirconia, and silicon nitride at solids loading above 50

vol.% [60, 63–65, 67]. Even with this strong interest to form complex ceramic structures, there is little work on developing bulk ceramics with preferentially aligned high aspect ratio powders. Recently, new investigations centered on fiber orientation during DIW have demonstrated the viability of this process to align high aspect ratio particles.[68, 69] In these studies, filament-based DIW was used to align high aspect ratio fibers in polymers[69] and pre-ceramic precursors,[68] however work done on aligning high aspect ratio powders (fiber or platelets) in ceramic suspensions is minimal.

The filament based DIW process from the previous and current work, uses a syringe style printing head that was supported by a gantry crane. This simple set up allowed for a motor to mechanically drive a syringe plunger. Applying a pressure to the syringe led to the flow of the aqueous-based ceramic suspension. Following this, the suspensions was extruded from the equipped nozzle. An image of the selected nozzle with dimensions is shown in Figure 1.6a.
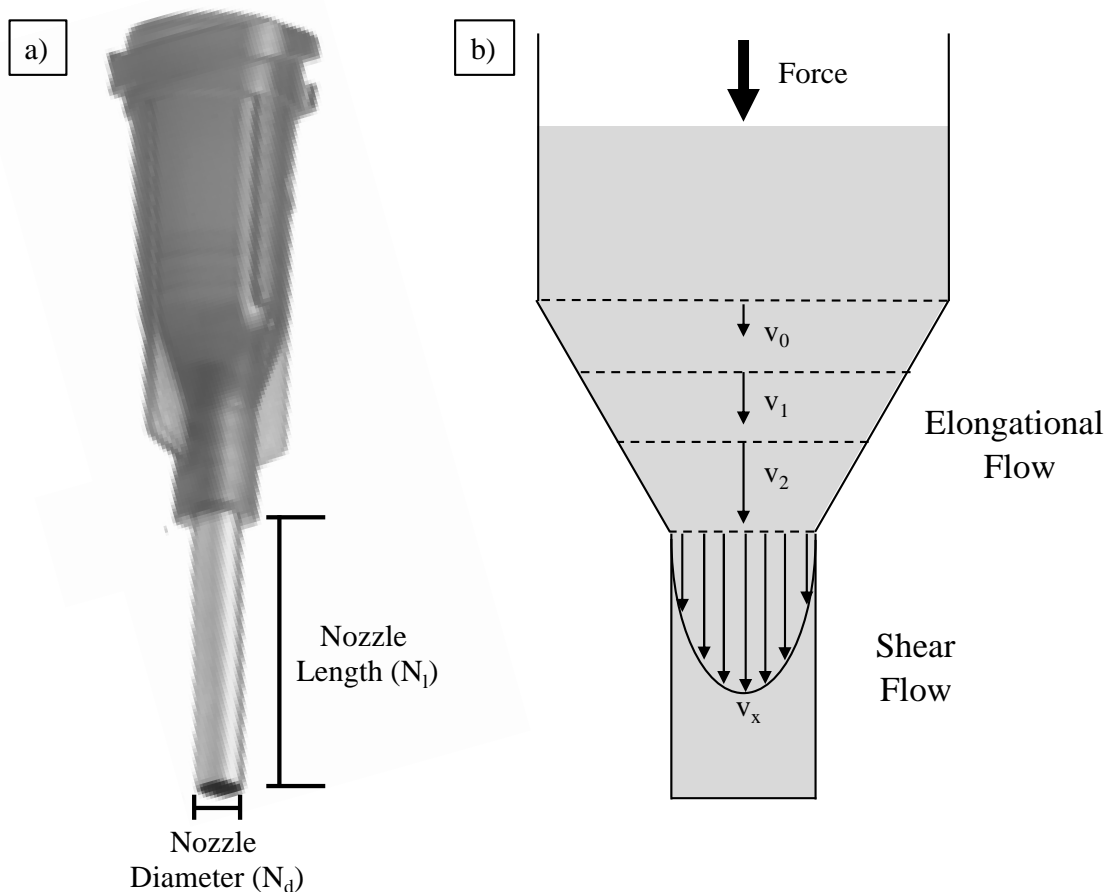
Figure 1.6. a) An image of the selected DIW nozzle, b) a simplified schematic of the nozzle with the excepted velocity gradients formed due to shear and elongational flows.

Upon the application of the pressure, the aqueous-based suspension will flow. First, it will be constrained by a change in cross-sectional area and following this it will enter an area of constant cross-section. A simplified schematic of this process with the velocity profiles developed in Section 1.2.1.1 and 1.2.1.2 is shown in Figure 1.6b. In the first area, the suspension will experience uniaxial elongational flow to conserve the volumetric flow rate as the cross-sectional area decreases.[32] In the second area, the suspension will experience pressure driven shear flow with the velocity gradient being highest at the nozzle edges.[31] As explained above, both of these profiles will lead to velocity gradients that can align high aspect ratio powders. It is expected that these velocity gradients will lead to the alignment of platelet and fiber morphology powders. However, considering that platelets have only one dimension that is constricted when compared to fibers, which have two dimensions, we expect to see biaxial alignment. This process will most likely result in two-dimensional texture, but the use of uniaxial hot-pressing could alleviate this. It is possible that the pre-alignment of platelets alumina in aqueous-based suspensions could lead to hot-pressed samples with increased alignment and optical properties.

The work discussed in Section 4 will aim to produce aligned platelet alumina from the DIW of aqueous-based ceramic suspensions. The developed suspensions were modified from previous work that can be found in the literature.[65, 70, 71] This was done by using a base 54vol.% equiaxed powder suspension. The suspensions were modified with platelet powder additions ranging from 5, 10, 15, 20vol.% of the total solids loading. To conserve the volume percent and additives, platelet additions were balanced with equiaxed powders. This study assesses the effects of platelet alumina solids loading on the rheological properties, the sintered grain orientation, and the sintered optical properties of transparent alumina produced via DIW.

1.2.2.5 Hot-pressing Equiaxed and Platelet Alumina Powders to Transparency

As explained in an earlier section, high aspect ratio powders are necessary to be able to take advantage of the particle alignment that comes from shear and elongational forming processes. Section 3 and 4 will established that viability of alternative process that use shear and elongational stresses to align alumina platelet powders. However, both of these studies found that it could be more beneficial to limit the use of platelet powders. For both the ceramic-filled thermoplastic processes and aqueous-based processes it was found that the use of platelet particles led to less desirable rheological properties. For processes that use ceramic-filled thermoplastic blends, it was

found that blends that exhibited higher temperature sensitivity constants and flow properties resulted in higher final alignments and increased optical properties. As will be discussed in Section 3, it was found that ceramic-filled thermoplastic blends prepared with platelet alumina possessed high measured torque and viscosity values at lower solids loadings when compared to blends from the literature and from this work that were prepared with equiaxed powders.[51] Additionally, further increasing the solids loading produced samples that were considered unworkable. From the rheology properties and formability that was exhibited by equiaxed powder blends it is postulated that the addition of equiaxed powders to platelet powder blends may lead to more desirable rheological properties which will increase the platelet alignment. For processes that use aqueous-based ceramic suspension, it was found that the additions of platelet powders, lead to increased yield stresses and viscosity and at platelet solids loadings greater than 20vol.% the suspensions become unworkable or dilatant. The texture analysis showed that as the amount of vol.% platelet powders increased the alignment of the cast and DIW samples decreased. For both the thermoplastic blends and aqueous-based suspensions, it seems that it would beneficial to use a mixture of equiaxed and platelet powder. To add to this, commercially available platelet alumina tends to be more expensive and has a lower purity when compared to equiaxed powder. Therefore, the use of equiaxed and platelet powder ratios may be a practical approach to obtain higher optical properties in a cost-effective manner. However, the densification behavior of the equiaxed and platelet powder ratios must first be understood.

The work discussed in Section 5 will report the sintering behavior of hot-pressed equiaxed and platelet powders with no intentional pre-alignment. Based off of previous work,[58] an initial sintering investigation was preformed to identify the optimum maximum pressure for the selected sintering parameters. Under the selected hot-pressing parameters, the effects of 0, 25, 50, 75, and 100wt.% equiaxed powder additions to platelet powders on the sintering behavior, optical properties, and grain alignment will be discussed.

2. EXPERIMENTAL METHODS

A portion of this chapter is published in the Journal of the American Ceramics Society

Willy's contribution to this collaborative effort includes project design, sample development and processing, rheology testing and analysis, binder burnout analysis, sintering and specimen analysis, rocking curve testing and analysis, optical analysis, and writing of the manuscript.

A portion of this chapter is published in the Journal of the American Ceramics Society

Willy's contribution to this collaborative effort includes help with project design, XRD data collection and analysis, and editing of the manuscript.

For the additive manufacturing investigation, Willy's contributions include project design, assistance with the DIW process, development of the suspensions, rheological testing and analysis, rocking curve testing and analysis, optical data analysis, optical image analysis and writing of the manuscript.

For the powder ratio investigation, Willy's contribution includes project design, powder preparation, hot-pressing, displacement data collection and analysis, rocking curve testing and analysis, optical sample preparation, optical image collection and analysis, optical data analysis, and writing of the manuscript.

2.1 Ceramic-Filled Thermoplastic Polymer Blends

2.1.1 Mixing of Ceramic-Filled Polymer Blends

The platelet powders used were RonaFlair White Sapphire alumina (Merck KGaA, Darmstadt, Germany) with a manufacturer reported purity of 99.8% and grade YFA02050 Serath alumina (Kinsei Matec Co., Ltd, Japan) with a manufacture reported purity of 98.0%. Both powders have a platelet morphology, as seen in Figure 2.1. The RonaFlair or large platelet powder

has a reported diameter of 11μm and a thickness of approximately 0.5μm while the Serath or small platelet powder has a reported diameter of 1.2μm and a thickness of approximately 0.07μm. BET surface areas of $2.00 \pm 0.02 m^2/g$ and $11.47 \pm 0.05 m^2/g$ were obtained for RonaFlair and Serath powders, respectively, using a TriStar II 3020 gas adsorption analyzer (Micromeritics Instrument Corporation, Norcross, GA). To have a comparison between platelet and equiaxed powders, AA-03 (Sumitomo Chemical Co., Ltd., Japan) alumina was used. This powder has a manufacture reported purity of 99.99%, diameter of 0.44μm, and BET surface area of $5.2 m^2/g$.
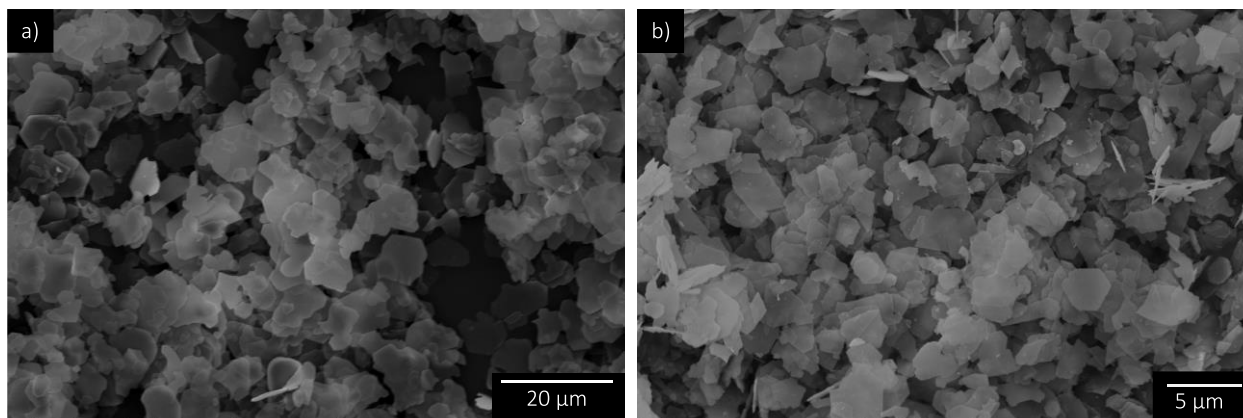
Figure 2.1. SEM micrographs of a). RonaFlair (large) alumina platelets with a reported average particle diameter of 11μm and b). Serath (small) alumina platelets with a reported average particle diameter of 1.2μm.

A thermoplastic binder system was modified and adapted from previous work on the coextrusion of fibrous monoliths[12, 13, 46–51, 72, 73] and green machining.[52] The development of the system and individual functions of each component is described in detail in the literature.[45, 53] A four component polymer blend consisting of EEA (MFI=6.0g/10min, poly[ethylene-co-ethyl acrylate], Dow Elastomers, Midland, MI), PiBMA (poly[ethylene-co-butyl acrylate], (Acryloid B67, Rohm and Haas, Philadelphia, PA), poly ethylene glycol (PEG1300, Mw= 1,300g/mol, Sigma–Aldrich, St. Louis, MO) and HMO (Heavy mineral oil, Fischer Chemical, Hampton, NH) was selected. Typically, a wax-based component (stearic acid) is added to act as a lubricant during shear mixing, however, this component was removed due to negative effects associated with polymer stability during mixing, pressing and binder removal.

A Brabender high-shear torque rheometer (Plasti-Corder PL 2100 Electronic Torque Rheometer, C. W. Brabender, South Hackensack, NJ) was used to initially mix the ceramic-filled

polymer blend. A detailed schematic of this setup was adapted from the literature[51] is presented in Figure 2.2 and the geometrical data is provided in Table 2.1.
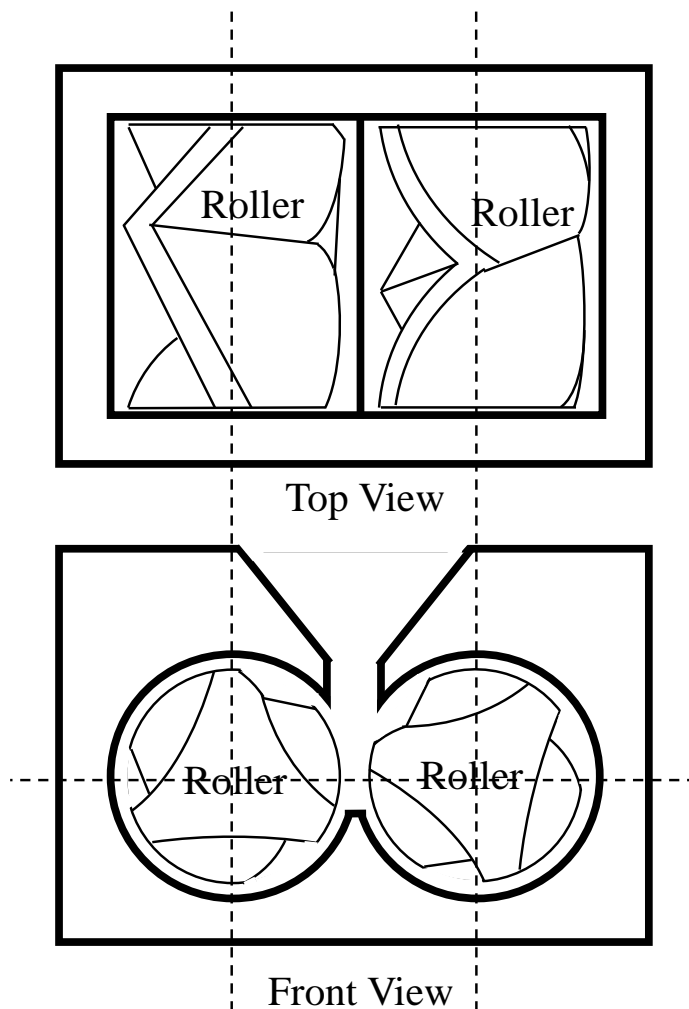
Figure 2.2. Schematic of the torque rheometer with roller-type mixing head adapted from Xu et al.[51]

Table 2.1. Geometrical data for the torque items rheometer adapted from Xu et al.[51]

Torque Rheometer Elements	Dimensions
Chamber Size	$60,000mm^3$
Radius of chamber (R_c)	19.65mm
Chamber length (L_c)	48.10mm
Gear ratio (g)	3:2
Roller length (L)	46.90mm
Radius of roller (Max)	19.47mm
Radius of roller (Min)	10.5mm
Effective internal radius (R_i)	17.4mm

During mixing, the shear mixer was equipped with a banbury blade geometry shown in Figure 2.3.
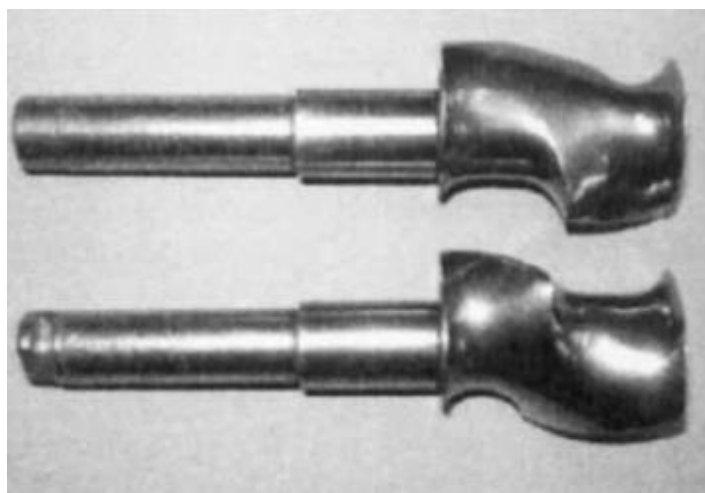
Figure 2.3. Image of the banbury blades used mix the ceramic-filled thermoplastic blends. Image found in the literature.[74]

Initial mixing parameters of 130°C and 20RPM were selected. The total amount of EEA was added and allowed to thoroughly blend. Once mixed, small increments of the selected powders were continuously added to the system. Throughout the entire mixing process, PiBMA and PEG1300 were slowly introduced. After all the powder was added to the system, the roller speed was increased to 60RPM and the remaining HMO was added. The blend was mixed at these parameters until the torque value stabilized (approximately 15 mins). It was then removed from

the mixer and chopped into roughly 1cm^2 pieces for further processing. The compositions of the ceramic-filled polymer blends are listed in Table 2.2.

Table 2.2. Ceramic-filled thermoplastic blend compositions.

Powder Type	Al$_2$O$_3$ [vol%]	EEA [vol.%]	PiBMA [vol.%]	HMO [vol.%]	PEG [vol.%]
RonaFlair-11μm (large)	40	44.9	4.6	0.5	10
	35	49.9	4.6	0.5	10
	30	54.9	4.6	0.5	10
Serath-1.2μm (small)	40	44.9	4.6	0.5	10
	30	54.9	4.6	0.5	10
AA-03, 0.44μm (equiaxed)	40	44.9	4.6	0.5	10

2.1.2 Torque Viscometry of Ceramic-Filled Polymer Blends

The viscosity-shear rate dependence of the mixed blends was measured using the torque rheometer. Examples in the literature[51, 75–80] have shown that mixers equipped with a torque meter and relatively small chamber are a viable tool when used to obtain the viscosity-shear rate behavior from the torque-RPM data in polymer-based systems. Xu et al.[51] and Santi et al.[80] showed that this type of analysis is not entirely accurate when large amounts of ceramic powder are introduced to the system but is still a feasible method to use as a comparative analysis between similar systems.

For the analysis, the torque rheometer was equipped with a roller-type mixing head with the same dimensions shown in the literature.[51] The sample chamber was loaded to 70% of the total volume (60 cm^3) with the ceramic-filled polymer blend and mixed at an initial temperature of 130°C with a roller speed of 20RPMS for 20mins. Once the torque and temperature were stable, the rotor speed was decreased to 10 RPM and mixed for an additional 5 minutes. Torque data was collected at 120, 130, 140, and 155°C for ten minutes to characterize the torque-temperature dependence. An exponential fit of the torque vs temperature graph was used to obtain the viscosity temperature sensitivity constant (*b*). This constant was used to account for temperature increases due to viscous dissipation and to correct the measured viscosity in future measurements through Equation 9:

$$\Gamma(T) = \Gamma(T) \exp[-b(T - T_o)] \qquad\qquad 9$$

Where $\Gamma(T)$ is torque as a function of temperature, b is the viscosity temperature sensitivity constant, T is the set temperature, and T_o is the measured temperature of the blend.[80] After the torque-temperature analysis, the temperature was set to 130°C and the roller speed was decreased to 5RPM. Torque data was collected at 5, 10, 20, 30, 50, and 70RPM in five minute intervals to obtain the torque-RPM dependence of each blend. To obtain the shear-rate and viscosity data, the analysis suggested by Bousmina et al.[77] was applied. In their analysis, they introduce a universal quantity that they termed the effective equivalent internal radius or R_i. This internal radius is useful because it is insensitive to the rheological behavior of the blend and is only dependent on the geometrical dimensions and gear ratio of the torque rheometer.[51, 77, 80] Calculating R_i is essentially a means of calibrating the torque rheometer and an explanation of the process is detailed below. A Newtonian silicone oil was used to obtain R_i from Equation 10:

$$R_i = \frac{R_c}{\left[1 + \frac{4\pi N}{n}\left(2\pi \cdot mLR_c^2 \cdot \frac{1 + g^{n+1}}{\Gamma}\right)\right]^{\frac{n}{2}}} \qquad\qquad 10$$

Where R_c is the chamber radius, N is the roller speed per second, n is the power law index, m is the melt consistency index, L is the roller length, Γ is the torque exerted on the roller shaft, and g is the gear ratio.[51, 77, 80] These values for the torque rheometer are listed in Table 2.1. Once R_i was obtained it was used in the following equations to calculate the shear rate (Equation 11) and viscosity (Equation 12) for each ceramic-filled polymer blend.

$$\dot{\gamma} \approx \frac{2\pi N}{\ln\left(\frac{R_c}{R_i}\right)} \qquad\qquad 11$$

$$\eta = \frac{\Gamma}{N} \frac{\left(\frac{R_c}{R_i}\right)^2 - 1}{8\pi^2 LR_c^2 \cdot (1 + g^2)} \qquad\qquad 12$$

A linear fit of the log(viscosity) dependence on the log(shear rate) was used to obtain the power law index (n) and melt consistency index (m) for each blend.

2.1.3   Uniaxial Warm Pressing of Ceramic-Filled Polymer Blends

A modified version of the process referred to as warm pressing[12, 13, 54] was used to align the platelet alumina. The blend was placed in a 7.6 by 3.8cm stainless steel die and held in a continuous load (250kg) at 150°C for one hour to form a preform. The preform, roughly 17.9mm thick, was removed from the die and placed between two metal plates coated with PTFE. Universal mold release (Smooth-On, Inc, Macungie, PA) was added to the surface of the PTFE to aid with lubrication and sample removal. For all blend compositions, a hydraulic press was used to apply a load of 4500 kg to the assembly at 150°C and held for approximately 15 minutes to form a sheet. Each sheet was shimmed to (2.0, 1.5, or 1.0mm) to obtain a homogenous thickness. Due to the PTFE layers, the expected target thicknesses were roughly 1.4, 0.9 and 0.4mm. The ability for a blend to reach the target thickness was dependent on the rheology of the system and the final thickness was reported in % overall reduction. The ceramic-filled polymer sheets cooled under load to room temperature, at which point, the load was removed, and the sheets were separated from the metal plates.

2.2   Aqueous-based Alumina Suspensions for Direct Ink Writing

2.2.1   Alumina Suspensions Preparation

Aqueous-based alumina suspensions were developed and characterized with A-16 alumina powder by Acosta et al.[70] and Wiesner et al.[71] Following this, the suspensions were modified for the direct ink writing process by Rueschhoff et al.[65] For this study, AKP-50 (Sumitomo Chemical Co., Ltd., Japan) high purity (99.99%) alumina powder with an average diameter of 0.2μm and RonaFlair (Merck KGaA, Darmstadt, Germany) white sapphire platelet alumina with an average diameter of 11 μm (mentioned above in 2.1.1) were selected as the ceramic powders. Poly-vinylpyrrolidone (PVP) with an average molecular weight of ~55,000 (55k) (Sigma–Aldrich, St. Louis, MO) was dissolved in RO water by mixing in a Flack Tek Inc. SpeedMixer (DAC 450, Flacktek, Landrum, SC). The PVP and water solution was mixed at 800 rpm for 4 mins, 1000 rpm for 4 mins, and 1200 rpm for 6 mins to ensure that all the PVP was completely dissolved in the water. Once the solution was mixed, alumina powders were incrementally added to the PVP and water solution. The solution and powders were mixed in 1 min. intervals at (800,1200, and 1500) rpm followed by an 1800 rpm mix for 10 secs. This process was repeated until the powder were

sufficiently dispersed. Once half of the total powders were added, the dispersant, Darvin 821A (R.T. Vanderbilt Company Inc.), was added. On the final mixing step, four (13.5mm in diameter and 12.8mm in height) cylindrical Al_2O_3 milling media (Union Process, Akron, OH) were added to suspensions to aid in the mixing process. Suspensions were ball milled for 24hrs to achieve uniformity. The components of each suspension are summarized in Table 2.3.

Table 2.3. Compositions of aqueous-based alumina suspensions.

Equiaxed Al_2O_3 [vol%]	Platelet Al_2O_3 [vol%]	Dispersant [vol.%]	PVP MW = 55k [vol%]	Water [vol%]
54	0	3.9	5.5	36.4
49	5	3.9	5.4	36.7
44	10	3.9	5.3	36.6
39	15	3.9	5.3	36.5
34	20	3.9	5.3	36.2

2.2.2   Rheological Characterization of Aqueous-based Suspensions

The rheological and viscoelastic properties of the Al_2O_3 suspensions were determined using a Malvern Bohlin Gemini HR rheometer (Malvern Instruments Ltd, Worcestershire, UK). The experimental set up used was identical to the one described in previous publication.[65, 66]

Suspensions were ball milled for 24hrs prior to testing. Loop flow curves were obtained by measuring the shear response for controlled shear rates of first the static response (shear rates increased logarithmically from 0.01 to $35s^{-1}$) and followed by the dynamic response (shear rates decreased logarithmically from 100 to $0.0035s^{-1}$). To assume a homogeneous mixture, a pre-shear rate of $20s^{-1}$ was applied for 10sec followed by an equilibration period of 30sec before the static response test. The Herschel-Bulkley model[81] for yield-pseudoplastic materials displayed in Equation 13, was used to fit both the static and dynamic curves.

$$\sigma = \sigma_y + k\dot{\gamma}^n \qquad\qquad 13$$

where σ is the shear stress, σ_y is the yield stress for the material, k is the consistency index, γ is the applied shear rate on the suspension, and n is the flow index.[65, 66, 81] The yield stresses, consistency indexes and flow indexes were calculated from the curve fits (R^2 >0.985) of the data.

Stress sweep analyses were performed for each suspension by measuring both the storage modulus (G') and loss modulus (G") for an applied oscillation stress ranging from 1 to 1000Pa at a frequency of 1Hz. The same pre-shear conditions mentioned above were applied to the suspensions before data collection. The equilibrium storage modulus and the gelation point (G"/G'=1) were obtained from this data.

2.2.3 Direct Writing Process

A commercially available syringe style printer with layer-by-layer deposition capabilities was used to direct write samples. Previous studies optimized the use of a modified Imagine 3D printer (Essential Dynamics, New York City, NY),[65, 66] however, a more advanced Hyrel 30M (Hyrel 3D, Norcross, GA) was employed in this study. The printer was equipped with an SDS30 syringe style printing head which can house a 30mL BD Luer-Lok tip syringe (part#302832). Nozzles with a tip capillary length of 35mm and internal nozzle diameter of 1.35mm and 1.75mm were used. An image of these nozzle is shown in Figure 1.6a. The technical specifications for the printer chassis, mechanics, software, and electronics can be found at the manufacture's website (Hyrel3D.com). The suspensions were deposited in layer by layer format onto a glass slide coated with a PTFE layer and an example of this process can be found in Figure 2.4a. The desired samples shape was a 46.5mm by 30mm infilled solid rectangle shown in Figure 2.4b/c. This sample size was selected based on the hot-press die dimensions. The bulk infilled sample was developed by stacking layers with repeating line paths on top of one another. Print files were developed in the slicing software that comes from the manufacturer. A few selected inputs that are used to develop the three-dimensional path are shown in Table 2.4.
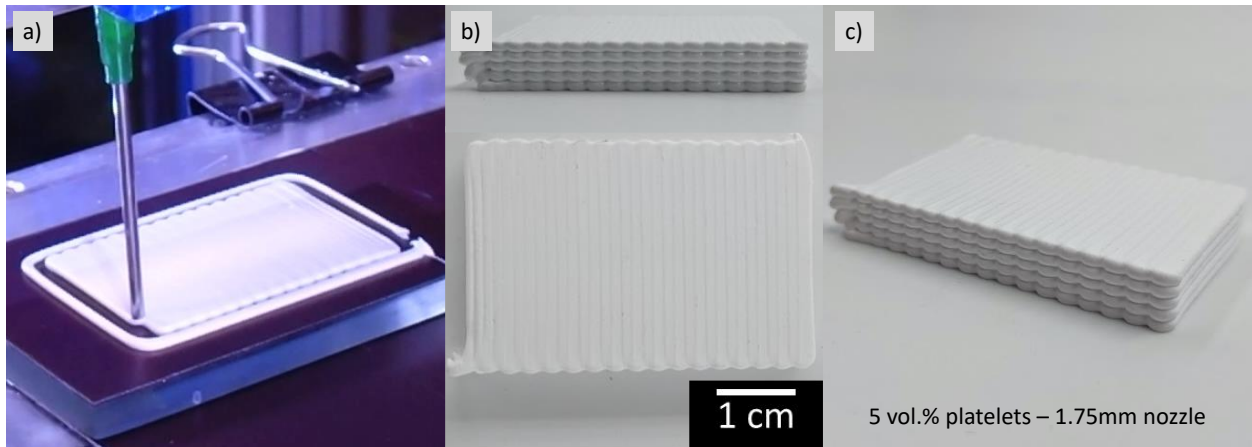
Figure 2.4. Image of an Al_2O_3 suspension being extruded in a layer-by-layer fashion to form the infilled rectangular sample. b) Side and top view images of sample produced via direct ink writing a 5vol.% platelet suspension with a 1.75mm nozzle diameter. c)profile view of the same sample.

Table 2.4. Settings used in the slicing software based on the nozzle parameters and optimization trails. These parameters were used to build the printing path file. Layer height is the height above the last layer the nozzle extrudes at. Nozzle diameter is used with the infill% to determine how far each print line should be spaced.

Nozzle	small flat/round	large round
layer height (mm)	0.9	1.4
nozzle diameter (mm)	0.9	1.7
infill (%)	75	50

During extrusion the printhead speed was set at 4mm/second. All suspensions were able to achieve a high-quality print with the slightly adjusted printing parameters. The pre-optimized processing parameters used to print the samples with different nozzle types are displayed in Table 2.5. Due to the different nozzle sizes the extrusion multiplier (flow rate modifier) was optimized for each print type and is listed in Table 2.5. To inhibit drying defects and to aid the printing process the surrounding humidity was saturated with a commercially available ultrasonic humidifier.

Table 2.5. Important control printing parameters for each nozzle. Layer height times the nozzle diameter is used to calculate the cross section of the print. Pulses/µl is used by the stepper motor to dispense in µl/sec. The multiplier modifies the flow rate

Nozzle	1.35mm	1.75mm
layer height (mm)	0.9	1.4
Nozzle diameter (mm)	1.2	1.7
Pulses/µl	48.6	48.6
Multiplier	1.5	0.45

Immediately after printing the glass slide containing the sample was placed into a humidity chamber to aide in drying. A water and sulfuric acid mixture was used to set the relative humidity of the chamber to above 70%. The samples were left in the chambers for > 48hrs.

2.3   Non-pre-aligned Equiaxed and Platelet Powder Ratios

2.3.1   Powder Preparation

The platelet powders used were RonaFlair White Sapphire alumina and AA-03 alumina equiaxed powders. More details on the powder and manufactures are provided in Section 2.1.1. The selected powders were weighed and separated into the following batches: 0,25,50,75,100wt.% equiaxed powder, with the remaining being platelet powder. Each batch had a total mass of a 100g and was individually washed in high-purity de-ionized water by roller-milling overnight. Then the batches were centrifuged, following this the water was decanted. This washing process (roller milling/centrifuging) was repeated two more times, then the batches were heated to 110°C and held at this temperature for 24hrs. This process was done in air to evaporate the remaining water. Once dried, the powder batches were sieved through a 250µm nylon mesh to break apart soft agglomerates. 6.0 grams of this sieved powder was poured directly into the hot-press die.

2.4   Texture Distribution Analysis

A texture analysis was performed to gain an understanding of the effect of processing conditions on the alignment. A rocking curve analysis was conducted on the (000.12) plane using a Panalytical Empyrean Diffractometer (Malvern Panalytical Ltd, Royston, UK). The machine was equipped with a bent Ge incident beam monochromator that is tuned to transmit Cu $K\alpha_1$

radiation. For both scans, incident slit geometry was fixed to 0.5° or 0.75mm while the detector active length was set to 0.715mm. A high resolution θ-2θ scan was collected at the Bragg's peak of interest (2θ = 90.6°, the basal plane that is perpendicular to the orientation plane). The data collection range was ± 1.24° with a step size of 0.005° and a dwell time of 1.0s. This scan was used to accurately locate the (000.12) plane and the 2θ axis was locked on the center of this peak for the following omega scan. The omega scan or rocking curve tilt range was ± 43.13°, with a step size of 0.25° and a dwell time of 1.0s. Preliminary analysis showed no repeatable treads in regards to alignment and sample position. Therefore, ten separate rocking curve analyses were performed on the ten green body samples collected from random locations on the pressed sheets to obtain an average value for the different processing conditions. For sintered samples, 3 separate rocking curve analysis were performed on both sides of the samples in different locations.

The data were corrected for defocusing and absorption phenomena in TexturePlus,[82] a software package developed at the National Institute of Standards and Technology, through explicitly determining the intensity distribution of the high resolutionθ-2θ scan (Bragg's peak).[30] Following this correction, the obtained texture profiles were fit to the March-Dollase equation (Equation 14):

$$F(f, r, \omega) = f \left(r^2 \cos^2 \omega + \frac{\sin^2 \omega}{r} \right)^{-\frac{3}{2}} + (1 - f) \qquad 14$$

where f is the volume fraction of textured grains (f=1), r is the orientation parameter, and ω is the specimen tilt angle or the angle between the texture axis and x-ray scattering vector.[11, 29, 83]The orientation parameter is obtained from the curve fit and is used to assess the alignment of the samples. It is important to note, that a lower orientation parameter corresponds to a higher alignment (r = 0; prefect alignment, r = 1; random orientation).[11, 29, 83]

2.4.1   Uniaxial Warm Pressed Samples

An average orientation parameter (r) was obtained from ten randomly selected green body samples and was used to characterize each bulk sheet. For sintered samples, an average orientation parameter (r) was obtained from 6 total scans with 3 scans from each side of the samples.

2.4.2   Direct Ink Writing Samples

An average orientation parameter (r) was obtained from a total of 6 scans (3 on each side of the samples). The orientation of the print lines relative to the X-ray beam path and rocking axis is illustrated in Figure 2.5.
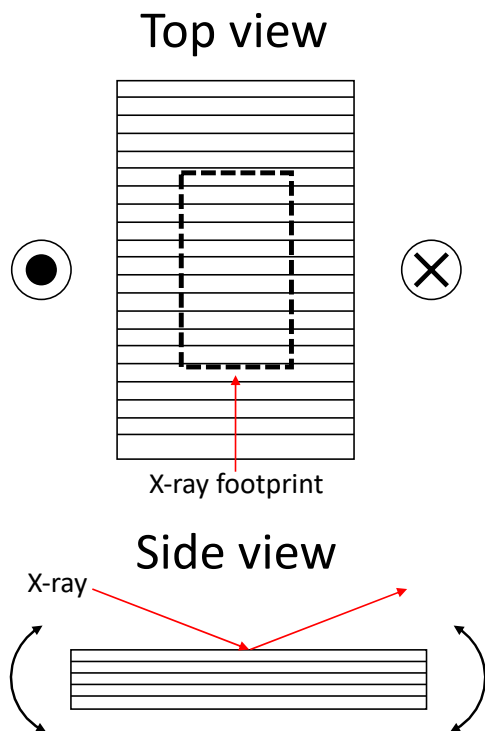
Figure 2.5. DIW sample setup for rocking curve analysis.

2.4.3   Sintered Ratio Samples

An average orientation parameter (r) was obtained from a total of 6 scans (3 on each side of the samples) similar to the sintered pre-aligned samples.

2.5   Binder Burnout

2.5.1   Ceramic-filled Thermoplastic Blends

Multiple 2.5cm diameter disks were punched from the ceramic-filled polymer sheets and individual disks were stacked on a crucible. The polymer was removed by heating at a rate of 1.5°C/hr to 500°C in flowing air, followed by an isothermal hold for 1hr. To mimic the procedure

by Schlup et al.,[58] 6g of the brown body disks were heat treated at 1100°C for 1 hour in air prior to being placed in the graphite hot-press die.

2.5.2   Aqueous-based Ceramic Suspensions

Based on the previous investigation,[65] the polymer was removed from the dried green bodies by heating up to 700°C at a rate of 1°C/min, holding for 1hr, then cooling to room temperature at 10°C/min. An atmosphere of flowing air was used.

2.6   Hot Pressing

The furnace used for hot-pressing was a Testorr series Centorr graphite furnace, mounted into a Model 312.21 MTS load frame. The furnace was controlled by a C-type thermocouple positioned near the edge of the graphite die for temperatures up to 1500°C, and a pyrometer aimed at the edge of the graphite die for temperatures above 1500°C. For all hot-pressed samples, the furnace was heated and cooled at a rate of 25°C/min. The assembled graphite dies were placed in the furnace and a vacuum was pulled for approximately 12hrs to achieve a 40 to 50 millitorr vacuum, then backfilled with gettered nitrogen at a desired temperature, which flowed for the remainder of the hot-press run.

2.6.1   Warm Pressed Ceramic-filled Polymer Sheets

A graphite die with an inner diameter of 25.4mm was used to hot-press pre-aligned samples. Molybdenum foil sheets (0.14 mm thick) were placed in between the alumina sample and the graphite spacers. A layer of graphoil (~0.26 mm thick) coated with a layer of boron nitride spray was placed between the molybdenum sheets and the graphite spacers. This assembly should prevent the alumina samples from bonding to the graphite spacers, and reduced carbon contamination from the graphite die.

Pre-aligned samples developed from ceramic-filled polymer blends were hot-pressed with a pre-load pressure of 0MPa, a maximum temperature of 1800°C, an isothermal hold time of 7hrs, and a maximum pressure of 10MPa. The maximum pressure was applied at a constant rate of 1.3MPa/min. A vacuum atmosphere was maintained from room temperature to 1550°C, then backfilled with flowing nitrogen for the remainder of the hot-press run. This process was

developed by Schlup et al.[58] and the reason for choosing the specific parameters can be found in the cited article. In addition to the pre-aligned samples, loose RonaFlair powder was poured into a graphite die and hot-pressed under the same parameters described above for comparison.

2.6.2 Additive Manufactured Samples

Hot-pressing was used to densify the samples produced through direct ink writing. A 30x45mm rectangular graphite die was assembled such that two layers of graphoil (each layer being 0.26mm thick), boron nitride spray, and a molybdenum sheet (0.14mm thick) separated the samples from the graphite spacers (similar to the previously mentioned set-up). Samples produced by additive manufacturing were hot-pressed with a pre-load pressure of ~0.7MPa that was applied at room temperature and maintained until 1400°C, a maximum temperature of 1825°C, an isothermal hold time of 5hrs, and a maximum pressure of 40MPa. At 1400°C, the max pressure 40MPa was applied at a rate of 1.33MPa/min while the furnace continued to heat. The pressure was reduced to ~0.7MPa prior to cooling. A vacuum atmosphere was maintained from room temperature to 1550°C, then backfilled with flowing nitrogen for the remainder of the hot-press run.

2.6.3 Non-pre-aligned Equiaxed and Platelet Powder Samples

The same 25.4mm diameter graphite die and set up mentioned in Section 2.6.1 was used to hot-press the non-pre-aligned equiaxed and platelet powders. For each equiaxed and platelet batch, 6.0 grams of sieved powder were poured into the graphite die, and uniaxially cold-pressed at approximately 7MPa to initially consolidate the powder. Test samples were hot-pressed with a pre-load pressure of 0MPa, a maximum temperature of 1800°C, an isothermal hold time of 5hrs, and a maximum pressure of 80MPa to characterize the densification behavior. Based on this behavior and other investigations conducted by Schlup et al., final samples were hot-pressed with a pre-load pressure of 0MPa, a maximum temperature of 1800°C, an isothermal hold time of 7hrs, and a maximum pressure of 20MPa. For both hot-pressing procedures, the maximum pressure was applied at a constant rate of 1.3MPa/min. A vacuum atmosphere was maintained from room temperature to 1550°C, then backfilled with flowing nitrogen for the remainder of the hot-press run. For this study, the max pressure was held during cooling until a temperature of 1100°C was

reached. At this temperature, the load was removed, and the sample was cooled to room temperature.

2.7   Sample Preparation

For UV-vis spectroscopy all samples were machine ground using a Supertec STP-1022ADCII surface grinder with a 100-grit metal-bonded diamond wheel attachment. For each pass, 0.015mm of material was removed. Even amounts of material were removed from the top and bottom surfaces of the samples leading to a final thickness 1.5mm. Both surfaces of the samples were polished using a Leco GPX 200 auto grinder, starting from 77µm and ending with 1µm diamond suspension. Long polishing times, sometimes 6hrs per step, were required to achieve a defect free surface. The polished samples resulted in final thicknesses ranging from 1.15 to 1.40mm. More details of the process can be found in another dissertation by Andrew Schlup.

2.8   UV-vis Spectroscopy

In-line transmission measurements were performed using a PerkinElmer Lambda 950 UV-VIS-NIR spectrophotometer equipped with an integrating sphere. Light was measured from 200 to 800 nm. For the optical loss analysis, a wavelength of 645nm was chosen to compare the specific optical properties (total transmission, in-line transmission, reflection, absorption, forward scattering, and backward scattering) based on results from the literature.[7, 84, 85] Total transmission, in-line transmission, reflection, and absorption are measured using the spectrophotometer, and from these values the forward and backward scattering are derived. More details about the set-up, equations, and analysis, can be found in other works[58] as well as the dissertation by Andrew Schlup. For total transmission, the sample was placed directly against the edge of the integrating sphere so that all light that passes through the sample can be measured. For in-line transmission, the sample was positioned approximately 60cm away from a 1.0 cm diameter aperture in front of the detector so that light with in a 0.5° cone is measured. Reflection was measured using an arrangement similar to that of Apetz et al,[7] where the sample was placed directly against an inlet on the back-side of the integrating sphere. Absorption was measured using a configuration similar to the reflection measurement, except a diffuse reflective cover was placed behind the sample. In addition to the

fabricated samples, the optical properties of a commercially available sapphire sample were measured and used as a basis and comparison.

2.9   Microstructures

After polishing, samples were thermally etched at 1600°C for 30mins in an air environment. Follows this, the samples were sputter-coated with Au-Pd, and analyzed with a FEI Quanta650, scanning electron microscope (SEM) at 10kV. However, due to the COVID-19 pandemic the resulting microstructure will not be shown in this work but my be available in future work.

2.10 Density Measurements

Archimedes' method was used to calculate the average bulk density of the sintered samples in accordance with ASTM C693-93.[86] A true density value of 3.97 g/cm3 was used for Al_2O_3 and the density of water was selected based on temperature.

3. ALIGNING α-ALUMINA PLATELETS VIA UNIAXIAL PRESSING OF CERAMIC-FILLED POLYMER BLENDS

To take advantage of shear and elongational stresses, it is desirable to have blends that exhibit thermoplastic polymer-like properties or behave more like the base polymer (EEA). Blends made with greater than 40 vol.% platelet powders (both RonaFlair and Serath blends) produced samples with processing defects and were considered unworkable. Many of these samples would crumble during removal from the warm pressing surfaces. However, samples made with equiaxed (AA-03) powders were able to reach higher solids loading and maintain polymer-like properties, which is similar to what is observed in the literature for EEA based systems.[13, 45, 48, 50, 51, 53–55] The use of platelet morphology powders is clearly influencing the behavior of the blends. As will be shown in a later section, blends where the polymer characteristics dominate resulted in higher alignment. Therefore, it is important to quantify the rheological behavior and connect it to the processing parameters and particle alignment.

3.1 Viscosity Dependence on Temperature

The torque-temperature dependence for RonaFlair (large) and Serath (small) blends are shown in Figure 3.1 at different solids loading. These curves reveal that each blend experiences a decrease in torque as temperature increases at a constant roller speed. This behavior is common for thermoplastic polymers and can be related to the weak intermolecular forces between polymer chains.[51, 77, 87] The solid lines correspond to an exponential fit of the data with all curve fits having an R^2 value > 0.92. The measured viscosity temperature sensitivity constant (*b*) for each blend is shown in Table 3.1. These values were used to determine the extent of the polymer-like properties of each blend and to correct the torque vs roller speed data to a reference temperature of 130°C by Equation 9:
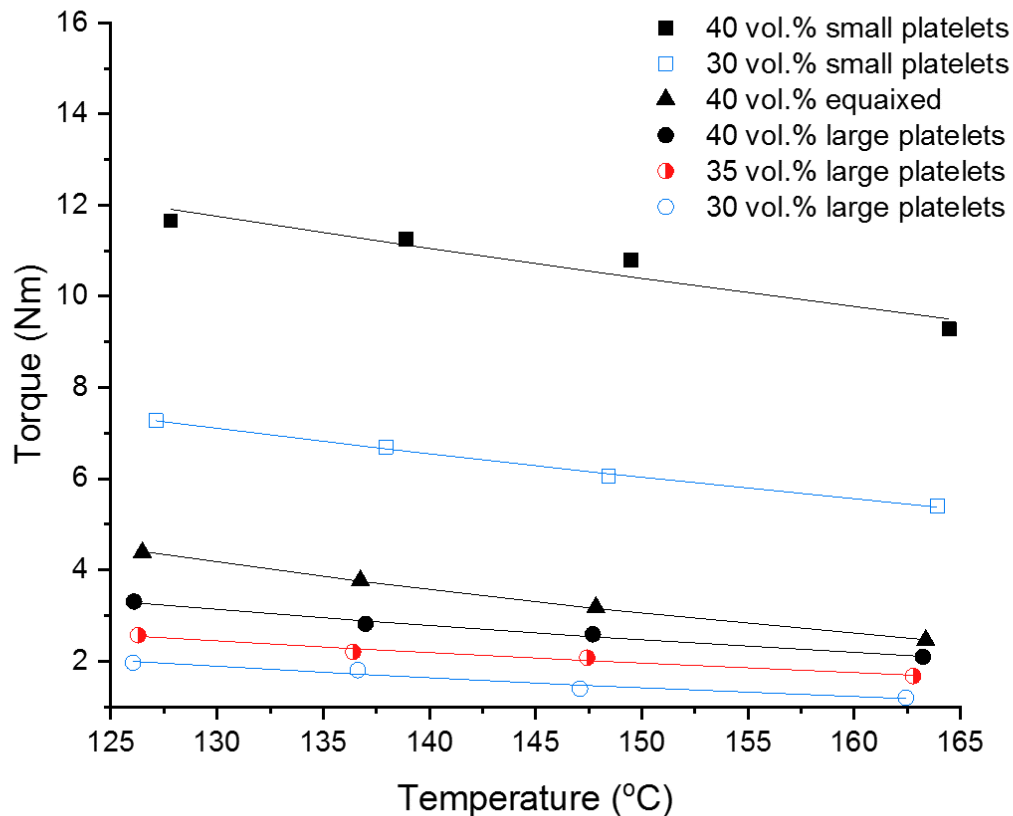
Figure 3.1. Torque vs temperature dependence of large platelets, small platelets, and equiaxed blends at different solids loading measured on a Brabender torque rheometer at a constant rotor speed of 10RPM. These curves reveal that each blend experiences a decrease in torque as temperature increases. The viscosity temperature sensitivity constant (b) for each blend is shown in Table 3.1.

Table 3.1 shows that an increase in solids loading decreases the temperature sensitivity constant for both platelet types. A higher *b* corresponds to higher viscous dissipation, which is typically explained by the thermal motion of polymer chains, chain flexibility, and the degree of chain entanglement.[80, 88] Therefore, in ceramic-filled blends with higher *b*, polymer interactions will dominate. To keep the total batch volume constant, a decrease in platelet solids loading was balanced with an increase in EEA. Adding more polymer to the system should increase the amount of polymer chain interactions, allowing polymer interactions to dominate over the mechanical interactions of the ceramic powders.[51] It is also possible that increasing powder content leads to

an increase in particle-particle and particle-polymer interactions. These interactions could lead to a decrease in polymer entanglement which will result in less viscous dissipation.

Table 3.1. Ceramic-filled thermoplastic blend compositions and measured viscosity data. The viscosity data was collected on a torque rheometer where b is the viscosity temperature sensitivity constant, n is the power law index and m is the flow consistency index.

Powder Type	Al_2O_3 [vol%]	EEA [vol.%]	PiBMA [vol.%]	HMO [vol.%]	PEG [vol.%]	b[$°C^{-1}$]	R^2	n	log(m)	R^2
RonaFlair-11µm (large)	40	44.9	4.6	0.5	10	0.012	.991	0.38	3.981	.995
	35	49.9	4.6	0.5	10	0.012	.976	0.46	3.806	.996
	30	54.9	4.6	0.5	10	0.015	.963	0.56	3.539	.997
Serath-1.2µm (small)	40	44.9	4.6	0.5	10	0.006	.921	0.14	4.745	.999
	30	54.9	4.6	0.5	10	0.008	.998	0.38	4.357	.980
AA-03 0.44µm (equiaxed)	40	44.9	4.6	0.5	10	0.016	.999	0.65	3.867	.997

In Table 3.1, blends made with large platelets have a higher *b* than blends made with small platelets, regardless of solids loading. As stated above, polymer interactions will be more dominant in ceramic-filled blends with higher *b*. Blends made with large platelets have fewer individual particles than blends made with small platelets (at a constant vol.%) due to the difference in particle size. Fewer particles could lead to the polymer interactions dominating over the particle-particle interactions in large platelet blends. Likewise, an increase in the total amount of particles in small platelet blends leads to more particle-polymer interactions and decreases chain entanglement.[51, 88] These mechanisms may explain why *b* and the viscous dissipation are greater for large platelet blends, and smaller for small platelet blends. However, this behavior is not observed in the equiaxed blend, which has the highest *b* (0.016°C^{-1}) of all blends and lowest particle size (0.44µm). This behavior must be a characteristic feature of platelet morphology powders. As stated earlier, it is desirable to have blends where the polymer interactions dominate. Therefore, blends with the highest *b* (large platelet) were considered ideal for forming processes to achieve particle alignment.

Figure 3.1 shows that an increase in the solids loading led to an increase in the measured torque for the different platelet blends. This trend is commonly observed in similar ceramic-filled polymer blends developed for co-extrusion[48, 51, 76] and green machining processes.[45] A study focusing on the rheological behavior of BaTiO$_3$/EEA blends found that an increase in solids

loading increased the torque and viscosity values at a constant temperature.[51] They claimed this behavior was due to an increase in the mechanical inter-particle interactions between the ceramic powders. In the literature, it is typical to have solids loadings greater than 50 vol.% in EEA based blends and still have workable samples,[13, 45, 48, 50, 51, 53–55] which is not the case for the blends produced in the current study. Blends produced with greater than 40 vol.% platelets had measured torque values lower than or equal to observed torque values for 55 vol.% equiaxed powder blends from the literature,[51] and were considered unworkable. Clearly, the use of platelets versus equiaxed powders is influencing the behavior of the blends.

3.2   Rheological Measurements

Figure 3.2 shows the log(viscosity) dependence on log(shear rate) at 130°C for large and small platelet blends at different solids loading. A 40 vol.% equiaxed blend is added for comparison. The solid lines correspond to linear curve fits with all $R^2 > 0.98$. The powder law index (or shear thinning exponent, n) and melt consistency index (m) were calculated from the fits and are shown in Table 3.1. All ceramic-filled polymer blends exhibited a pseudo plastic or shear thinning behavior with $n < 1$. It is important to note that the shear thinning exponent obtained by a torque rheometer has been found to not be in agreement with data obtained on a parallel plate rheometer, as described by Xu et al.[51] They claimed that this deviation from the expected behavior is probably due to the blends having yield stresses, as well as the relationship between log(torque)–log(shear rate) being non-linear at lower shear rates.[51] However, they did find that the melt consistency indexes and the overall trends obtained by a torque rheometer and parallel plate rheometer were in agreement.
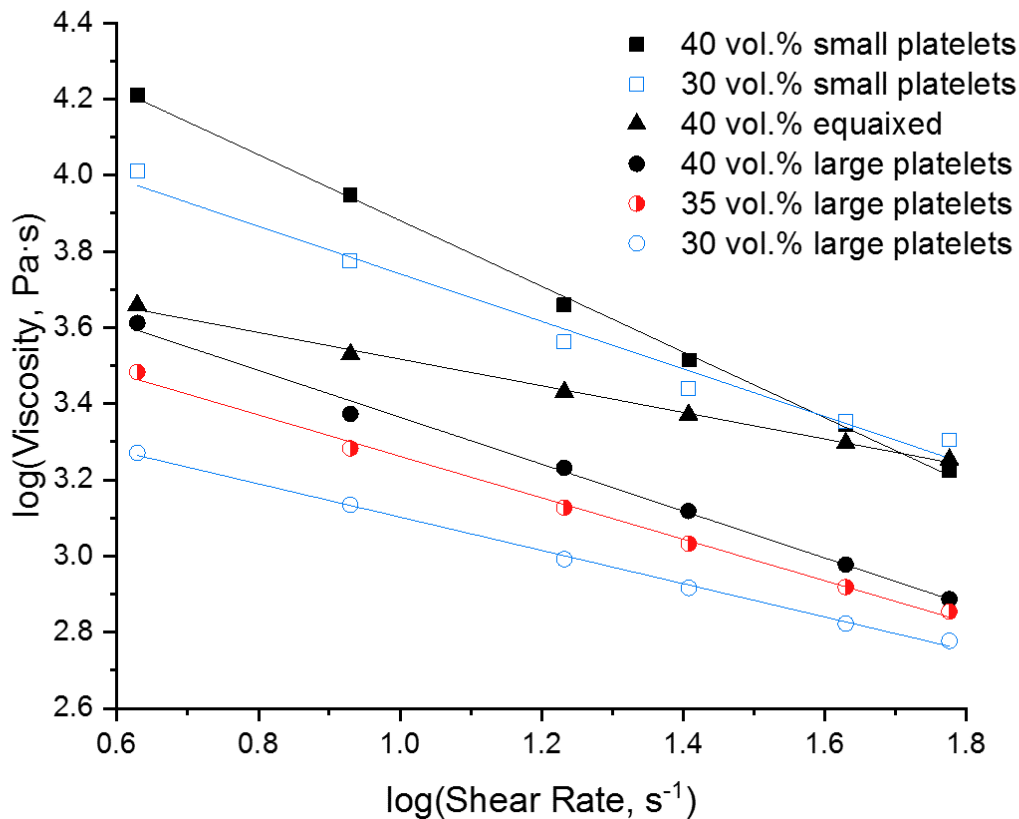
Figure 3.2. Log (viscosity) - log (shear rate) dependence of large platelets, small platelets, and equiaxed blends at different solids loading measured on a Brabender torque rheometer at 130°C. Increasing the solid loading resulted in an increase in viscosity for respective platelet type. All polymer blends exhibited a uniform shear thinning behavior with n < 1.

From Figure 3.2 it was found that an increase in solids loading led to an increase in the viscosity for a given shear rate, regardless of powder type. This behavior is commonly observed in the literature for ceramic-filled polymer blends and could be attributed to the increased polymer-particle interactions, interparticle interactions and collisions.[51] It was also found that an increase in solids loading led to a decrease in the shear thinning exponent (n) and an increase in the flow consistency index (m) for both platelet powders, as shown in Table 3.1. Both trends are observed in the literature for blends that were developed for co-extrusion.[48, 51, 76]

Blends made from large platelets exhibited lower viscosity values than blends made with small powders, regardless of solids loading and shear rate. Recall in Section 3.1, blends made with

large platelets will have fewer individual particles due to the difference in particle size. Fewer particles could lead to fewer particle-particle interactions. Additionally, it is known that geometrical characteristics of ceramic powders have a significant effect on particle packing density, particle arrangement, and rheological properties.[17] Anisometric particles with the ability to freely rotate will readily orient due to imparted shear stresses.[35, 37] Since the large platelet blends experience less particle-particle interactions, the platelets should be able to rotate more freely and eventually orient parallel to the direction of shear. Xu et al.[51] claimed that particle orientation can result in laminar flow and lead to a reduction in the resistance to shear. It is possible that the large platelet blends have lower viscosities because there are fewer particles and the morphology of the particles are more susceptible to orientation.

Figure 3.2 shows the 40 vol.% equiaxed blend has a higher viscosity than the large platelet blends and a lower viscosity than the small platelet blends. According to previous logic on particle size and particles per volume the equiaxed powder should have a higher viscosity than both platelet blends, which is not the case. This is most likely due to the difference in particle morphology, specifically, the surface area. Recall in Section 2.1.1, the surface area of the equiaxed powders being higher than the large platelets and lower than the small platelets. These differences in surface area could explain the viscosity behavior. It is well understood in the field of colloidal processing that increasing the specific surface area, leads to increases in the number of particle-particle interactions and thus increases the viscosity.[89, 90] Additionally, the flow behavior of the equiaxed blends is different than the platelet blends. The 40 vol.% equiaxed blend had the highest shear-thinning exponent (n=0.65) and the lowest flow consistency index (log (m) = 3.867) of all blends, as shown in Table 3.1. It is well understood that anisotropic powders will be susceptible to shear stresses and align, decreasing the resistance to shear, resulting in significantly more shear thinning when compared to spherical powders.[51, 89] Even though the equiaxed blend has a higher viscosity than all the large platelet blends and experiences less shear thinning than all blends, it was the most workable blend. An image of the blend after mixing is shown in Figure 3.3a.
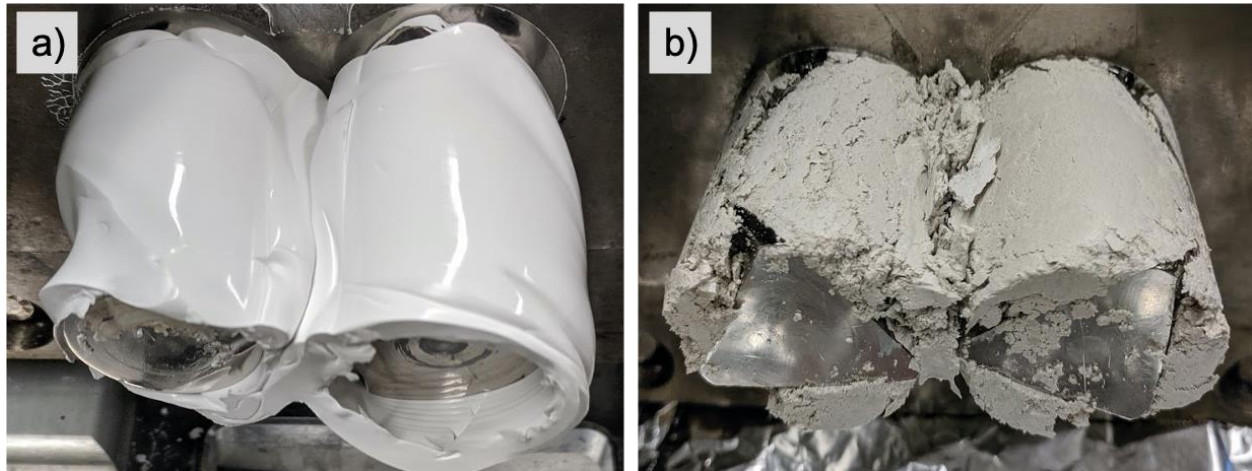
Figure 3.3. a) image of the 40vol.% equiaxed blend after mixing, b) image of the 40 vol.% small platelet blend after the rheological test.

This behavior could be due to the equiaxed blend experiencing more viscous dissipation and dominating polymer interactions. It may be possible to use mixtures of equiaxed and platelet powders to develop blends with more optimized rheological properties or behaviors similar to the base polymer (EEA) in future studies.

As stated above, blends made with platelet solids loading greater than 40 vol.% were considered unworkable. They also may have experienced issues with polymer degradation. This behavior was most apparent in blends produced with 40 vol.% small platelets. At higher shear rates, the viscosity values are lower for the 40 vol.% small platelet blends than the 30 vol.% small platelet and 40 vol.% equiaxed blends. This behavior was not expected. During the analysis, the roller speed, which is proportional to the shear rate, is slowly increased from low to high RPM over the course of 180mins. Visual inspection showed that the behavior of the 40 vol.% small platelet blend changed from the beginning of the analysis to the end. After the rheological test, this blend had a chalk-like appearance and behaved more as a dry powder blend (crumbled apart) than a polymer blend. An image of the blend after the test is shown in Figure 3.3b. From The shear thinning exponent (n = 0.14) was the lowest in this study and lower than blends produced in the literature,[48, 51, 76] indicating that this blend is more prone to degradation than the other blends in this study.

3.3 Texture Analysis of Pressed Sheets

The orientation parameter (r) and grain misalignment angle (full width at half maximum (FWHM)) were obtained from a rocking curve analysis and these values are listed in Table 3.2. A lower orientation parameter (r) and lower FWHM are associated with higher alignment. For this analysis, the alignment reference plane was normal to the pressing direction. Ten samples were analyzed from each pressed sheet to obtain an average r and FWHM. Each blend (solids loading and platelet type) was pressed to a target thickness of roughly 1.4, 0.9, and 0.4mm (accounting for the PTFE coating) to obtain a percent reduction of 92.2, 95.0, and 97.8%, respectively. The final pressed sample thickness was measured and is reported in Table 3.2 as percent reduction.

Table 3.2. Texture distribution data for ceramic-filled thermoplastic blends uniaxially pressed to varied thicknesses. Orientation parameter (r) obtained from curve fits of the March-Dollase equation. The 95% confidence interval of the reduction, FWHM and orientation parameter are shown for each sample having a data population of 10.

Powder Type	Shim (mm)	vol.%	Reduction			FWHM (°)			r			R^2
RonaFlair-11µm (large)	1.4	40	92.40	±	0.05	28.28	±	1.20	0.401	±	0.013	>.99
		35	92.62	±	0.03	19.53	±	1.01	0.360	±	0.012	>.99
		30	92.77	±	0.04	14.32	±	0.52	0.295	±	0.007	>.99
	0.9	40	94.16	±	0.08	21.59	±	1.40	0.383	±	0.015	>.98
		35	95.09	±	0.04	19.80	±	0.94	0.363	±	0.011	>.99
		30	95.25	±	0.03	15.34	±	0.48	0.309	±	0.006	>.99
	0.4	40	94.79	±	0.13	21.80	±	1.43	0.384	±	0.015	>.99
		35	95.41	±	0.52	19.26	±	1.43	0.356	±	0.018	>.98
		30	97.01	±	0.10	11.16	±	1.16	0.251	±	0.017	>.99
Serath-1.2µm (small)	1.4	40	91.30	±	0.08	25.39	±	0.89	0.420	±	0.009	>.98
		30	92.47	±	0.03	20.24	±	1.06	0.368	±	0.012	>.98
	0.4	40	91.72	±	0.32	25.99	±	1.35	0.429	±	0.013	>.98
		30	95.09	±	0.28	20.99	±	0.98	0.379	±	0.006	>.98
AA-03, 0.44µm (equiaxed)	0.4	40	97.04	±	0.20	--	±	--	--	±	--	--

Figure 3.4 shows the average orientation parameter vs. percent reduction for large platelet blends made with different solids loading. For all large platelet solids loadings (30, 35, 40vol.%),

each blend was able to reach the target reduction of 92.2% (within ~ 0.5%); however, this is not true for other target reductions. An example of this is shown in Table 3.2 where both the 40 and 35 vol.% blends were not able to reach a target reduction of 97.8%. Instead, these samples reached a final reduction of 94.8 and 95.4%, respectively. For these samples, the metal plates did not fully seat on the shims under the applied load (4,000kg). It was evident that these blends required a higher load to reach larger reductions. However, preliminary tests showed that forcing the sample to flow at higher loads may be negatively impacting the alignment, which could be due to particle jamming.[91] Additionally, blends with 30 vol.% large platelets were able to reach all the target percent reductions under the applied load. It seems that the ability of each blend to reach the target percent reduction is connected to the extent of the polymer behavior (temperature sensitivity constant (b)) and flow properties (shear thinning exponent (n) and flow consistency index (m)), which is related to the solids loading (i.e. polymer content) and leads to differences in the final alignment. To support this claim, the 40 vol.% equiaxed blend was pressed to a target reduction of 97.7% and was able to reach an average reduction of 97.04% (reported in Table 3.2). This value is similar to the percent reduction obtained from the 30 vol.% large platelet blend when pressed to the same target percent reduction. Both of these blends had higher temperature sensitivity constants and shear thinning exponents.
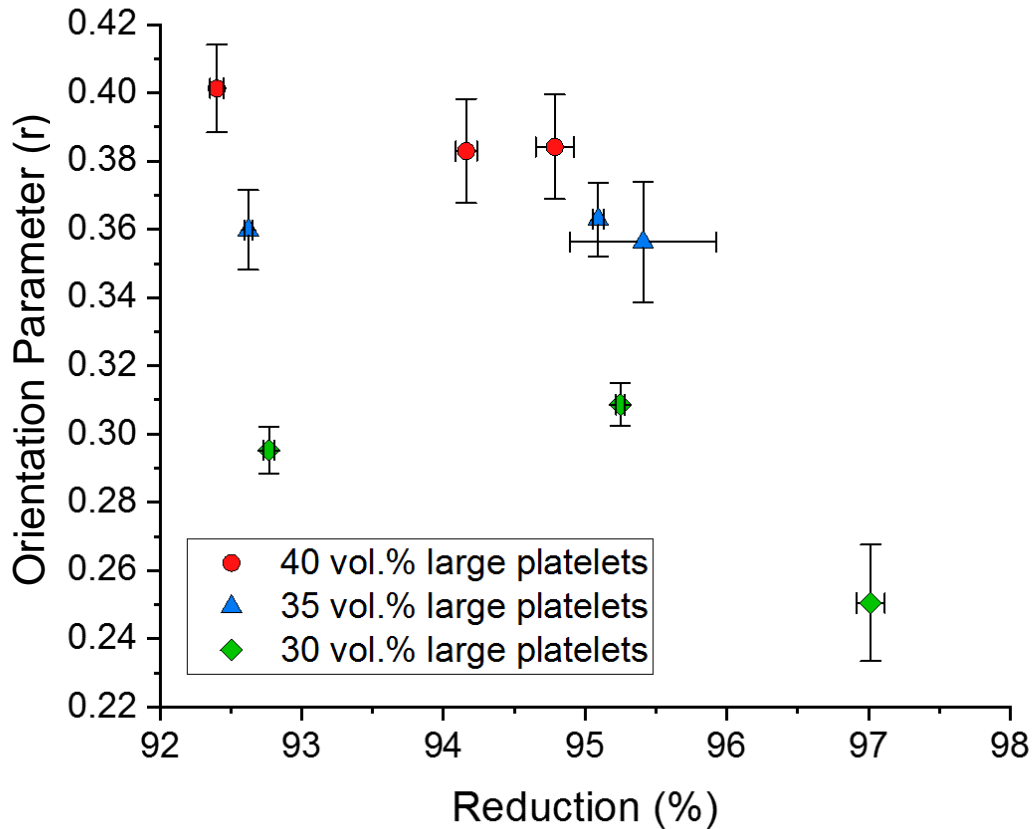
Figure 3.4. Orientation parameter (r) vs. percent reduction dependence of large platelet and small blends at different solids loading. The 95% confidence interval for both the orientation parameter and percent reduction are shown for each sample having a data population of 10.

It was found that decreasing the solids loading resulted in sheets that were able to undergo more reduction and obtain lower orientation parameters. As mentioned above, decreasing the ceramic solids loading led to an increase in the temperature sensitivity constant (*b*) and increased the flow properties (higher shear thinning exponents (n) and lower flow consistency indexes (m)), which resulted in pressed sheets with higher percent reductions. Decreasing the ceramics solids loading may have allowed the polymer interactions to dominate, resulting in blends that reach higher reductions and undergo more bi-axial extensional flow during warm pressing. It is expected that this increased amount of flow allows for higher velocity gradients that will induce platelet alignment.[35, 37] It is also possible that decreasing solids loading decreases particle-particle

interactions,[51] allowing the platelets to rotate more freely and align parallel to the direction of flow.[35, 37]

Also, observed in Figure 3.4 is that the pressed sheets tend to reach a characteristic minimum orientation parameter for different solids loadings. Further increases in the reduction do not result in further alignment, which is apparent in the 40 and 35 vol.% large platelet blends. Sheets produced with 40 and 35 vol.% solids loading had a characteristic minimum orientation parameter of roughly 0.39 and 0.36, respectively. It seems that this minimum alignment was obtained at a target reduction of 92.2%, and further alignment was not obtained with an increase in percent reduction. However, sheets produced with 30 vol.% solids loading did experience further alignment after pressing to target percent reductions higher than 95.0%. It appears that the 30 vol.% blend experiences a characteristic minimum orientation parameter at higher percent reductions, (> 97%). As suggested above, decreasing the solids loading will lead to a decrease in the particle-particle interactions, allowing the platelets to rotate and further align. This could explain why the lower solids loading blends are able to reach a higher alignment.

Figure 3.5 shows the average orientation parameter vs. percent reduction for sheets developed from small and large platelet blends. From the plot, it is clear that blends developed with small platelets experience far less alignment when compared to the large platelet blends with the same solids loading. For small platelet blends, the same trends with solids loading, temperature sensitivity constant, flow properties, and target percent reduction that were observed in large platelet blends are present. However, blends produced with small platelets experience inferior rheological properties when compared to large platelet blends. All small platelet blends had lower temperature sensitivity constants and poorer flow properties when compared to large platelet blends. Due to the poor rheological properties, small platelet blends were not able to reach the target percent reductions, which leads to less bi-axial extensional flow during warm pressing. As discussed earlier, the small platelet blends will have more individual particles per volume leading to an increase in particle-particle interactions, which results in inferior rheological properties and less final alignment.
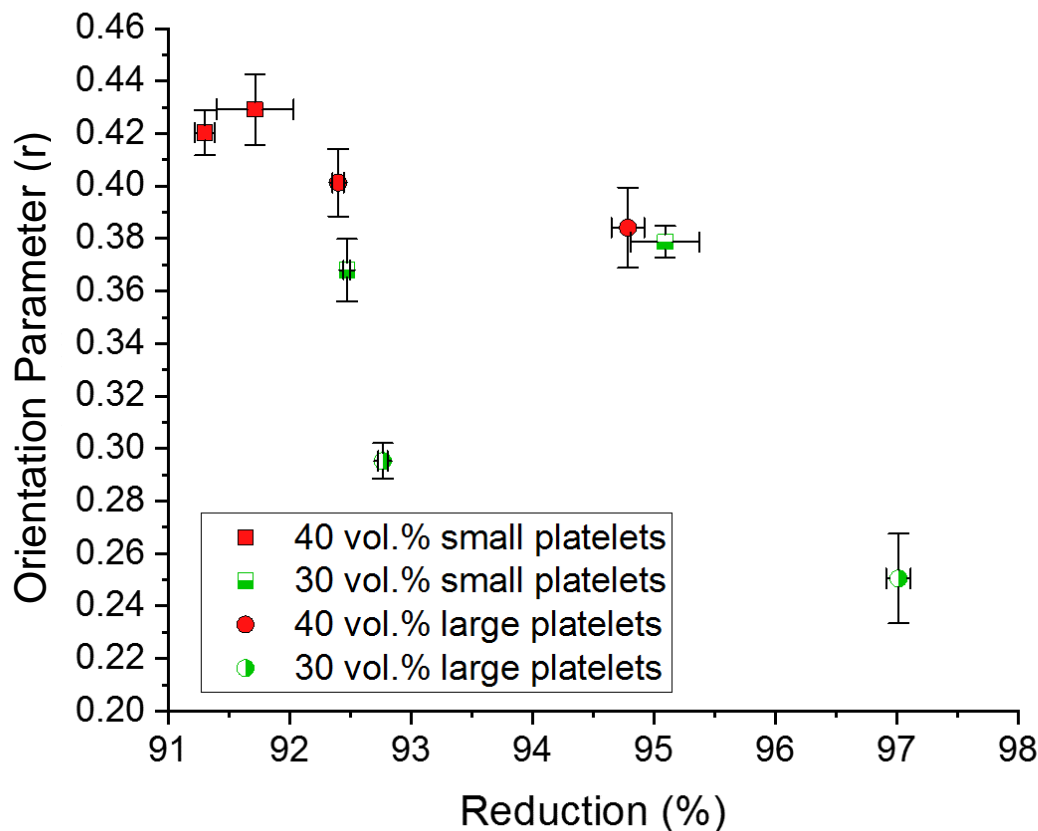
Figure 3.5. Orientation parameter (r) vs. warm pressing thickness dependence of large platelet and small blends at different solids loading. The standard error of both the orientation parameter and thickness are shown for each sample having a data population of 10.

It was determined that the 30 vol.% large platelet blends produced the highest average alignment. This blend was able to reach a higher percent reduction due to the rheological properties and experienced more bi-axial elongational flow. Pressing this blend to a target percent reduction of 97.8% had a final alignment of r = 0.251 ± 0.017, with FWHM = 11.16° ± 1.16° compared to sheets with the lowest alignment: r = 0.429 ± 0.013, with FWHM = 25.99° ± 1.35° being produced with 40 vol.% small platelet blends at a target percent reduction of 97.8%. It is possible to develop blends with a lower solids loading (< 30 vol.%) which may be able to achieve higher alignment. However, blends with lower solids loading were not investigated in this study because the resulting brown body densities would lead to samples that are too fragile for handling during hot-press die preparation. Also, it is important to note that the addition of more polymer necessitates slower

binder burnout rates and longer processing times, therefore, the 30 vol.% large platelet blend pressed to a target percent reduction of 97.8% was chosen to produce a final pre-aligned hot-pressed sample.

3.4   Analysis of Hot-Pressed Samples

In the previous study by Schlup et al.[58] the hot-pressing parameters were developed for 100% platelet powder compacts. This analysis also found that a considerable amount of alignment was obtained from the hot-pressing of non-pre-aligned powders through a qualitative XRD alignment analysis. The X-ray diffraction spectra of the surface normal to the hot-pressing direction for non-pre-aligned platelet alumina, and an equiaxed alumina sample from this study are shown in Figure 3.6. A commercially available single crystal sapphire sample is added for comparison. This data shows that the (006) and (00$\underline{12}$) peaks are significantly more intense for the hot-pressed platelet alumina samples than the equiaxed alumina samples. These peaks correspond to the basal plane of the alumina or normal surface of the physical platelets. Another interesting trend is that all the other peaks that are observed in the equiaxed powders are either absent or have significantly low intensities. Since there is little to no intensity for other peaks this means that the other crystallographic directions are not aligned in this direction which is similar to the observed behavior for the single crystal sapphire. Similar trends were observed by Yi et al.[6] in transparent alumina that was produced in a high magnetic field. The behavior found by Schlup et al. was the basis for the current study since it showed that the hot-pressing of platelet alumina could lead to transparent alumina with improved crystallographic alignment and transparency. Based on this previous study[58] and the literature on the alignment of alumina[1, 5–7] uniaxial warm pressing was selected as a possible pre-alignment process to be used with hot-pressing. It was expected that this process would lead to an improvement in the final sintered crystallographic alignment of transparent alumina. The following section will discuss quantify this alignment and the connection between this texture and the final optical properties.
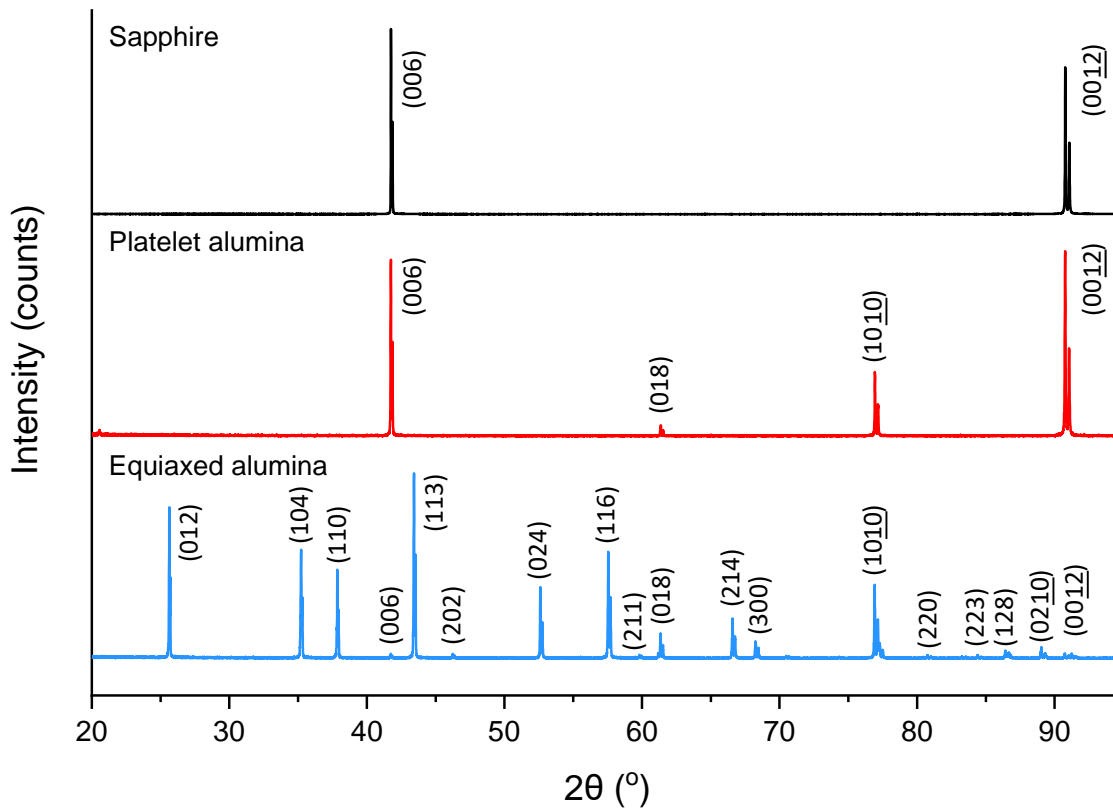
Figure 3.6. X-ray diffraction spectra of single crystal sapphire, hot-pressed non-pre-aligned platelet alumina, and hot-pressed equiaxed alumina.

The rocking curves of pre-aligned and non-pre-aligned hot-pressed samples are shown in Figure 3.7. From the data, it can be seen that the pre-aligned sample has a higher peak intensity than the non-pre-aligned sample, therefore having higher alignment. The pre-aligned sample had an average alignment of $r = 0.254 \pm 0.011$ and a FWHM $= 11.38° \pm 0.75°$, while the non-pre-aligned sample had an average alignment of $r = 0.283 \pm 0.007$ and a FWHM $= 13.40° \pm 0.53°$. It seems that pre-aligning platelets with uniaxial warm pressing is improving the final alignment of the sintered samples. It is expected that this 14.5% decrease in the grain misalignment angle (FWHM) over non-pre-aligned samples will lead to an improvement in the transparency.[7] In a previous investigation, it was found that the hot-pressing procedure is affecting the alignment of the samples.[58] However, there is no significant change to the alignment when comparing the green body sheet to the pre-aligned hot-press sample.

59
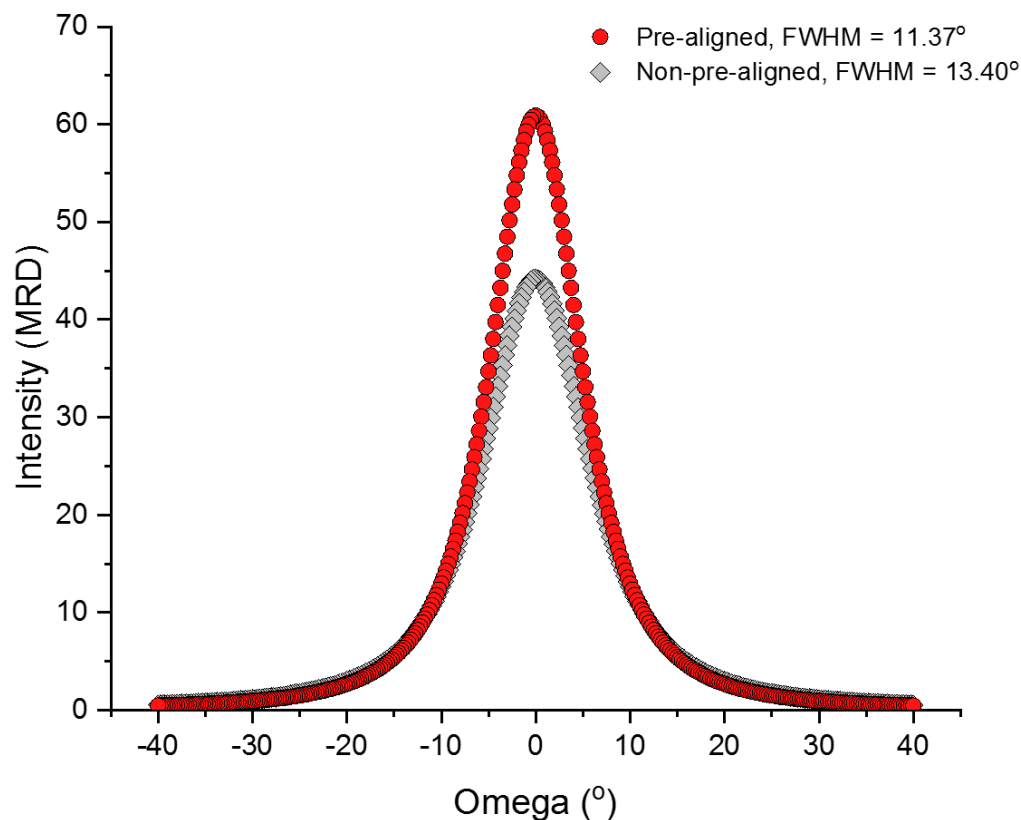
Figure 3.7. XRD rocking curves of hot pressed non-pre-aligned and pre-aligned large platelet powders (30 vol.% large platelets blends). Pre-alignment through uniaxial warm pressing is increasing the final alignment of the transparent sample. Curves are March-Dollase fits of the data.

Figure 3.8 shows the in-line transmission as a function of wavelength for the hot-pressed samples, as well as a single crystal sapphire standard. The pre-aligned sample has a higher in-line transmission compared to non-pre-aligned sample. This indicates that pre-aligning the platelets with the uniaxial warm pressing procedure is improving the optical properties. To the knowledge of the author, this is the 2nd highest in-line transmission reported for transparent polycrystalline alumina in the literature.[5–7, 84, 85]
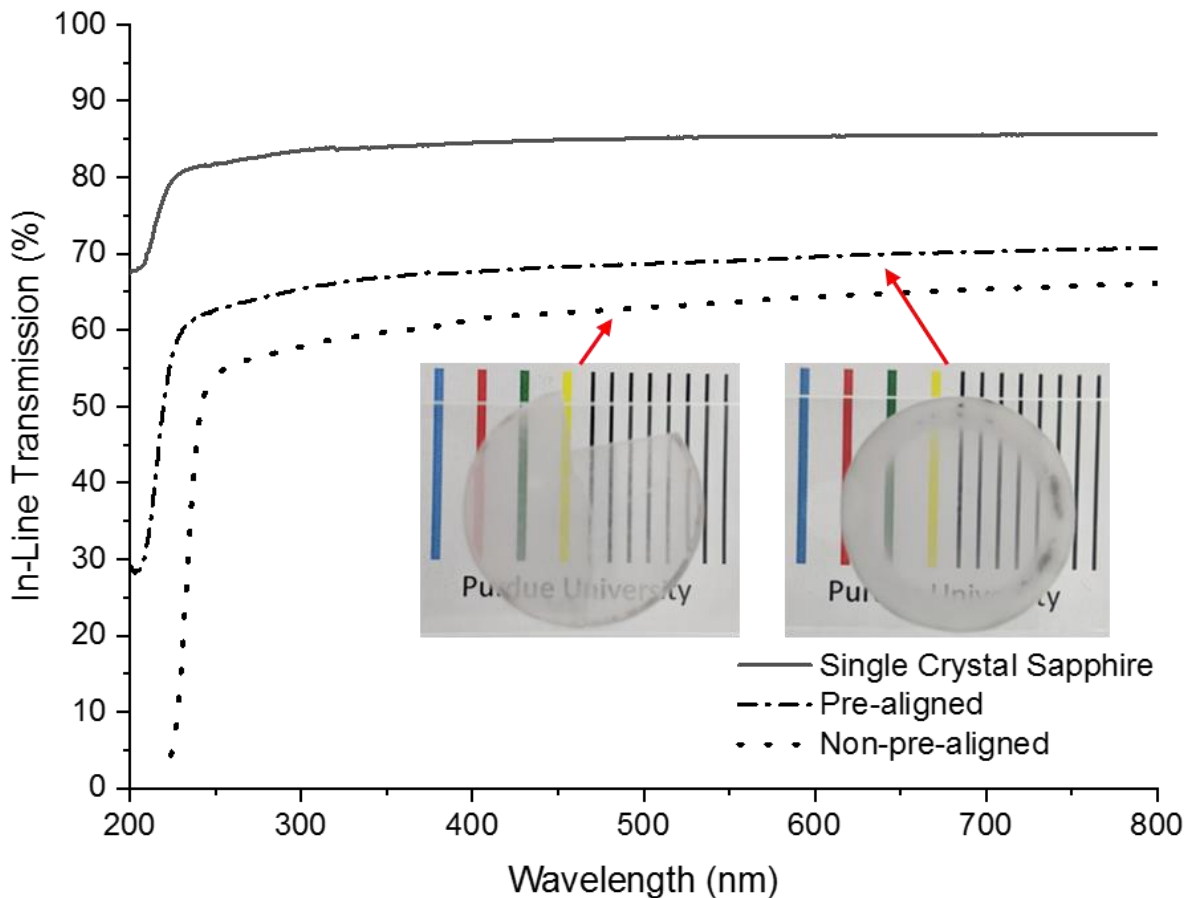
Figure 3.8. UV-vis analysis of dense non-pre-aligned, pre-aligned, and single crystal sapphire. a) In-line transmission as a function of wavelength, normalized to t = 0.8mm and b) light transmission at 645nm for each sample. Samples are placed 2cm above the text. Pre-alignment of the platelet alumina leads to an increase in the in-line transmission when compared to non-pre-aligned alumina.

Figure 3.9 shows the light transmission at 645nm for the different optical loss mechanisms. The pre-aligned sample has less forward scattering losses than the non-pre-aligned sample, which indicates lower birefringent scattering due to crystallographic alignment.[7] Both hot-pressed samples have approximately 4% absorption losses, which is indicative of trapped secondary phases. [7] As explained in previous work,[58] this absorption was minimized by performing a heat treatment at 1100°C prior to hot-pressing. The non-pre-aligned sample has effectively no backward scattering losses, while the pre-aligned sample has approximately 1% backward scattering losses. According to Apetz et al.[7], backward scattering is indicative of residual porosity. In the case here it was found that the pre-aligned sample has a lower density (99.48%) than the non-pre-aligned

sample (99.89%TD), which is in agreement with the backscattering data as well as a density gradient as can be seen in the outer perimeter of the pre-aligned sample in Figure 7a. The specimens with pre-aligned platelets may have a higher packing density than those that are non-pre-aligned as the oriented platelets will have a higher packing factor.[17] This lower packing density may result in a lower effective stress during hot-pressing suggesting that pre-aligned platelets may require a higher hot-pressing pressure than non-pre-aligned platelets to ultimately eliminate residual porosity and improve the final optical properties.[92] The effect of different hot-pressing pressures on pre-aligned samples is explored in other work by Schlup et al. and will not be considered in this current work. However, the data from his study can be used to show the repeatability of the uniaxial warm pressing and hot-pressing process.
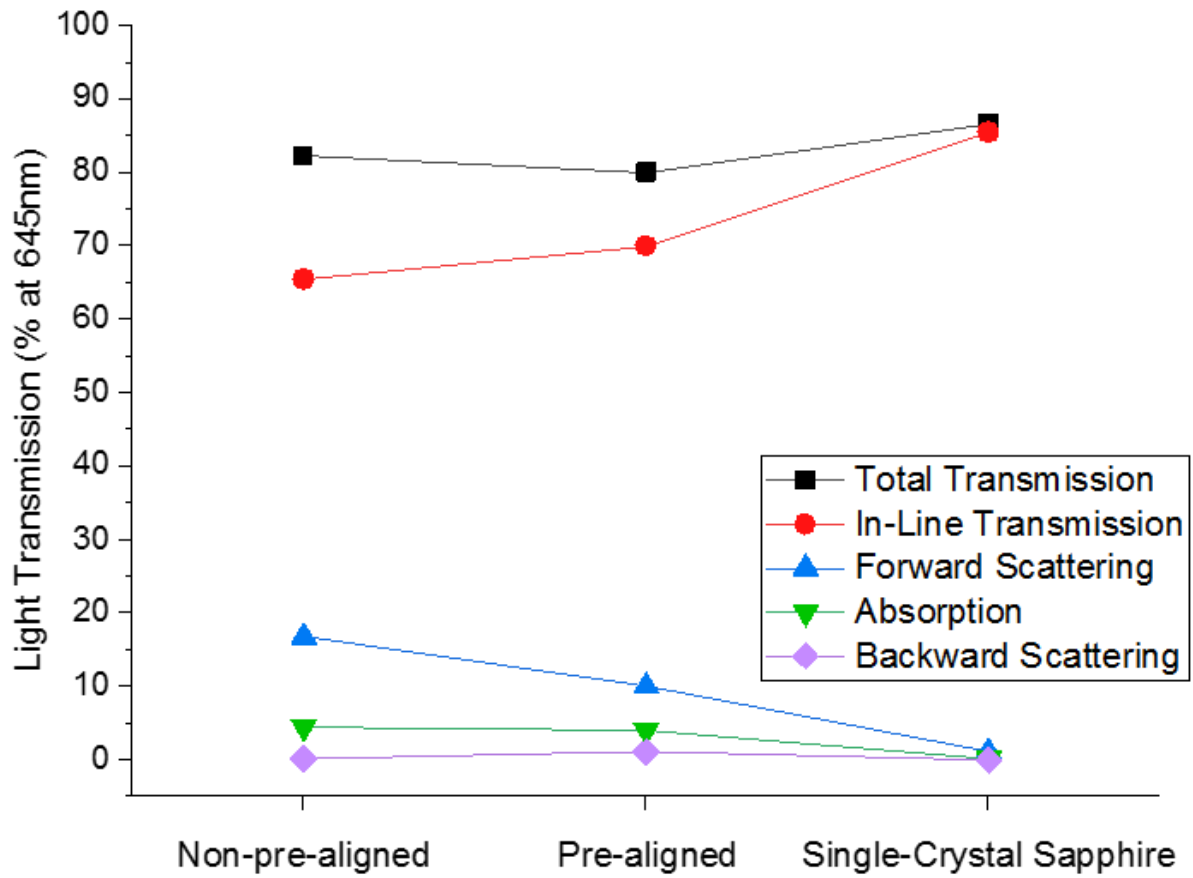
Figure 3.9. UV-vis analysis at 645nm of dense non-pre-aligned, pre-aligned, and single crystal sapphire samples normalized to thickness of 0.8mm. Samples are placed 2cm above the text.

Figure 3.10 shows the effect of maximum hot-pressing pressure ranging from 5 to 25MPa on the orientation parameter for pre-aligned and non-pre-aligned platelet alumina. This data was used by Andrew Schlup in his dissertation to investigate the effect of max pressure on the texture, optical properties, and density gradients of platelet alumina and details relating to these observations can be found there. For this study, the data can be used to show the difference in texture between pre-aligned and non-pre-aligned alumina. The previous data showed that the pre-alignment process improve the texture and optical properties of one sample. The data in Figure 3.10 shows is that the pre-alignment process when paired with hot-pressing increases the alignment of the alumina samples when compared to the non-pre-aligned sample. This means that the process is repeatable and could be a reliable and valuable alternative to magnetic alignment.
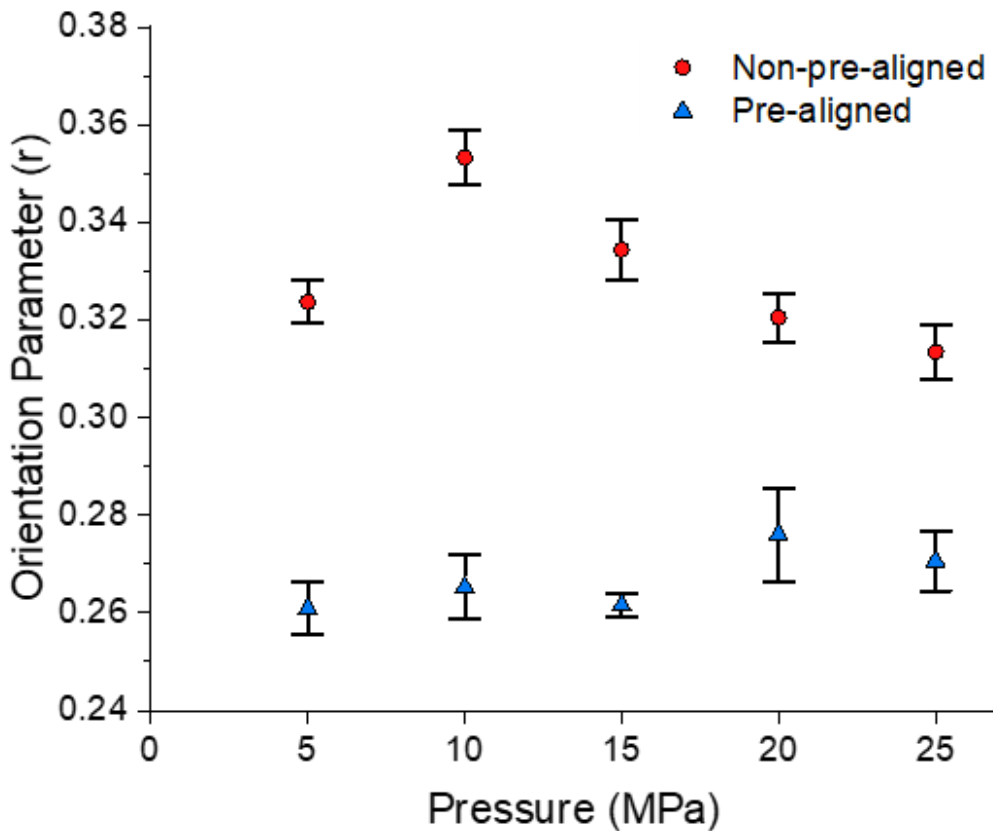
Figure 3.10.Orientation parameter (r) vs max pressure for pre-aligned and non-pre-aligned samples. The pre-aligned samples have repeatably higher alignment when compared to the non-pre-aligned samples.

3.5 Summary and Conclusions

Uniaxial warm pressing was used to align platelet alumina in polyethylene-based copolymers. The effects of alumina platelet solids loading and platelet diameter on viscosity, percent reduction, and final alignment were investigated. For both platelet types (large and small), decreases in the solids loading led to increases in the temperature sensitivity constant (*b*) and flow properties (higher shear thinning exponents (*n*) and lower flow consistency indices (*m*)). The use of small diameter platelet powders had a negative impact on the flow properties. Blends that exhibited higher temperature sensitivity constants and flow properties resulted in pressed sheets with higher percent reductions and higher final alignment. It was determined that the 30 vol.% large platelet blend was ideal for final alignment and demonstrated an average orientation value (r) and grain misalignment angle (FWHM) of 0.25 ± 0.02 and $11.16^{\circ} \pm 1.62^{\circ}$, respectively. This blend was further processed and used to produce a transparent sample that demonstrated increased optical properties when compared to non-pre-aligned samples. This sample exhibited a final orientation parameter of $r = 0.254 \pm 0.011$, a grain mis-alignment angle of $FWHM = 11.38^{\circ} \pm 0.75^{\circ}$, and an in-line transmission of 70.0% at 645nm. Additionally, further texture analysis showed that the pre-alignment process obtains repeatably higher alignment values compared to non-pre-aligned samples when conducted across multiple hot-pressed samples. Furthermore, it is expected that the addition of equiaxed powder to the platelet blends will improve the rheological properties and increase the final alignment. Section 5 will investigate the sintering behavior, alignment, and optical properties of equiaxed and platelet powder mixtures to see if powder combinations can obtain reasonable optical properties.

4. ALIGNING α-ALUMINA PLATELETS VIA DIRECT INK WRITING FOR SINTERED TRANSPARENCY

Willy's contributions to the current investigation include project design, assistance with the DIW process, development of the suspensions, rheological testing and analysis, rocking curve testing and analysis, optical data analysis, optical image analysis and writing of the manuscript.

In DIW, the rheological properties of the aqueous-based ceramic suspensions are designed to have both a static and dynamic yield stresses.[93] Once the applied extrusion shear stresses exceed the suspension yield stress, the suspension flows and parts can be constructed by stacking the extrudate in a controlled fashion, building up the part layer by layer. After exiting the nozzle and the removal of the shear stress the yield stress of the suspension quickly develops again, prohibiting the formed part from slumping due to either gravity or its own weight [63, 65, 70, 71, 94]. Therefore, it is important to design suspensions with the requisite yield stresses to be able to build infilled samples. Previous work,[65, 66] was centered on the development of suspensions with rheological properties that led to high printability and minimized processing defects for single walled or outlined shapes. Based on the optimal parameters from these investigations, the current suspensions were modified to meet new printability criteria for infilled samples so that all suspensions had high printability. As will be shown in a later section, suspensions with lower yield stresses, viscosities, and platelet loadings resulted in higher alignment for DIW samples. Even though the printability is not being investigated, it is still important to quantify the rheological behavior and connect it to both the processing parameters and particle alignment.

4.1 Rheological and Viscoelastic Characterization of Suspension

Loop flow curves demonstrating the dependence of shear stress on applied shear rate for the alumina suspensions are shown in Figure 4.1 for varied platelet loading (0-15vol.%) suspensions.
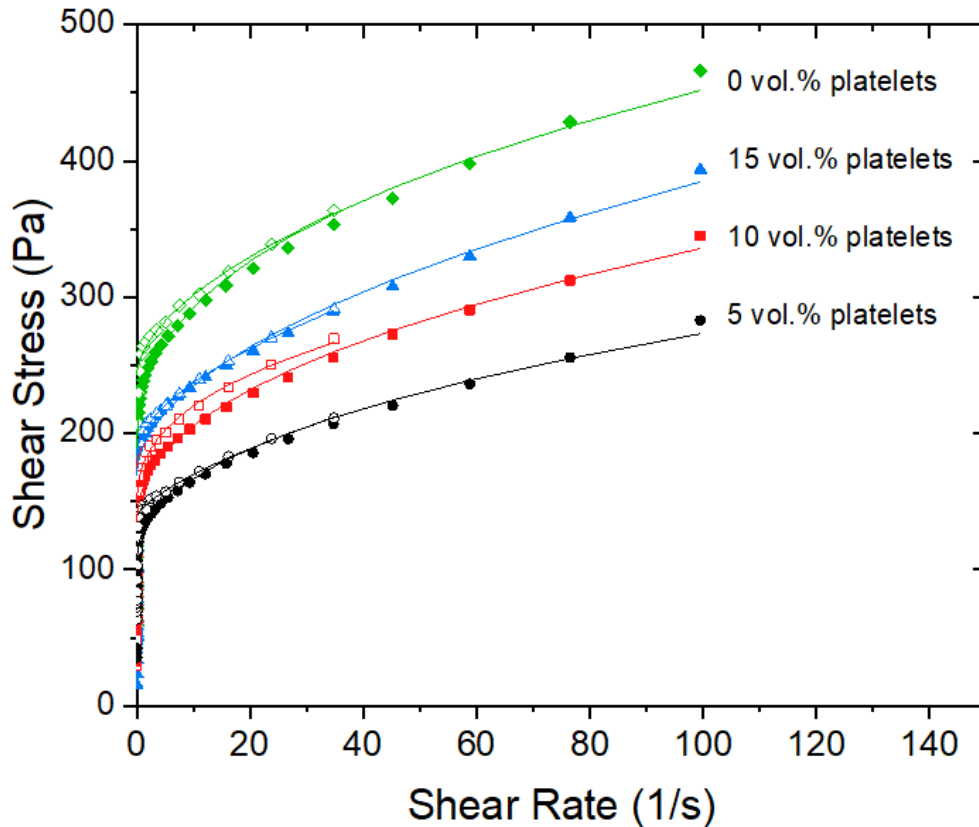
Figure 4.1. Loop flow curves of suspensions with varying platelet loadings. Infilled symbols correspond to the static response (shear rates increased logarithmically from 0.01 to 35 s^{-1}) and solid symbols correspond to the dynamic response (shear rates decreased logarithmically from 100 to 0.0035 s^{-1}). The solid lines correspond to a fit of the Herschel-Bulkley fluid model with fitting parameters ($R^2 > 0.99$) for each data set shown in The flow curves reveal that all suspensions behaved in a yield-pseudoplastic manner with the flow index (n) values being less than 1, which indicates a shear-thinning behavior.[95] It has been shown in the literature,[63, 64, 94, 96] as well as in previous work,[65, 66] that yield-pseudoplastic suspensions are ideal for continuous filament-based DIW. The solid lines correspond to a fit of the Herschel-Bulkley fluid model (Equation 13),[81] and the obtained rheological parameters are listed in Table 4.1. The 20vol.% platelet suspensions were tested but the data was unreliable due to the limitations of the machine. Simply, the measured shear stresses were too high and caused discontinuities in the data. This analysis technique replicates the shear rate and shear stress response formed in the suspension during printing. The obtained static

yield stress ($\sigma_y{}^{stat}$) relates to the suspensions ability to inhibit extrusion from the syringe before printing and the obtained dynamic yield stress ($\sigma_y{}^{dyn}$) relates to the layer shape retention and layer rigidity during stacking.[93]

Table 4.1. The 20 vol.% platelet suspensions are not are shown due to the limited capabilities of the testing machine.

The flow curves reveal that all suspensions behaved in a yield-pseudoplastic manner with the flow index (n) values being less than 1, which indicates a shear-thinning behavior.[95] It has been shown in the literature,[63, 64, 94, 96] as well as in previous work,[65, 66] that yield-pseudoplastic suspensions are ideal for continuous filament-based DIW. The solid lines correspond to a fit of the Herschel-Bulkley fluid model (Equation 13),[81] and the obtained rheological parameters are listed in Table 4.1. The 20vol.% platelet suspensions were tested but the data was unreliable due to the limitations of the machine. Simply, the measured shear stresses were too high and caused discontinuities in the data. This analysis technique replicates the shear rate and shear stress response formed in the suspension during printing. The obtained static yield stress ($\sigma_y{}^{stat}$) relates to the suspensions ability to inhibit extrusion from the syringe before printing and the obtained dynamic yield stress ($\sigma_y{}^{dyn}$) relates to the layer shape retention and layer rigidity during stacking.[93]

Table 4.1. Alumina suspensions with corresponding Herschel-Bulkley curve fitting parameters for yield-pseudoplastic fluids for both static and dynamic behavior. The equilibrium storage modulus is provided along with the gelation point (G"/G'=1).

Platelet Alumina [vol%]	$\sigma_y{}^{stat}$ [Pa]	k_s [Pa·s^n]	n_s	R^2	$\sigma_y{}^{dyn}$ [Pa]	k_d [Pa·s^n]	n_s	R^2	G'_{eq}(Pa)	G"/G'=1
0	242.6	16.1	0.56	.992	185	43.0	0.40	.988	17299	126.2
5	138.3	6.7	0.68	.992	104	23.3	0.43	.988	17036	140.0
10	145.1	30.9	0.39	.988	132	26.3	0.44	.991	16401	114.6
15	184.9	14.5	0.56	.995	169	20.3	0.51	.990	13816	94.1
20	-	-	-	-	-	-	-	-	-	-

To keep the total batch solids loading constant at 54 vol.% the addition of platelet powders was balanced with a decrease in equiaxed powders. It was found that the subsitution of platelet

powders decreases both the dynamic and static yield stress below that of the base 54 vol.% equiaxed powder suspension. Similar to the arguments presented in Section 3.2, the geometrical characteristics of ceramic powders will have an effect on the particle packing density, particle arrangement, and the rheological properties.[17, 89, 90] Due to the platelet powders being significantly larger than the equiaxed powders there will be fewer individual particles for the same volume. Fewer particles could lead to an increases in the mean interparticle spacing leading to a reduction in the interaction volume between the particles (particle-particle interactions) thus decreasing the resistance to shear and decreasing the yield stress.[97, 98] In addition to this, it is known that the combination of large and small powders can lead to an increase in packing factor as well as a more efficient packing structure.[17] A more efficient packing structure can lead to more free space which will make it easier for an equivalent volume of particles to be moveable, therefore lowering the yield stress. It is also possible that the unique geometrical characteristics of the platelets allow for orientation parallel to the direction of shear which will further lead to a reduction in the resistance to shear.[35, 37, 51]

Additionally, Figure 4.1 shows that increasing the platelet loading from 5vol.% to 15vol.% leads to an increase in the yield stresses. It is commonly known that an increase in the solids loading of colloidal suspensions will lead to an increase in the yield stress and the resistance to flow.[70, 98] However, in this case the total overall solids loading is not being increased since it is held constant at 54vol.%. Therefore, the anisotropic characteristics of the platelet powders are likely influencing this behavior. As explained earlier, the replacement of equiaxed powders with platelet-like powders will decrease the total individual powders per volume. Therefore, decreasing the number of individual particles should decrease the yield stress. However, as more platelet powders are added to the system and more equiaxed powder are removed, the complex behavior of the platelet interactions should begin to dominate at the lower shear rates, and thus causing the yield stress to increase.[17, 89, 90] Anisotropic powder suspensions are known to produce distinctive rheological profiles when compared to suspensions developed from equiaxed powders due to the unique and irregular shape of the powders.[17, 37, 89, 90] The irregular morphological characteristics makes these powders more resistance to flow at lower shear rates due to the random orientation and larger volume occupation.[17, 37, 90] This complex behavior increases the likelihood that the particles will interact and could explain the increases in the yield stress behavior as the platelet content is increased. This observation is supported by the fact that the suspensions developed with

20vol.% platelets had significantly higher shear stresses for the applied shear rates and maxed out the capabilities of the rheometer. In addition to this, preliminary samples developed with 25vol.% platelets displayed dilatant behavior and were considered to be an un-printable suspension.

Figure 4.2 show the viscosity versus shear rate relationships for the different suspensions with platelet solids loading ranging from 0-15vol.% a) for shear rates increased logarithmically from 0.01 to 35s^{-1} and b) shear rates decreased logarithmically from 100 to 0.0035s^{-1}. All suspensions behaved in a uniform shear-thinning manner within the forming range (> 10s^{-1}).[65, 66, 99]
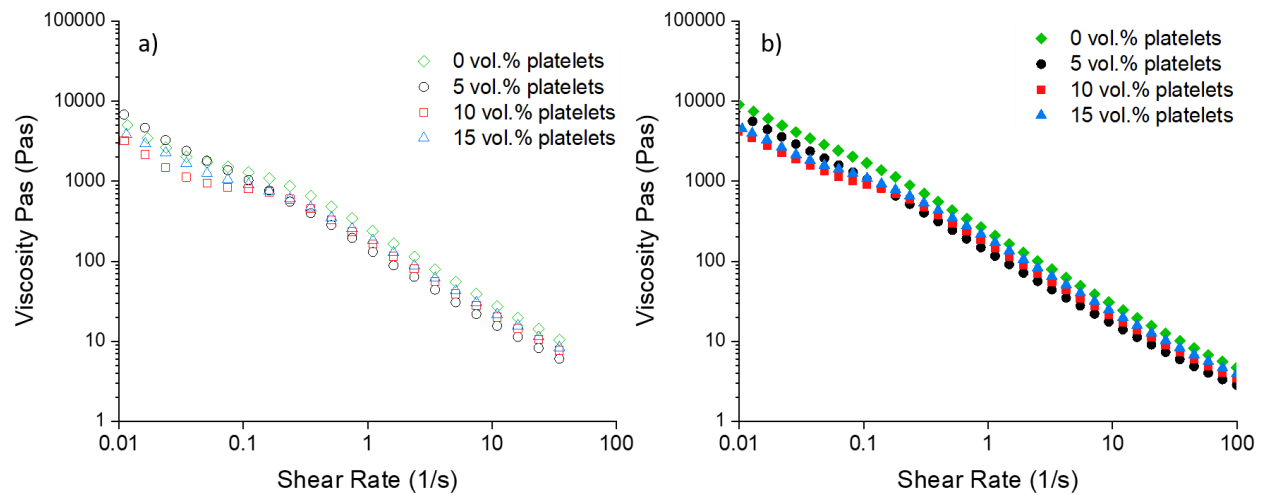
Figure 4.2. Log viscosity vs log shear rate plots of suspensions with varied platelet loadings a) shear rates increased logarithmically from 0.01 to 35 s^{-1} and b) shear rates decreased logarithmically from 100 to 0.0035 s^{-1}. Viscosity data illustrates the uniform shear thinning behavior of all the suspensions within the forming range (>1s^{-1}).

In regard to platelet solids loading, a trend similar to the yield stress behavior was observed for the viscosity behavior within the shear forming range (> 1s^{-1}). It was found that the subsitution of platelet powders decreases both the dynamic and static viscosity values below that of the base 54 vol.% equiaxed powder suspension within the forming range. Similar arguments described above on the inter-particle interactions, packing factor, and particle geometry can be used to explain the observed behavior.[17, 63, 96–98, 100, 101] The parameters obtained from the Herschel-Bulkley fluid model fit shown in Table 4.1 reveal no clear relationships between the platelet loading and consistency index (k). Also, it is interesting to note that the viscosity behavior at lower applied shear rates is different than the behavior observed at higher (>1s^{-1}) shear rates. This could explain why there are no observable trends between the platelet loading and consistency index. In addition

69

to this, the behavior in the lower shear rate range is not the same for the two different analysis (static and dynamic), however, the trends are consistent within the DIW forming range.[64, 65, 94, 102] The flow index (n) for the static response also shows no clear relationship with platelet loading. However, for the dynamic response it was found that an increase in the platelet loading led to an increase in the flow index. An increase in the flow index indicates that the suspension is experiencing less shear thinning.[65, 66] It was expected that an increase in the platelet powder content would lead to an increase in the shear thinning behavior due to the alignment of the platelet particles. This behavior is common in asymmetric particles suspensions and leads to suspensions with highly shear thinning behavior.[17, 37, 89, 90] However, this is not the case for the current suspensions.

Plots of the modulus versus shear stress for the suspensions with platelet solids loading ranging from 0-15vol.% are shown in Figure 4.3 a) 0vol.% and b) 5vol.% platelets Figure 4.4 a) 10vol.% and b) 15vol.% platelets. Additionally, the loss factor (tan δ = G"/G') for each suspension is displayed.
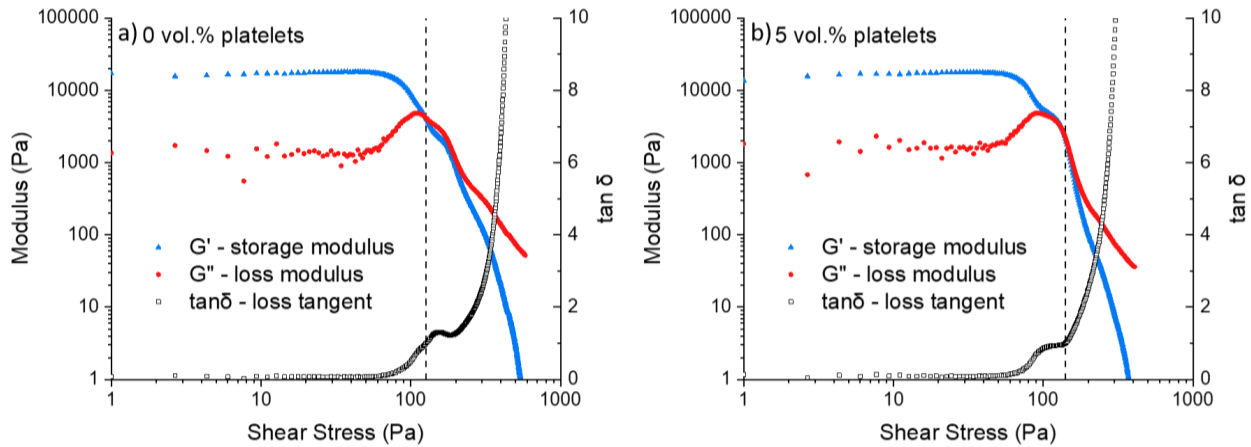
Figure 4.3. Log modulus vs log oscillation stress plots obtained at a frequency of 1 Hz for suspensions with varying platelet additions a) 0 vol.% platelets and b) 5 vol.% platelets. Tan δ (G"/G') plots are provided. The gel strength (G'$_{eq}$) was obtained from the linear viscoelastic region and a vertical dashed line signifies the gelation point (G"/G'=1).
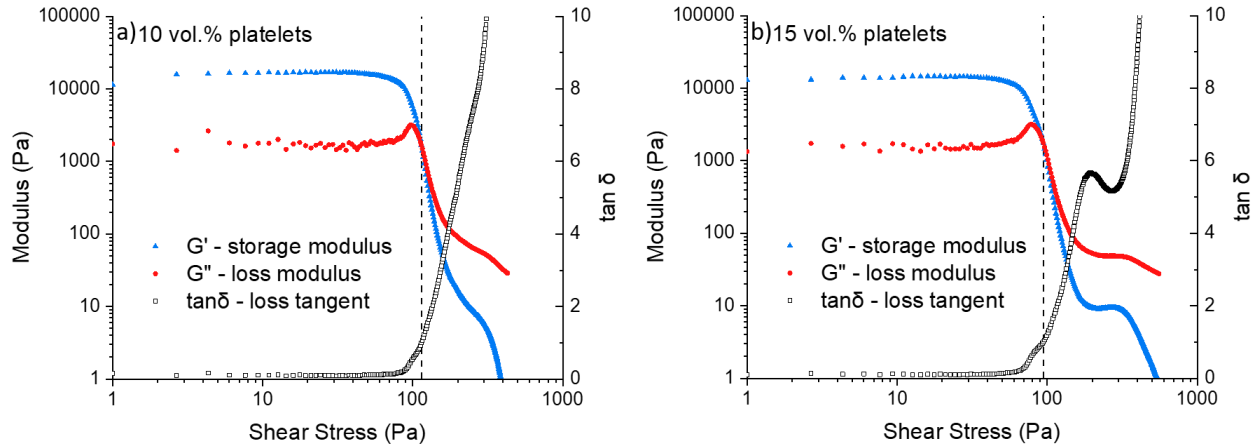
Figure 4.4. Log modulus vs log oscillation stress plots obtained at a frequency of 1 Hz for suspensions with varying platelet additions a) 10 vol.% platelets and b) 15 vol.% platelets. Tan δ (G"/G') plots are provided. The gel strength (G'_{eq}) was obtained from the linear viscoelastic region and a vertical dashed line signifies the gelation point (G"/G'=1).

All suspensions initially displayed linear viscoelastic behavior in the lower shear stress region which can be characterized by a constant modulus response. Within this region, the suspensions had higher storage modulus values than loss modulus values which corresponds to viscoelastic solid-like behavior.[93] After this linear region, the values of both moduli start to decrease at different rates. This transition leads to a region where the loss modulus is higher than the storage modulus which corresponds to viscoelastic liquid-like behavior.[93] The point at which G"/G'=1 is called the gelation point and marks this transition from a solid-like elastic dominant behavior to a liquid-like viscous dominant behavior. The calculated gelation point for each suspension is listed in Table 4.1 and shown with a hashed line in Figure 4.3 and Figure 4.4.

The equilibrium storage modulus (G'_{eq}) was obtained from the linear viscoelastic region and these values are reported in Table 4.1. It was found that the substitution of platelet powders into the suspensions led to a decrease in the equilibrium modulus, indicating a decrease in gel strength. Increasing the platelet content from 0vol.% to 15vol.% decreased the equilibrium storage modulus from 17299Pa to 13816Pa, respectively. It has been shown that suspensions with higher equilibrium moduli or gel strength will exhibit stronger shape retention for the deposited layers.[64, 66, 93] It is also important to note that all suspensions exhibited significantly higher equilibrium storage moduli than previously found for boron carbide suspensions developed for DIW.[66] It seems

71

that this decreases in equilibrium storage modulus did not impact the quality of the print as all samples were considered to have an acceptable print quality.

After this linear viscoelastic region, the suspensions reach the respective limit and transitions from a solid-like to liquid-like behavior at the gelation point (G"/G'=1)[93] Typically, a behavior of this nature is linked to a breakdown of the particle-gel network structure.[94] From the values reported in Table 4.1 it can be seen that increasing the amount of platelet powders from 5vol.% to 15vol.% leads to a decrease in the shear stress at which this transition happens. This means that the addition of platelet powders is causing the suspension gel network to breakdown at lower shear stresses. It is unclear way this is happening as there is little research that reports or links this behavior to morphology. It is possible that the platelet powders are interacting with the polymer and breaking down this network. It is also, possible that the morphology of the platelet powders is not is not well suited for the network. Lastly, as discussed earlier, the platelet particles will align under higher shear stresses. This could be the cause for the decrease in gel point.

The loss modulus curves show the amount of the deformation energy that is lost during shearing due to internal friction. Evaluating the loss modulus curves of these suspensions shows that all the suspensions follow a relatively constant loss modulus value in the linear viscoelastic region. After this flat section, the curves rise and reach a maximum then drop steeply. It is important to note that this loss modulus peak happens before the gelation point. This behavior is well characterized in the literature and this peak behavior is described as the development of micro cracks with in the suspension.[103, 104] The development of theses micro cracks, leads to deformation energy loss due to the now broken and freely movable bridge fragments around the micro cracks exhibiting internal viscous friction in the form of heat.[103, 104] Following this, the micro cracks will grow and form a continuous macro crack. During this process, the loss modulus starts to dominate over the storage modulus and the suspensions start to flow.[103, 104] For the developed suspensions, it was found that the peak loss modulus behavior changes as the amount of platelet loading is increased. Both the base 0vol.% suspension and the 5vol% suspensions steadily rise and have a broad peak. The 10vol.% and 15vol.% platelet suspensions have a much smaller and distinct peak. From the data it seems that the addition of platelets into the suspensions is causing the structural breakdown of the network to take place at lower shear stresses and more abruptly. It is possible that the unique morphologically structure of the platelets leads to a different network structure that breaks down more quickly due to alignment and exhibits less viscous dissipation.

Another important feature of this analysis is the loss tangent or damping factor. The loss tangent is the ratio of storage modulus to loss modulus. Comparing the loss tangent curve for each of the suspensions supports the previous observation. For the base 0vol.% platelet suspension there is a small peak in the data after the gelation point at a shear stress of roughly 105Pa. This peak is apparent in all the other suspensions loss factor plots and corresponded to the loss modulus peak previously discussed. This behavior is different for the other suspensions and further supports the micro crack argument made in the previous paragraph. Looking at the 5, 10, and 15vol.% platelet suspensions loss factor plots shows that this peak decreases in intensity and is shifted to a lower shear stress, as the platelet content is increased. More importantly, in the 15vol.% plots, this peak is almost entirely flattened out and another distinctive peak is observed at 110Pa. This peak corresponds to a secondary plateau region where both the storage and loss modulus are constant. The suspension is still behaving in a liquid-like fashion, how ever it seems that a secondary network has formed. It is not clear what mechanisms are causing this. It is likely due to a increased amount of platelet particles in the suspensions. Further investigations and discussion will be provided in future work.

4.2   Texture Analysis

Similar to the texture previous analysis, the orientation parameter (r) and grain misalignment angle (full width at half maximum (FWHM)) were obtained from a rocking curve analysis. The orientation parameter and FWHM for the cast and DIW samples along with the R^2 values are reported in Table 4.2. A lower orientation parameter (r) and lower FWHM are associated with higher grain alignment. For this analysis, the alignment reference plane was normal to the hot-pressing direction and the printing lines were oriented perpendicular to the x-ray rocking axis as shown in Figure 2.5. Six rocking curve analysis were done for each pressed sample to obtain an average r and FWHM. For each suspension samples were processed through DIW with a nozzle size of 1.35 or 1.75mm and a sample cast from the same suspension was added for comparison.

Table 4.2. Texture distribution data for cast and DIW samples developed from the different suspensions. Orientation parameter (r) obtained from curve fits of the March-Dollase equation. The 95% confidence interval for the orientation parameter and FWHM are shown for each sample having a data population of 6.

Platelet Al_2O_3 [vol%]	Processing conditions	Orientation parameter (r)			FWHM [^{o}]			R^2	Density (%TD)
0	Cast	--	+/-	--	--	+/-	--	--	98.67
	$N_d = 1.75$	--	+/-	--	--	+/-	--	--	99.10
	$N_d = 1.35$	--	+/-	--	--	+/-	--	--	98.81
5	Cast	0.450	+/-	0.024	28.26	+/-	2.71	.970	100
	$N_d = 1.75$	0.253	+/-	0.007	11.33	+/-	0.48	.988	99.52
	$N_d = 1.35$	0.262	+/-	0.004	11.95	+/-	0.25	.989	99.50
10	Cast	0.439	+/-	0.034	27.12	+/-	3.20	.947	100
	$N_d = 1.75$	0.280	+/-	0.007	13.19	+/-	0.51	.991	99.50
	$N_d = 1.35$	0.292	+/-	0.005	14.04	+/-	0.35	.987	100
15	Cast	0.396	+/-	0.049	23.21	+/-	4.77	.974	100
	$N_d = 1.75$	0.326	+/-	0.007	16.68	+/-	0.56	.985	99.67
	$N_d = 1.35$	0.281	+/-	0.004	13.23	+/-	0.28	.990	99.63
20	Cast	0.435	+/-	0.019	26.62	+/-	2.05	.958	100
	$N_d = 1.75$	0.323	+/-	0.006	16.50	+/-	0.47	.985	99.61
	$N_d = 1.35$	0.318	+/-	0.010	16.12	+/-	0.80	.983	99.55

The rocking curve or texture distributions are shown in Figure 4.5 a) for 5vol.% platelets and b) for 10vol.% platelets and Figure 4.6 a) for 15vol.% platelets and b) 20vol.% platelets.
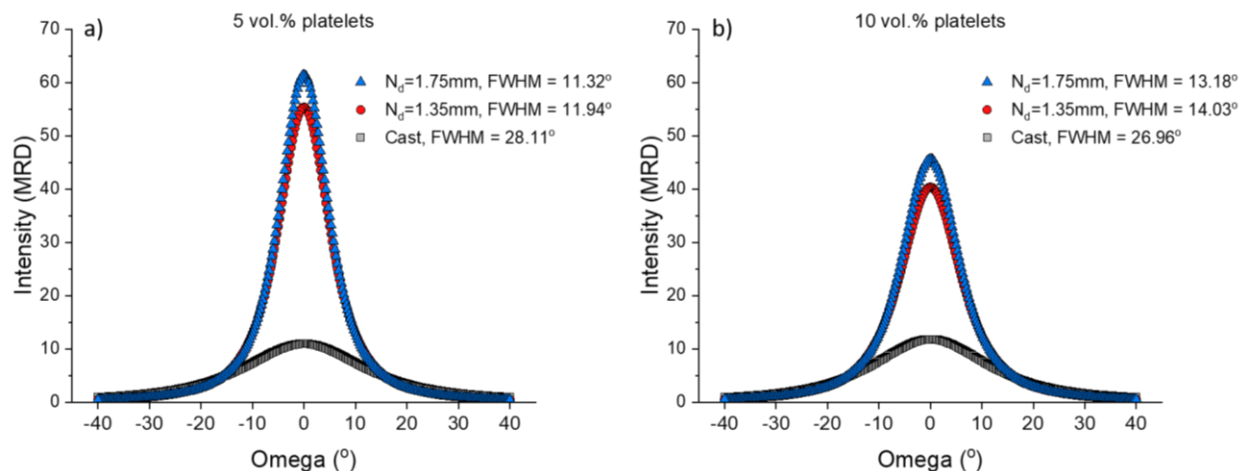
Figure 4.5. XRD rocking curves of hot-pressed samples processed through DIW with a nozzle diameter of 1.75mm and 1.35mm for a) 5vol.% platelets and b) 10vol.% platelets. A sample that was cast from the same suspension is show for comparison. Curves are March-Dollase fits of the averaged data.
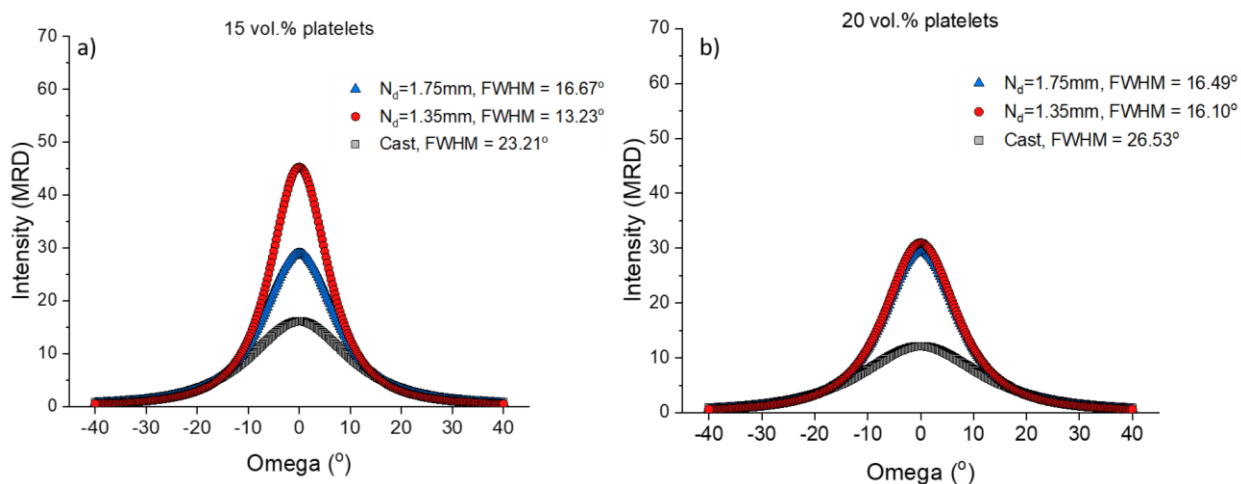
Figure 4.6. XRD rocking curves of hot-pressed samples processed through DIW with a nozzle diameter of 1.75mm and 1.35mm for a) 15vol.% platelets and b) 20vol.% platelets. A sample that was cast from the same suspension is show for comparison. Curves are March-Dollase fits of the averaged data.

As previously mentioned, a higher peak intensity will correspond to higher alignment. From the data and plots it can be seen that for all suspensions the DIW samples have significantly higher alignment when compared to cast samples. From this data, it is clear that the DIW process is aligning the platelets within the samples when compared to casting. However, the relationship between nozzle size and alignment is not clear. The rocking curve plots show that the average

75

alignment for the larger nozzle (1.75mm) when paired with the 5 and 10vol.% suspensions is higher than the smaller nozzle (1.35mm) but this trend flips when using the 15 and 20vol.% suspensions. Considering the 95%CI reported in Table 4.2 ,reveals that this trend is only statically significant for the 15vol.% samples. The data for the 5,10,20vol.% samples for the small and large nozzle are not statically different as determined by a studentized t-test. Therefore, it is not entirely clear whether using a nozzle with a 1.75mm diameter or a 1.35mm diameter impacts the final alignment. An investigation by Compton et al.[69] on the fabrication of lightweight cellular composites with aligned high aspect ratio fibers proposed that above a critical nozzle size the alignment would decrease. This critical nozzle size was never established in the literature and connected to the dimensions of the elongated phase. However, it could be that both of these nozzle sizes were above this critical dimension which led to an inconsistence trend. It is also, possible that the hot-pressing process and preparation is leading to this variability in the data. A closer look at the microstructure may reveal more information on this behavior.

Another relationship of interest is how the platelet loading impacts the final alignment. Figure 4.7 plots the orientation parameter (r) vs. vol.% platelets dependence of cast and DIW samples.
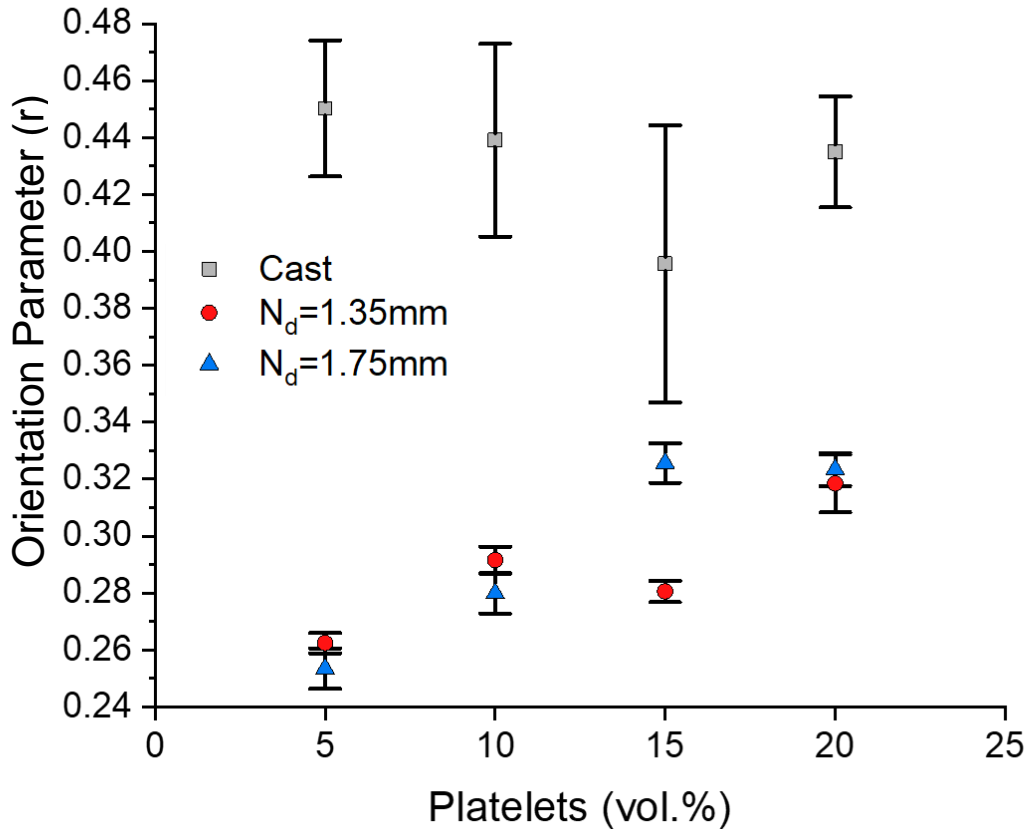
Figure 4.7. Orientation parameter (r) vs. vol.% platelets dependence of cast and DIW samples. The 95% confidence intervals for the orientation parameter are shown for each sample having a data population of 6.

For samples that were cast from the selected suspensions, the data shows no statically significant relationship between alignment and platelet content. All samples that were cast had a relatively high orientation parameter and a large variation in the data. Samples that were processed with DIW, showed lower orientation parameter and less variation in the data. Additionally, the data shows that as the platelet loading increases from 5 vol.% to 20vol.% the orientation parameter increases. Connecting this behavior to the rheological properties reported in Section 4.1, a correlation can be established. It was found that suspensions that have higher platelet loading have higher viscosity and yield stress. Similar to the arguments presented above, the geometrical characteristics of ceramic powders will have an effect on the particle packing density, particle arrangement.[17, 89, 90] The irregular morphology of the platelets will impact the flow behavior and

the alignment of the system.[89, 90] Further increasing the number of platelets in the system will increase the likelihood that the particles will interact. This can decrease the flow properties of the system which should could decrease the alignment and explains the observed alignment behavior in regards to platelet solids loading for DIW samples.

4.3   Optical Analysis

For the UV-vis analysis, the 0vol.% samples were not analyzed in this study due to a majority of the sample breaking during removal from the hot-press die. Moreover, the samples that were considered salvageable were not able to be polished due to a brittle nature. An image of a hot-pressed sample that was cast from a 0vol.% suspension is shown in Figure 4.8. The surface of this sample is severely pitted, and the density was measured to be 98.67%TD which is too low to exhibit transparency. Compared to the samples developed with 5vol.% suspensions there is no visible transparency and thus this sample was removed from the analysis.
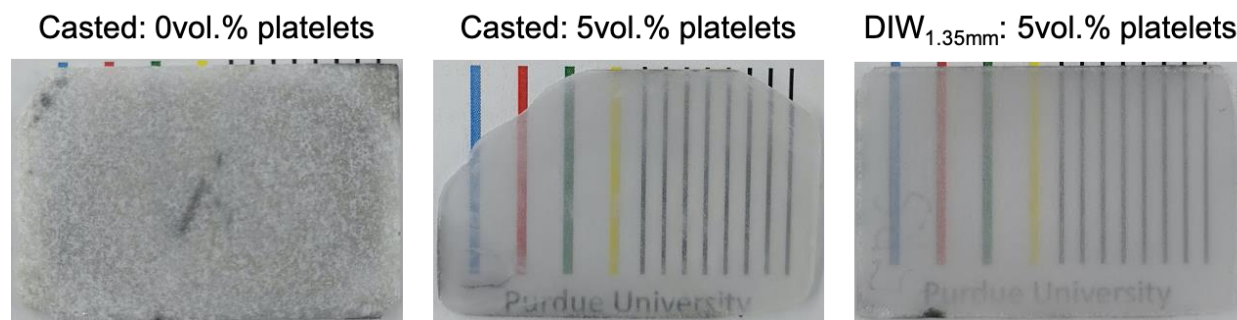
Figure 4.8. Optical images of hot-pressed samples placed flat on piece of paper. The samples containing 5vol.% platelets were polished to transparency.

Figure 4.9 shows the in-line transmission as a function of wavelength for the cast and DIW samples made from the 5vol.% and 20vol.% platelet suspensions, as well as a single crystal sapphire standard. The 5vol.% and 20vol.% samples were chosen for the optical analysis because the samples produced through DIW possessed the highest and lowest alignment values, respectively.
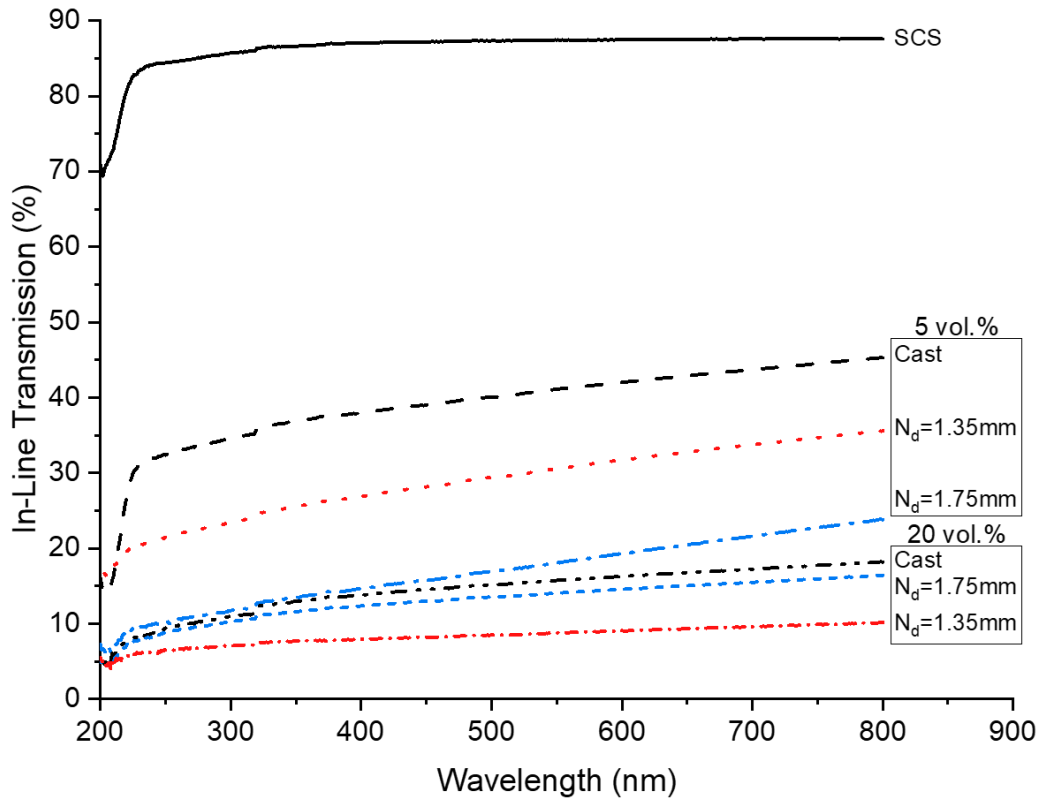
Figure 4.9. UV-vis analysis of cast and DIW samples produced from 5 vol.% and 20vol.% suspensions. In-line transmission as a function of wavelength, normalized to t = 0.8mm. A single crystal sapphire (SCS) sample is included for comparison.

All samples produced with the 5vol.% platelet suspensions had higher percent in-line transmission within the visible spectrum than samples produced with the 20vol.% platelet suspensions. This data suggests that having a lower platelet loading leads to improved optical properties for both processing routes. For samples produced through DIW, the alignment data showed that an increase in the platelet loading increased the orientation parameter and decreased the alignment. The in-line transmission data of the DIW samples follow the predicted trends discussed earlier and found in the literature on grain alignment and optical transparency.[7, 58, 84, 105–108] However, the samples produced trough casting do not follow this alignment and optical properties trend. The average orientation parameters obtained for all the cast samples are similar and not statically different, therefore the optical properties of these samples should be similar assuming the density and impurities of the samples are similar. The 5vol.% cast sample had significantly higher in-line transmission than the 20vol.% cast sample. Additionally, both cast

samples had significantly lower alignment values when compared to the samples that were produced through DIW. From this data, it would be expected that both cast samples would have the lowest in-line transmission values within the data set. This is not the case for the obtained data. The 5vol.% and 20vol.% cast samples had higher in-line transmission when compared to the respective samples produced through DIW. This trend was unexpected and is contradictory to the previous work on uniaxial warm pressing.[105] To add to this, these results do not match the results found in the literature as well as the hypothesis that grain alignment improves the optical properties.[7, 58, 84, 105–108] Comparing the bulk density data presented in Table 4.2 shows that for both the 5vol.% and 20vol.% platelet loadings suspensions that the cast samples have higher densities than the DIW samples. This density data shows that samples produced from the DIW process are not attaining the same relative densities as the cast samples. This is one possibility that could explain this unpredicted trend, however, a more comprehensive analysis will provide more information.

A more in-depth analysis can be done on the optical properties by measuring the different loss mechanisms for each sample. These loss mechanisms are associated with different microstructural features and from this information it can be established which features are impacting the optical properties of the individual samples. Figure 4.10 shows the light transmission and optical loss mechanisms at 645nm for the cast and DIW samples made from the 5vol.% and 20vol.% platelet suspensions. A single crystal sapphire standard was added to this analysis as a basis for comparison.
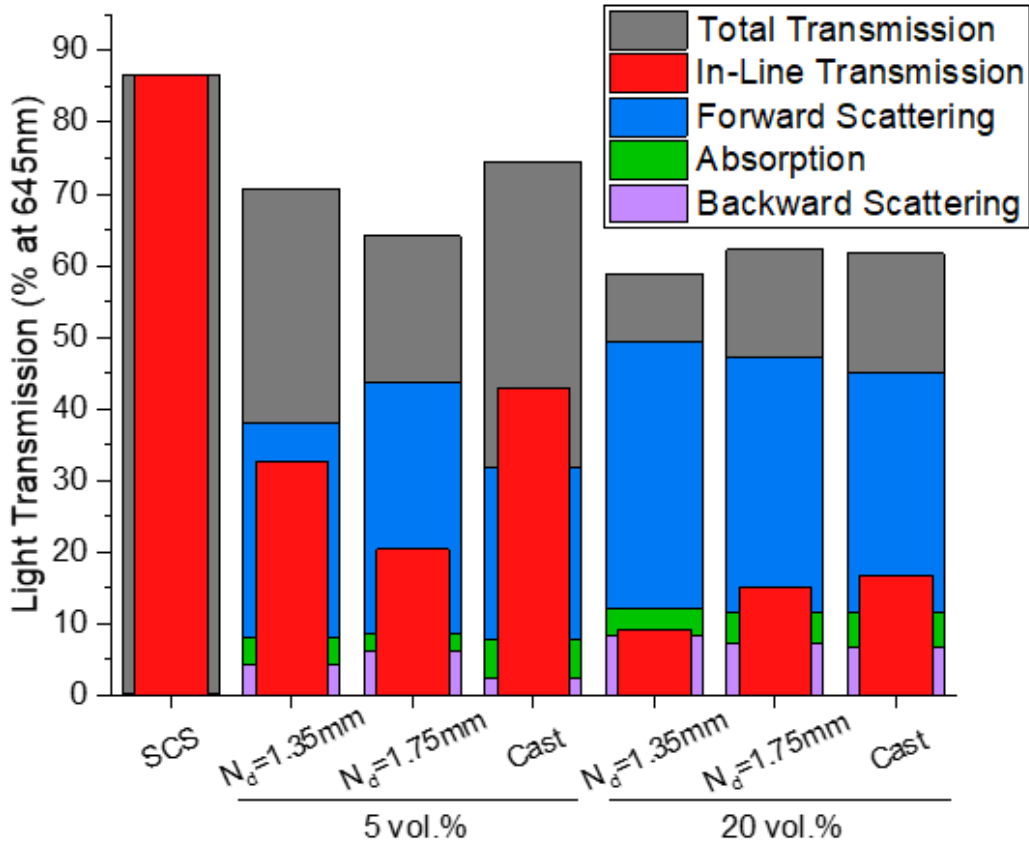
Figure 4.10. Light transmission at 645nm for cast and DIW samples produced from 5vol.% and 20vol.% suspensions. All samples were normalized to a thickness of 0.8mm. A single crystal sapphire (SCS) sample is included for comparison.

The optical loss mechanisms for transparent ceramics are absorption, backward scattering, and forward scattering. Absorption losses in polycrystalline alumina are caused by secondary phases.[7,58] The data shows that samples produced from the 5vol.% platelet suspensions had slightly less absorption than samples produced with the 20vol.% platelet suspensions. It is possible that increasing the platelet powder is increasing the amount of impurities in the total powder. As stated in Section 2.2.1, the purity of the equiaxed powder is 99.99% and the purity of the platelet powder is 99.8%. Having impurities in the platelet powder will lead to an increase in the absorption losses of the final samples.

Backward scattering losses are caused by residual porosity within the matrix.[7, 58] The data shows that the 5vol.% platelet suspensions have slightly less backward scattering losses when compared to the 20vol.% platelet suspensions. However, this data does not entirely match the bulk density data in Table 4.2. The density data shows that cast and DIW samples have comparable densities for analogous samples. This means that the backwards scattering losses should be the same for the respective samples. It is important to consider that the Archimedes method is a bulk measurement. Furthermore, the UV-vis analysis was performed on a local part of the sample and should be more sensitive to the local porosity within the area of optical consideration. Further analysis on the microstructure may show local porosity within the samples. Looking at the trends within the respective suspension groups, both cast samples have lower backwards scatter losses when compared to DIW samples of the same suspension. This observation is supported by the Archimedes density analysis. This would partially explain the unexpected trend that was observed for the cast samples with less alignment and higher in-line transmission.

It is well understood that forward scattering losses are due to differences in the refractive index. These index mismatches are caused by either residual porosity or grain misalignment between the anisotropic grains.[7] Typicality, in high density samples it is assumed that the majority of forward scattering loses are due to crystallographic mis-alignment[58, 105] The data shows, that all samples produced with 5vol.% platelet suspensions have less forward scattering losses at 645nm than samples produced with 20vol.% platelet suspensions. There are no clear trends connecting this behavior to the bulk densities of the samples since the data presented in Table 4.2 shows that the cast and DIW samples of the 5vol.% suspensions have similar densities to the analogous 20vol.% platelet samples. However, the backwards scattering data does show differences in the residual porosity between the analogous 5vol.% and 20vol.% samples. These differences are small which makes it hard to determine the influence that the porosity has on the forward scattering losses but the trends within these samples have a similar pattern for backwards and forward scattering. Meaning that samples with higher backwards scattering had higher forwards scattering. Under the selected hot-pressing parameters, it seems that samples produced with 5vol.% suspensions, whether cast or DIW, may be able to reach higher grain alignments leading to less forward scattering losses at comparable densities.

Both the 5vol.% and 20vol.% cast samples have lower forward scattering losses than the respective DIW samples. For platelet loadings, the cast samples had lower grain alignment when

compared to DIW samples. Due to this, both cast samples should have higher forward scattering losses than all DIW samples, however, this is not the case. The density data and backwards scattering data shows that samples produced from the DIW process are not able to achieve the same relative densities having more residual porosity than the cast samples.[7, 58] As explained above, residual porosity does contribute to the forward scattering loss mechanism. At the higher densities of the cast samples, the forward scattering mechanisms should be almost purely due to misalignment rather than porosity. This density data may explain the lower in-line transmission values and higher forward scattering losses exhibited by the highly aligned DIW samples. However, the amount of residual porosity within the DIW samples is relatively small and it is not clear if this is the case. Another possible explanation for the observed behavior is that the selected texture analysis is not adequate. The rocking curve analysis is limited to one-dimensional texture (the rocking plane) and is not able to obtain the complete alignment behavior of samples that possess two-dimensional (outside the rocking plane) or more complex texture. A more advanced pole figure analysis or EBSD characterization may prove useful for these samples.

To gain an understanding of the out of plane texture, a simple preliminary rocking curve analysis was performed on a few DIW samples rotated 90° from the original testing orientation. This testing orientations that were used are shown below in Figure 4.11.
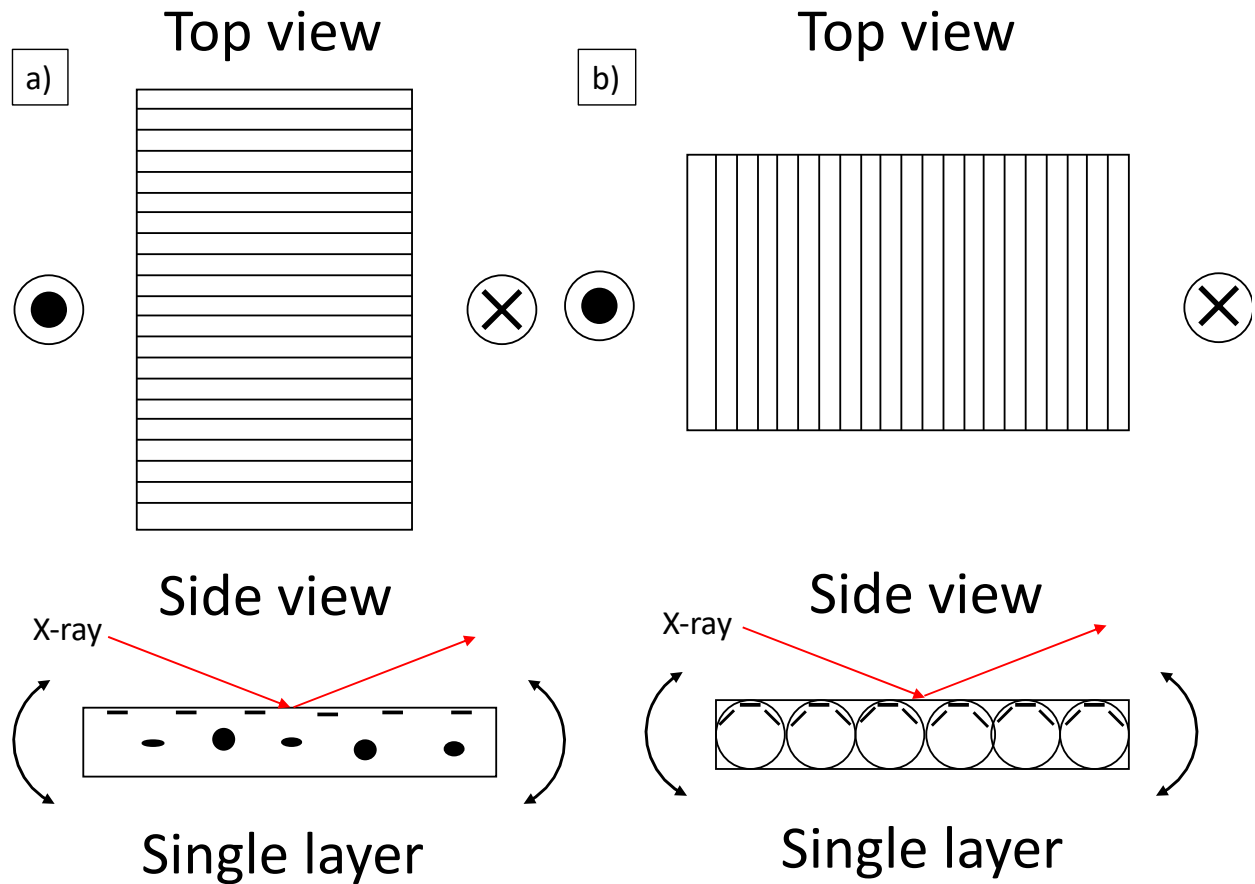
Figure 4.11. Rocking curve analysis setup for the DIW samples a) the set-up used to analyze the main DIW samples with the print lines perpendicular to the rocking axis and b) the sample rotated 90° so that the print lines are parallel to the rocking axis. A schematic of the print lines is shown to illustrate the platelet alignment relative the rocking axis.

The orientation parameters obtained on DIW samples that were rotated 90° were significantly higher than the previously obtained orientation parameters. This means that the DIW samples have lower alignment when oriented parallel to the rocking axis. A more in-depth analysis will need to be done to properly characterize the alignment of these samples, but this preliminary test shows that the alignment behavior of the DIW samples is complex. This behavior is interesting and to further understand it a microstructural analysis and pole figure analysis will need to be performed as well. Nevertheless, the current hypothesis of the author is that the samples simply have biaxial alignment. In Figure 4.11, a simple schematic of the individual layers and the expected platelet alignment is shown below the test set-ups. The platelets are expected to align parallel to

the direction of flow (parallel to the print lines), which is commonly observed in the fabrication of polymer matrix composites from extrusion-based processes (DIW and fused deposition).[68, 109, 110] Since, the platelets have two-dimensional texture, they should preferentially align to a secondary axis or to the dimensions of the nozzle while still aligning in the primary axis or the direction of flow. The single layer schematic in Figure 4.11a shows the expected alignment of the platelets. This arrangement, which corresponds to the set-up used in the main rocking curve analyze, should lead to an analysis that gives a higher alignment value since the platelets will align to the print lines and perpendicular to the rocking axis. Any secondary axis alignment will not contribute to the texture data since this this alignment is out of the rocking plane. However, when the sample is rotated 90°, as is shown in the single layer schematic in Figure 4.11b, this secondary alignment will contribute to the data. The platelets on the top and bottom surface of the nozzle will be aligned to the rocking axis but the platelets that align around the other edges of the nozzle will be aligned off the rocking axis. As the samples is rocked through the rocking plane, the platelets that are aligned on this secondary axis or along the edges of the nozzle with result in an intensity at mis-aligned angles. This will result in a sample that has a higher orientation parameter or a boarder texture distribution. This preliminary hypothesis may explain the observed behavior, but further investigation is needed to establish the complex texture of the DIW samples.

4.4   Microstructure

As explained above, the shear and elongational flow profiles developed in DIW should lead to velocity gradients that can align high aspect ratio powders. Considering that platelets have only one-dimension that is constricted, this capillary extrusion-based process should lead to biaxial alignment as opposed to the uniaxial alignment that was developed in the previous study.[105] It was understood that the DIW process is most likely resulting in two-dimensional texture, but it was the hope that the use of uniaxial hot-pressing could alleviate some of this behavior. From the above texture analysis and optical analysis, it is clear that the data is not in agreement with the accepted Rayleigh-Gans-Debye theory,[7] which states that an increases in the grain alignment will lead to an increases in the optical properties. A closer look at the DIW samples may provide information on the data discrepancies. A visual inspection of the polished DIW samples revealed that there are characteristic features left over from the DIW process. Further investigation shows, that all of the DIW samples have lines with high and low transparency. It seems that these lines corresponds to

the print lines within the samples. An example of this macrostructural characteristic is shown in Figure 4.12.
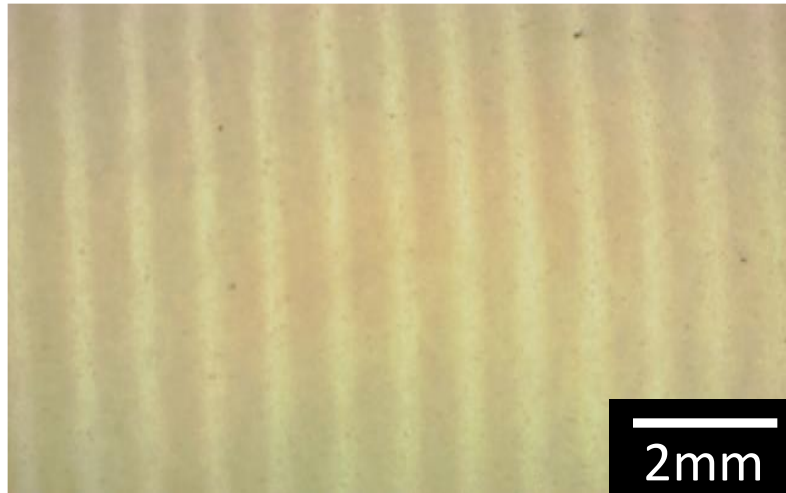
Figure 4.12. Optical micrograph of sintered and polished sample produced through DIW a 20vol.% suspension.

This optical image shows that the sample is retaining the print lines from the DIW process even after the samples have been hot-pressed. This is a unique observation because it was expected that the hot-pressing process would remove a majority of the preprocessed behavior. A microstructural analysis will need to be performed to identify this behavior. The current hypothesis is that the smaller or lighter regions correspond to the edges of the filament where the alignment should be highest due to the shear stresses.[32, 68, 109, 110] While the larger or darker lines correspond to the inner part of the filament where the shear stresses should be lowest. Simply, these lines may have different alignments that are impacting the optical properties making one line more transparent (lighter) than the other. It is also, possible that these lines corresponded to porosity or particle segregation. Whether or not these hypotheses are true or not, these features do explain the above observed discontinuities in the alignment and optical data for the cast and DIW samples. The DIW samples have local regions of higher and lower transparency which will negatively impact the optical properties. This retained microstructure may not be beneficial to transparent samples, but it may find use in composite based structure, or layered structures. A microstructural analysis will need to be performed to further understand this behavior.

4.5   Summary and Conclusions

An additive manufacturing process termed DIW was used to produce alumina samples from aqueous-based ceramic suspensions to be hot-pressed to transparency. A 54vol.% equiaxed powder suspension was used as a basis and then modified with 5, 10, 15, 20vol.% platelet powder additions. To conserve the volume percent and additives, platelet additions were balanced with equiaxed powders. The effects of platelet alumina solids loading on the rheological properties, the final sintered grain orientation, and the final sintered optical properties of transparent alumina produced via direct ink writing were analyzed. An increase in the amount of platelet powders from 5-20vol.% increased the dynamic yield stress from 104Pa to 169Pa and decreased in the equilibrium storage modulus from 17,036Pa to 13,816Pa. All samples exhibited requisite rheological properties to obtain high quality samples. It was found that the DIW process significantly increased the alignment in one orientation when compared to samples cast from the same suspensions. An optical analysis showed that sample developed with 5vol.% platelet suspensions had higher in-line transmission values across the visible spectrum when compared to samples developed with 20vol.% suspensions. A sample cast from a 5vol.% platelet suspensions had the lowest grain alignment but possessed an in-line transmission of 42.8% at 645nm, which was the highest of the samples produced in this study. An optical loss analysis showed, that this sample had the lowest backwards scattering losses due to a low amount of residual porosity and this result was supported by the density data. It seems that the processing of samples through DIW is leading to residual porosity within the system. It is believed that the alignment of the DIW samples is complex due to the biaxial alignment of platelets. A more advanced texture analysis will need to be conducted in the future to properly characterize the grain alignment of the DIW samples. Additionally, it was found that the samples produced through DIW showed visual evidence of retained layers after sintering. This retained microstructure is not beneficial to developing high transparency samples and could be the cause for disagreement between the alignment and optical data.

5. HOT-PRESSING OF EQUIAXED AND PLATELET ALUMINA POWDERS TO TRANSPARENCY

Willy's contribution to this collaborative effort includes help with project design, XRD data collection and analysis, and editing of the manuscript.

Willy's contribution to the current investigation includes project design, powder preparation, hot-pressing, displacement data collection and analysis, rocking curve testing and analysis, optical sample preparation, optical image collection and analysis, optical data analysis, and writing of the manuscript.

Previous research investigated the sintering behavior and resulting optical properties of non-pre-aligned platelet alumina powder during hot-pressing. In that study, the effects of the hot-pressing parameters (maximum temperature, powder calcination, pre-load pressure, maximum pressure, and isothermal hold time) on the densification and optical properties of platelet-morphology alumina were reported.[58] This previous study established the basis for the processing conditions used in the current equiaxed and platelet powder ratio sintering analysis. From this previous study,[58] it was found that samples fabricated by hot-pressing calcined platelet alumina powder with a pre-load pressure of 0MPa, maximum temperature of 1800°C, maximum pressure of 10MPa, and an isothermal hold time of 7hrs yielded the highest optical properties. In that study, it was found that using higher max pressures (>10MPa) led to samples with lower densities and optical properties. It was suggested that the lower densities at higher pressures could be a result of a pore swelling phenomenon and it may be possible to mitigate this phenomenon by maintaining the max pressure during cooling. Articles investigating the spark plasma sintering of alumina have reported processes conditions were a maximum load is applied until the temperature decreases to 1000°C.[111–113] In the previous study by Schlup et al.[58] it was proposed that holding the max pressure during cooling would inhibit the surrounding matrix from readily deforming at higher temperatures. To add, removing the load at lower temperatures would provide insufficient thermal

energy inhibiting the surrounding alumina microstructure from deforming from pore swell. It is the hope that these modified parameter will lead to a decrease in the amount of pore swell. Therefore, in this equiaxed and platelet ratio sintering analysis, the max pressure was maintained during cooling and removed at a temperature of 1100°C. In addition to this modification, the isothermal hold time was reduced to 5hrs. The previous work,[58] established that at least 5 hours is required to obtain adequate optical properties (T_{ILT}>60%) for non-pre-aligned powders. To save time and resources a 5hr isothermal hold time was selected over the slightly more optimal 7hr hold time.

A particular area of interest that was investigated in this previous analysis was the displacement behavior of the hot-pressed samples. By looking at the displacement rate data for samples that were hot-pressed at a max pressure of 2.5MPa to 80MPa an interesting inflection in the data was observed around 10MPa. Samples hot-pressed at a max pressure of 2.5MPa and 5MPa continued to displace at a significant rate after reaching their respective max pressure and for samples that were hot-pressed at max pressures above 10MPa the displacement rate became constant. It was found that hot-pressing platelet powder at a pressure of 10MPa, which roughly corresponded to this inflection point, resulted in optimal optical properties. To explain this behavior, it was proposed that at pressures below 10MPa the powder compact is still experiencing particle rearrangement and a considerable amount of porosity remains leading to the significant displacement rate after the max pressure is applied. At pressures above 10MPa, it is assumed that particle rearrangement was completed, and the powder bed had nearly densified. Meaning that the addition of higher pressures would result in the powder compact bed experiencing linear-elastic strain and a decrease in optical properties. Additionally, when a max pressure greater than 20MPa was applied to the samples a spontaneous change in the displacement rate was observed. It was proposed that this spontaneous change could correspond to a recrystallization phenomenon previous proposed by Heuer et al.[14, 114–116] as the "critical strain". It is possible that these observations are characteristic of the platelet powders and that equiaxed powder will behave differently during sintering. Due to this, an analysis on the displacement and displacement rate behavior during sintering was conducted on equiaxed and platelet ratio powders to gain an understanding of the sintering behavior and to identify if the inflection point is different for the equiaxed powders and thus different for the different powder ratios.

5.1 Sintering Behavior

To understand the sintering behavior and to identify the optimal maximum pressure parameters of the ratio powder compacts a sintering analyzed was conducted. This analysis consisted of using the sintering parameters detailed in Section 2.6.3 and applying a maximum pressure of 80MPa. Applying this high maximum pressure allows for the identification of the inflection point and the spontaneous change in displacement rate. If samples are to have a range of behaviors it will be important to characterize these behaviors. The normalized displacement vs time behavior of the different equiaxed and platelet powder ratios is shown in Figure 5.1. In the plot, the 100/0 label corresponded to a powder sample that is composed of 100% equiaxed powders while the 75/25 sample corresponded to a powder sample that is composed of 75% equiaxed powders and 25% platelet powders. The rest of the samples are labeled accordingly.
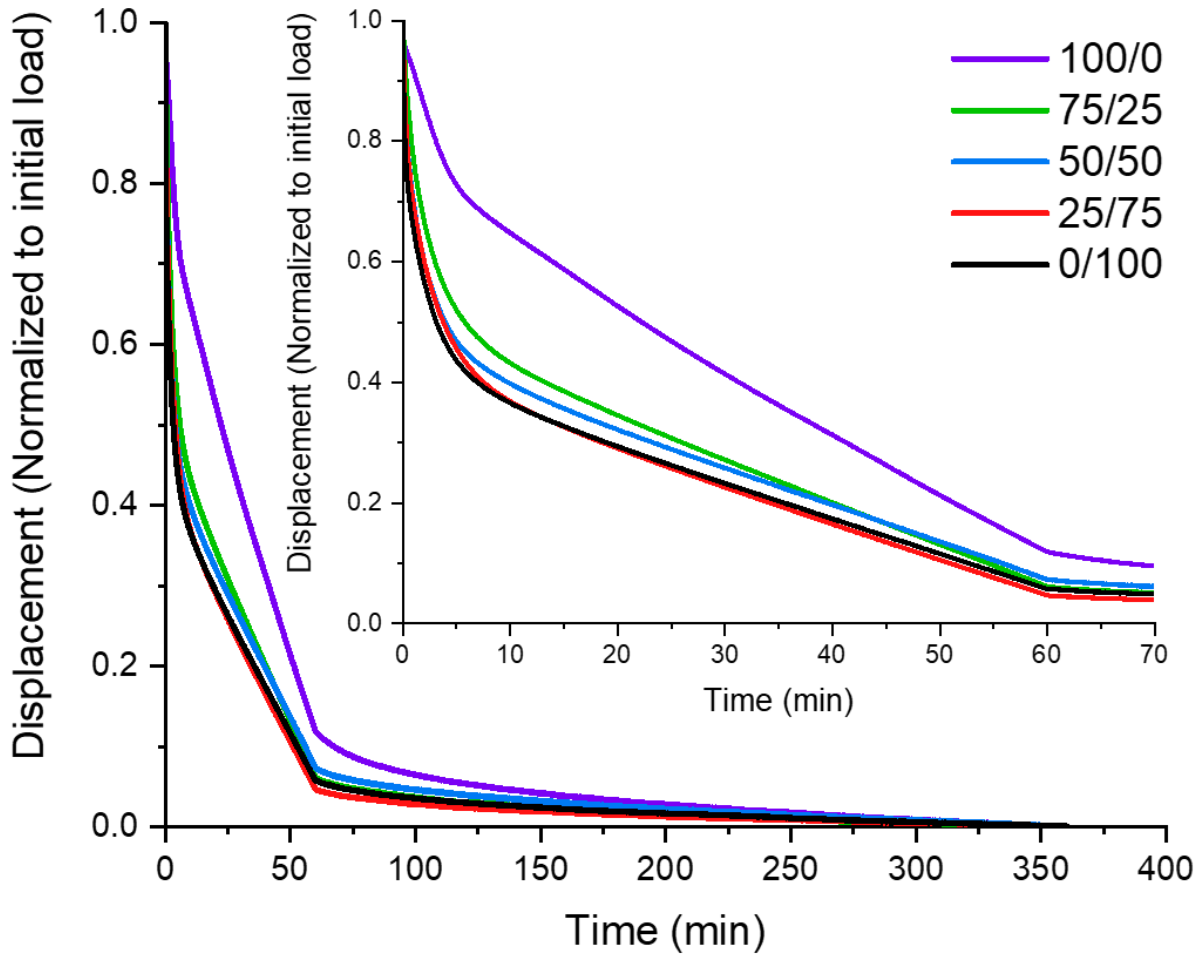
Figure 5.1. Powder compact displacement (normalized to the initial load) vs hot-press time for the powder ratio samples. The initial time corresponds to when a load of 0.1kN is detected.

The displacement data collection was initiated at a load of 0.1kg as this was deemed to be the point of initial contact with the powder. For all the samples the displacement data was normalized to the respective initial value to be comparable. Therefore, the samples all start at an initial value of 1 and end at a final value of 0 since the hot-press is applying a compressive load. The displacement data shows that all samples experience a significant displacement initially. Following this there is an inflection in the data and then an area were the individual displacement rates are constant. At about 60mins, all the samples show a sharp inflection. This secondary inflection point corresponds to the time when the maximum pressure (80MPa) is reached. After this point the samples continue to displace a small amount while the isothermal temperature and load is held constant.

The displacement data shows that all the equiaxed and platelet ratio powders experience different displacement profiles during the sintering process. Taking a closer look at the zoomed in plot in Figure 5.1 better illustrates the differences in the displacement data. For the following explanation the separate parts of the plot will be referred to as zone 1: from the initial displacement value to the first inflection (time = 0 to time ~ 8mins), zone 2: from the first inflection to the second inflection (time ~8mins to time ~60mins), and zone 3: from the second inflection to the end (time > 60mins).

In zone 1, the 100% equiaxed sample experiences significantly less overall displacement when compared to the other samples. From here the samples that experience the least amount of displacement to most displacement are as follows; 75% equiaxed (75/25), 50% equiaxed (50/50), 25% equiaxed (25/75), and 0% equiaxed (0/100). This shows that as the amount of platelet powders are increased the amount of initial displacement increases. It is well known that equiaxed alumina powder of this type will pressurelessly sintering to high densities at temperatures above 1600°C.[6, 8, 108] Therefore, it is possible that the equiaxed powder compact is densifying during the heating process and when the load is applied the sample is more resistance to displacement. While the samples with platelets experience less densification and readily deform during the load application. How this might relate to the final densification and optical properties will be discussed in a later section.

At the start of zone 2, a similar tread continues with displacement, however, after some time the 25% equiaxed sample (25/75) starts to experience more displacement than the 0% equiaxed (0/100) sample. Also, at a later time the 75% equiaxed (75/25) sample starts to experience

more displacement than the 50% equiaxed sample. Before zone 3, the order of the sample in terms of lowest displacement to highest are 100% equiaxed, 50% equiaxed, 75% equiaxed, 0% equiaxed, and 25% equiaxed. This change in behavior may be significant, however, it may also be an artifact of the process. The tolerances of the hot-press die have been minimized as much as possible but the use of graphoil can lead to possible 'play' within the system. To add to this, even though the mass of the samples are held constant it is possible to have issues associated with human error when loading the powder into the hot-press die. To see if these behaviors are significant a more in-depth analysis of the displacement rate will need to be discussed.

At the start of zone 3, the samples have reached the maximum pressure and continue to displace during the isothermal temperature and constant applied load for 5hrs, until the final displacement is reached. The lowest to highest displacement order remains the same as that just before zone 3. At this part of the process, the samples are expected to be undergoing what Heuer et al. refers to as 'sinter-forging'. During this isothermal temperature hold the alumina samples are experiencing primary recrystallization followed by a full densification.[14, 58, 114–116]

To get a better understanding of the sintering behavior, it is beneficial to convert the displacement vs time data to a displacement rate. This was done by taking the derivative of the normalized displacement data. A displacement rate vs time plot is shown in Figure 5.2.
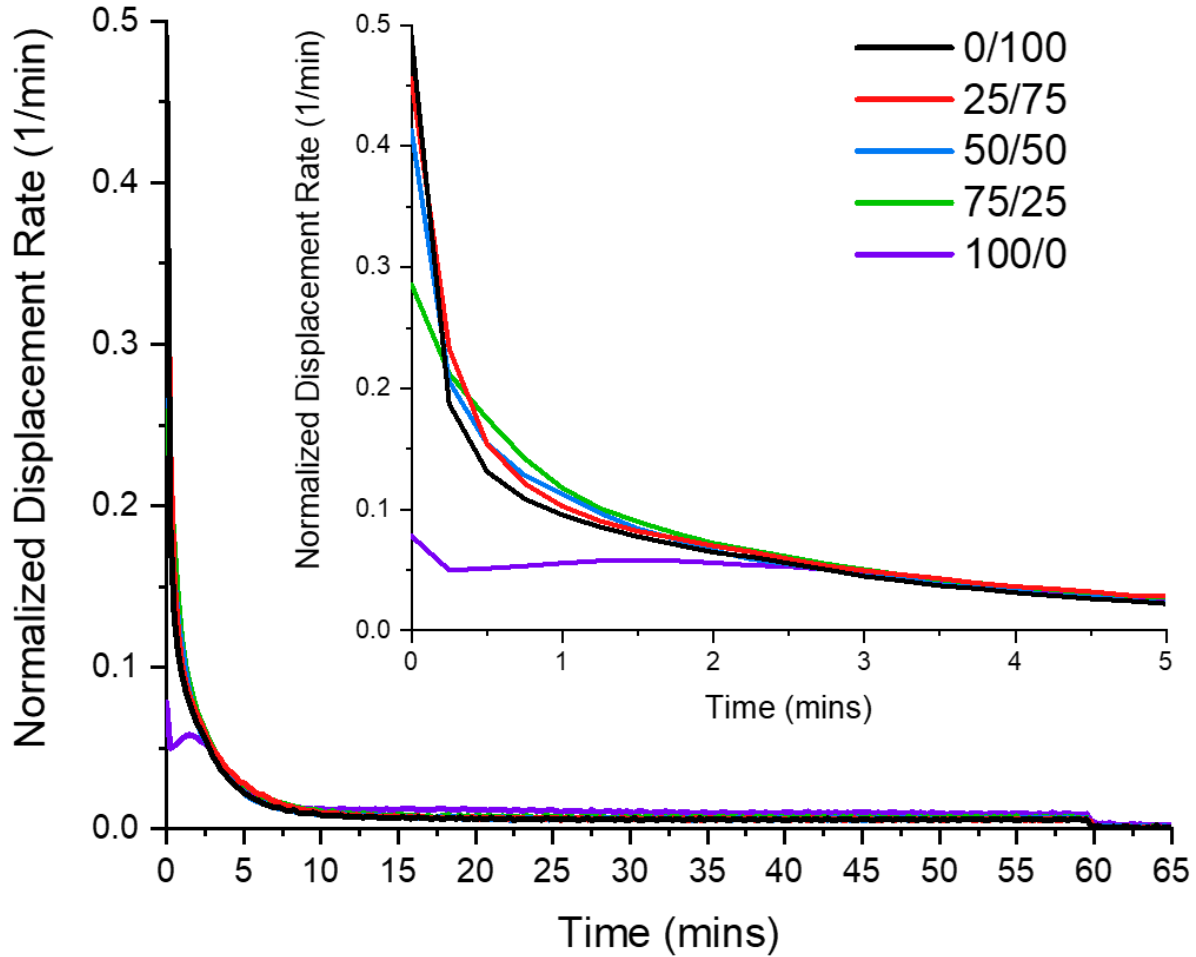
Figure 5.2. Normalized displacement rate vs hot-press time for the powder ratio samples. The initial time corresponds to when a load of 0.1kN is detected.

This data, much like the data presented in the previous literature[58] shows that the samples experience an initial displacement rate that decreases to a constant rate at around 10mins. All samples experienced a similar inflection point at around the same time and the data basically overlaps at around 5mins. This demonstrates that the initial hypothesis stating samples with equiaxed powders may exhibit inflection points at different times or at different loads during the sintering process was incorrect. Based on this observation, the powders in this study will be hot-pressed at a pressure that corresponds to this inflection point. This process will be similar to the previous study that found that hot-pressing at a load that corresponds to this inflection point leads to optimal optical properties.[58] Unpublished results on work that investigated the sintering behavior of pre-aligned and non-pre-aligned samples found that using a maximum pressure within

the range of 15 to 20MPa resulted in samples with the highest optical properties. Based on these results a max pressure of 20MPa was chosen for this study.

Another important feature of this plot is the initial displacement rates for the individual samples. All samples start at different displacement rates during the time of initial loading. The data shows that increasing the amount of equiaxed powders leads to a decrease in the initial displacement rate. This is most likely due to the increases driving force for sintering and densification for the equiaxed powders. As mentioned above, this specific equiaxed alumina powder will pressurelessly sintering to high densities at temperatures above 1600°C.[6, 8, 108] Also, it is well established in the literature that finer powders with higher surface areas will have an increased driving force for sintering.[17] So it is possible that the adding in equiaxed powders is leading to the samples densifying at lower temperatures and this densification is inhibiting the rate at which the powder bed displaces. Work on the densification behavior of pre-aligned and non-pre-aligned powders showed that the platelet powders experience little densification before the load application. This work supports the claim that the platelet powders are not experience the same amount of densification as the equiaxed powder prior to the load application and isothermal temperature hold. This work is presented in a dissertation by Andrew Schlup.

All the samples seem to densify in a similar manner except for the equiaxed powders. The samples with platelet powders all experience a displacement rate that decreases with time. However, this is not the case for the equiaxed powder, since this powder experiences an initial displacement rate followed by a local minimum or plateau. Immediately after this plateau, the displacement rate increases again to a local maximum that is followed by a continuous decrease. This behavior is interesting when compared to the other powder samples. Since this is not a spontaneous change in behavior the sample is most likely plasticly deforming as the load is increased. Again, it seems that the samples have densified and are resisting displacement. Once, a high enough load is applied, the displacement rate increases meaning the samples are densifying or forging. After this increases in displacement rate, the sample then continues a displacement rate similar to the other samples. The possibility of this behavior and how it is connected to the final transparency of the samples will be discussed in the following section.

5.2   Optical Analysis

From the displacement analysis a max pressure of 20MPa was selected and the equiaxed and platelet powder ratios were hot-pressed under these conditions. To gain an understanding of how the processing parameters are impacting the optical performance of the different ratio powders an optical analysis was performed. All samples were polished to transparency under the conditions listed in Section 2.7 to determine the optical properties. A qualitative comparison of the samples was performed by collecting images of each sample placed 2cm above a color scale and text. The optical images of the samples are shown in Figure 5.3.
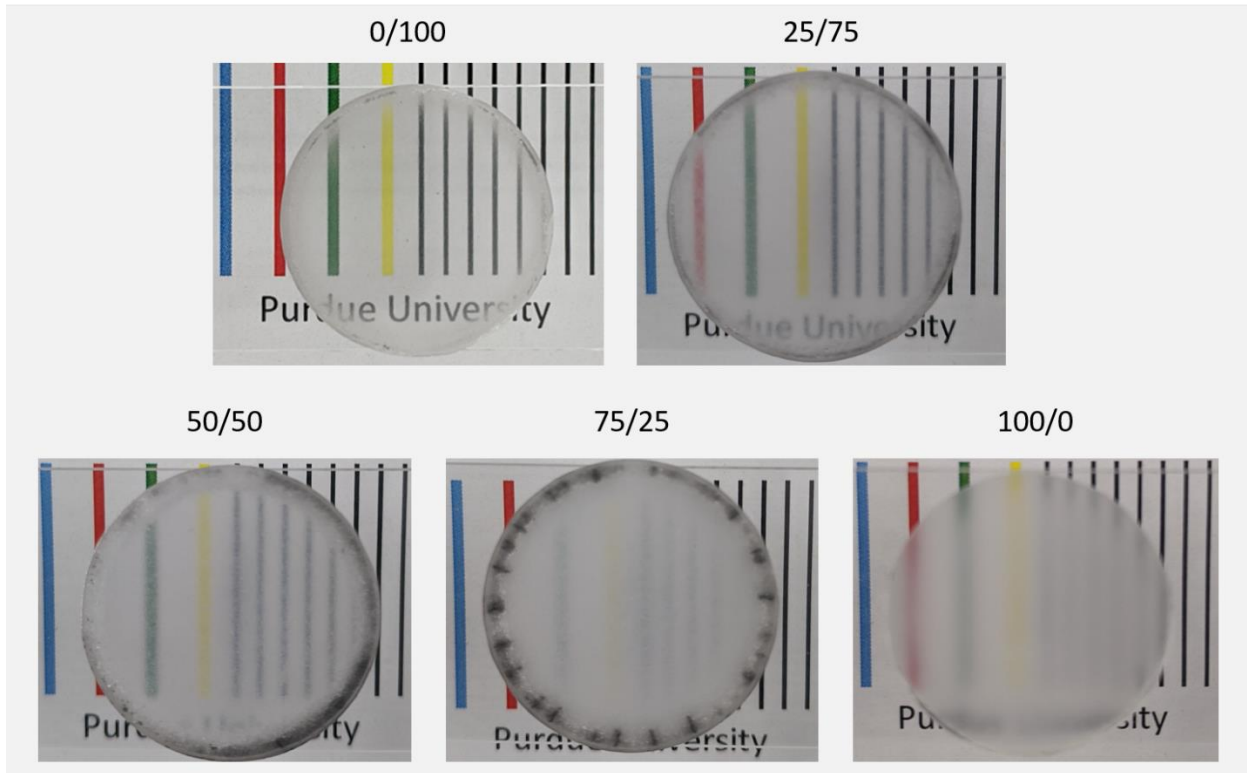
Figure 5.3. Optical images of the different ratio samples. Samples were placed 2cm above the text.

All samples displayed some level of transparency when elevated above the text. It is clear from the images that the 0% equiaxed or platelet sample has the highest transparency and clarity. From this visual analysis, it is clear that the addition of equiaxed powders leads to a decrease in the transparency and an increase in haze. From the images it is hard to tell whether the 75/25 or the 100/0 samples has a lower transparency, however, this will be quantified in the following section. Additionally, discolorations around the edge of the samples that are similar to the ones

found in previous studies was apparent on the 25/75, 50/50, and 75/25 samples.[58] This discoloration was significant for the 50/50 and the 75/25 samples. After removal from the hot-pressing die it seemed that the outer edges of these samples had reacted with the graphoil and die. For the 0/100 sample there seems to be more haze on the edges, but it is significantly less discolored than the other samples. This discoloration is not apparent on the 100/0 sample.

To quantify the optical properties a UV-vis analysis was performed on the samples. Figure 5.4 shows the in-line transmission as a function of wavelength for the ratio powder samples, as well as a single crystal sapphire standard.
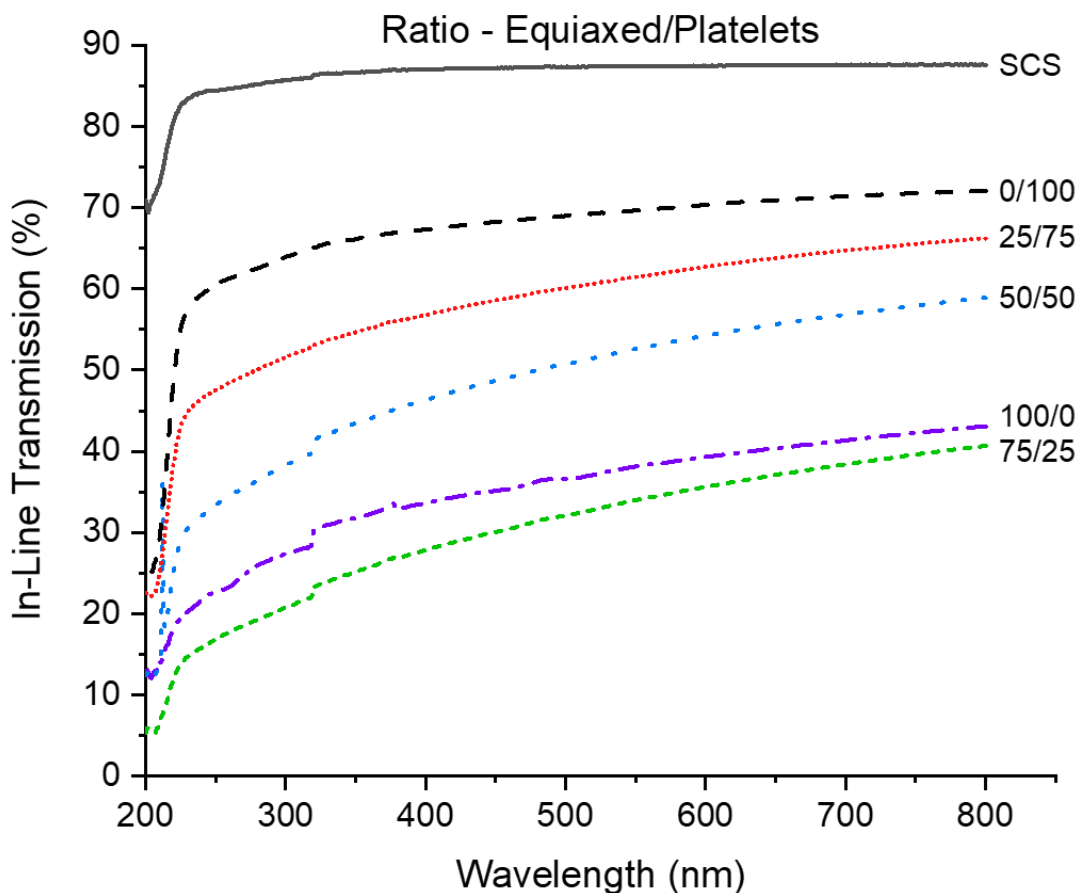
Figure 5.4. UV-vis analysis of non-pre-aligned equiaxed and platelet ratio samples. In-line transmission as a function of wavelength, normalized to t = 0.8mm. A single crystal sapphire (SCS) sample is included for comparison.

The 0/100 or 0% equiaxed sample had the highest in-line transmission values over the visible spectrum when compared to the other ratio powder samples. Similar to the results of the optical images, the addition of equiaxed powders led to a decrease the in-line transmission. In the

above optical images, it is difficult to determine whether the 75/25 or the 100/0 had lower optical properties. The in-line transmission data shows that the 100% equiaxed samples had significantly higher (~7-9%) in-line transmission in the lower wavelength region (200-600nm) than the 75% equiaxed sample. Toward the higher wavelength (>700nm) this difference decreases to roughly 3%.

Also, the data shows that the curve 'flattens' or displays a more homogenous behavior over the entire optical spectrum as the platelet powder content is increased. This is similar to the behavior that was discussed in previous literature.[58] This behavior is explained by the Rayleigh-Gans-Debye theory,[7] which is shown Equation 15:

$$T_{ILT} = (1 - R_s)\exp\left(\frac{-3\pi^2 r^2 \Delta n^2 d}{\lambda_0^2}\right) \qquad 15$$

Where r is the grain size, Δn is refractive index mismatch, d sample thickness, and λ_0 the wavelength. This theory explains that in-line transmission will increase with smaller grain sizes and lower refractive index mismatch, and will decrease at lower wavelengths.[7] It is important to note that, the refractive index mismatch has a much greater effect on the in-line trans-mission because it varies to the second power compared to the first power for the grain size. In the previous study,[58] it was concluded that since the platelet alumina samples had such a large grain size, the high and relatively homogeneous in-line transmission must mean that the refractive index mismatch is low. As previously mentioned, a low refractive index mismatch is related to high crystallographic orientation.[5–7] This implied that the samples must have some degree of alignment and this theory was supported with a simple qualitative X-ray diffraction based texture analysis that is shown in Figure 3.6. This previous analysis showed that the hot-pressing of platelet morphology alumina is leading to samples with increased crystallographic alignment over samples produced with equiaxed alumina. Applying this logic to the current data, shows that the addition of platelet powders leads to higher grain alignment. This higher grain alignment is leading to more homogeneous in-line transmission across the visible spectrum and increased optical properties. However, a more in-depth analysis of the different loss mechanisms will provide more information on the optical behavior.

Figure 5.5 shows the light transmission and optical loss mechanisms at 645nm for the ratio powder samples, as well as a single crystal sapphire standard.
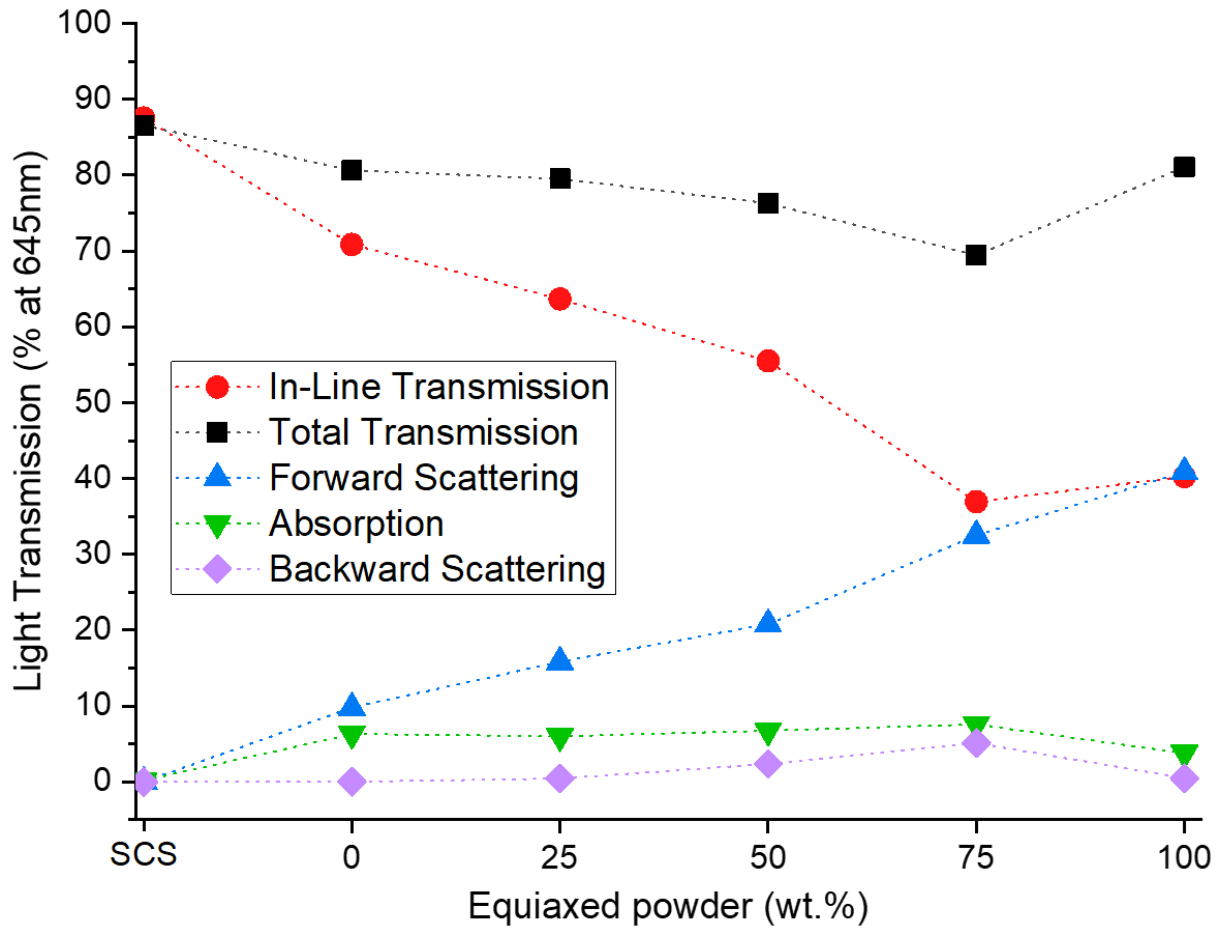
Figure 5.5. Light transmission at 645nm vs. powder ratio. All samples were normalized to a thickness of 0.8mm. A single crystal sapphire (SCS) sample is included for comparison.

The optical loss mechanisms for transparent ceramics are absorption, backward scattering, and forward scattering. As mentioned before, absorption losses in polycrystalline alumina are caused by secondary phases.[7, 58] The data shows that all the hot-pressed ratio sample with platelet additions have similar adsorption values. However, the 100% equiaxed sample does display a slightly lower adsorption value when compared to the sample with platelet additions. This behavior is most likely due to the lower purity of the platelet powders when compared to the equiaxed powders. As stated in Section 2.2.1, the purity of the equiaxed powder is 99.99% and the platelet powder 99.8%. It is possible that the impurities in the platelet powder are leading to increased absorption losses in the final samples.

Backward scattering losses are due to residual porosity within the matrix.[7, 58] The data shows that the backwards scattering losses marginally increase as the amount of equiaxed powders increase. This means that the addition of equiaxed powders in decreasing the density of the samples. At the moment this data has yet to be supported with a density analysis but should be in future work. Connecting this data to the displacement rate data for platelet samples, shows that samples that had the highest initial displacement rates have the lowest backwards scattering values, meaning that the porosity has been minimized. It seems samples that experience the higher displacements and displacement rate lead to samples with lower porosity and higher optical properties. Meaning that there is most likely an optimum temperature at which the max pressure needs to be applied for the different samples since it was proposed that samples with equiaxed powder are experiencing densification prior to the load application. Doing so could lead to higher densities and higher optical properties. It is also interesting to note that this backwards scattering data provides a reason for the 75% equiaxed samples having lower in-line transmission values than the 100% equiaxed samples. This is due to the increased backwards scattering mechanisms, meaning that the 100% equiaxed sample is denser than the 75% equiaxed sample.

Forward scattering losses are due to differences in the refractive index and these differences are caused by either residual porosity or grain misalignment.[7] The data shows, that as equiaxed powders are added the ratio samples the forward scattering losses increases. A small portion of these losses will be due to the aforementioned porosity. However, the remaining losses will be due to grain misalignment. As mentioned in previous studies,[58, 105] the use of platelet morphology powders leads to final sintered samples with a higher degree of crystallographic alignment compared to equiaxed powders. The ability to align the platelet leads to a reduction in the forwards scattering losses and increases the optical properties of the samples. The previous studies,[58, 105] only looked at the use of 100% platelet powders. Prior to this study, substituting equiaxed powders into the platelet powder compact has yet to be characterized under the optimized hot-pressing conditions. Form the forward scattering data, it is clear that these samples are becoming less aligned as the percentage of equiaxed powders increases. To support this observation a quantitative texture analysis was preformed.

5.3   Texture Analysis

Similar to the previous texture analysis, the orientation parameter (r) and grain misalignment angle (full width at half maximum (FWHM)) were obtained from a rocking curve analysis and these values are listed in Table 5.1. A lower orientation parameter (r) and lower FWHM are associated with higher alignment. For this analysis, the alignment reference plane was normal to the hot-pressing direction. Six separate rocking curve analysis were conducted on each sample to obtain an average r and FWHM. A texture analysis was not performed on the 100% equiaxed powder sample since the intensities of basal plane peaks from randomly oriented or equiaxed alumina (0006 and 000.12) are intrinsically weak, making the correction factor susceptible to noise and background errors.[29, 30]

Table 5.1. Texture distribution data for sintered powder ratio samples. The orientation parameter (r) obtained from curve fits of the March-Dollase equation. The 95% confidence interval for the orientation parameter and FWHM are shown for each sample having a data population of 6.

Sample ID (equiaxed/platelet)	Orientation parameter (r)			FWHM [^{0}]			R^2	Density (%TD)	Grain size (μm)
0/100	0.321	+/-	0.005	16.26	+/-	0.40	.982	99.79	52.1
25/75	0.385	+/-	0.005	21.96	+/-	0.32	.985	--	--
50/50	0.411	+/-	0.014	23.64	+/-	0.98	.973	--	--
75/25	0.509	+/-	0.022	34.63	+/-	2.61	.961	--	--
100/0	--	+/-	--	--	+/-	--	--	--	--

Figure 5.6 shows the average orientation parameter (r) vs. wt.% equiaxed powders. It is clear that as the amount of equiaxed powders are increased the orientation parameter increases and therefore the alignment decreases. This trend is in agreement and supports the forward scattering behavior observed above.
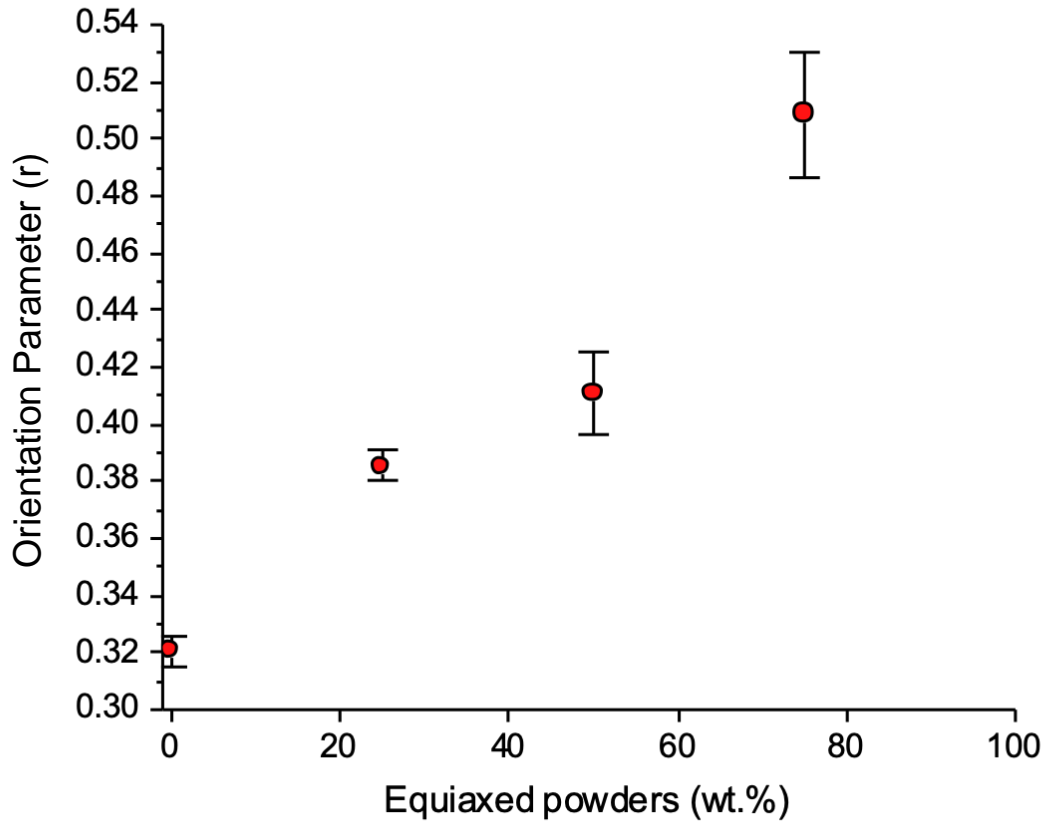
Figure 5.6. Orientation parameter (r) vs. wt.% equiaxed powders. The 95% confidence intervals for the orientation parameter are shown for each sample having a data population of 6.

It was initially expected that the sintered samples would behave similar to templated grain growth samples.[9–11, 25–27] Meaning that the platelets would template the equiaxed matrix and result in an aligned microstructure. However, it is not clear if this is happening and a closer look at the microstructure will better characterize the sample. Relating this alignment behavior back to the displacement rate data, shows that samples that have a higher initial displacement rate have higher alignment. As explained above, it is possible that the equiaxed powders are sintering before a load is applied. This is most apparent for the 100% equiaxed powder sample were there are inflections in the data indicating that the powder compact was resistance to deformation. The addition of equiaxed powder may be inhibiting the alignment of the powders by 'locking' in the initial randomly aligned microstructure before the load is applied. It is possible that the application of the load is where the sample gains a considerable amount of alignment and a current study by Schlup

et al. is investigating this alignment behavior and the results are showing that the platelet powders are gaining a considerable amount of alignment during the load application. This work is explained in a dissertation by Andrew Schlup. Applying the load at a lower temperature prior to densification may result in more alignment and increased optical properties.

The 75% equiaxed powders sample had a significantly low grain alignment with an orientation parameter and FWHM of 0.509 ± 0.022 and 34.63° ± 2.61°, respectively. As a comparison, samples from the previous study in Section 4 that were casted (should experience little pre-alignment) from 80wt.% equiaxed alumina suspensions had a significantly higher alignment when compared to this sample. The orientation parameter and FWHM of the casted sample was 0.435 ± 0.019 and 26.62° ± 2.05°, respectively. It is important to note, that these sample were sintered under a different sintering profile. The maximum temperature was higher, and the pressure was applied at a lower temperature. This data supports the hypothesis that the samples in the current study were not sintered under optimized parameters for equiaxed powders. It is possible that the casting process allowed for some amount of alignment over the powder compact process, however, the difference in FWHM between these samples is significant. Further investigation into the sintering behavior will need to be conducted to find if the load application temperature results impacts the final sintered alignment. From the data, it seems that it would be beneficial to continue to modify theses previously applied parameters in future studies.

5.4   Summary and Conclusions

The addition of equiaxed powders into platelet ceramic-filled thermoplastic blends could significantly increases the rheological properties possibly leading to an increase in the alignment during uniaxial pressing. However, before these blends are developed the sintering behavior of hot-pressed equiaxed and platelet powders were investigated. An initial sintering investigation paired with current work by Schlup et al. identified the optimum maximum hot-pressing pressure to be 20Mpa. The effects of 0, 25, 50, 75, and 100wt.% equiaxed powder additions on the sintering behavior, optical properties, and grain alignment were investigated. This analysis found that an increase in the amount of equiaxed powders decreased the initial powder compact displacements rate which impacted the finally grain alignment and optical properties. An increase in the wt.% equiaxed powders from 0wt% to 75wt% decreases the in-line transmission from 70.9% to 40.2%, respectively at 645nm. Additionally, the optical loss analysis showed that the addition of equiaxed

102

powders lead to increases in the backwards scattering which is indicative of residual porosity. Additionally, an increase in the wt.% equiaxed powders from 0wt% to 75wt decreased the alignment from ($r = 0.321 \pm 0.005$; FWHM = $16.26^{\circ} \pm 0.40^{\circ}$) to ($r = 0.509 \pm 0.022$; FWHM = $34.63^{\circ} \pm 2.61^{\circ}$), respectively. It is clear that under these hot-pressing conditions that the use of equiaxed powders is detrimental to the optical properties and grain alignment. However, the hot-pressing displacement rate data and backwards scattering data suggest that samples with equiaxed powders may need different sintering parameters to further optimize the densities and alignment. It seems that samples with equiaxed additions are sintering before the hot-pressing load is applied. This could be inhibiting the powder compact from deforming and aligning the platelet powders. Further analysis of the microstructure could provide information on this behavior. Additionally, a more in-depth sintering analysis could lead to more optimized sintering parameters. Lastly, the use of the pre-alignment process could be used to align these powders alleviating the issues with pre-sintering before the load is applied.

REFERENCES

1   A. Krell, J. Klimke, and T. Hutzler, "Transparent compact ceramics: Inherent physical issues," *Opt. Mater. (Amst).*, **31** [8] 1144–1150 (2009).

2   A. Krell, J. Klimke, and T. Hutzler, "Advanced spinel and sub-um Al2O3 for transparent armour applications," *J. Eur. Ceram. Soc.*, **29** [2] 275–281 (2009).

3   D.C. Harris, L.F. Johnson, L.R. Cambrea, L. Baldwin, M. Baronowski, D.E. Zelmon, W.B. Poston, J.D. Kunkel, *et al.*, "Refractive index of infrared-transparent polycrystalline alumina," *Opt. Eng.*, **56** [7] 077103-1–11 (2017).

4   J.G.J. Peelen, "Transparent hot-pressed alumina. II Transparent versus translucent alumina," *Ceramurg. Int.*, **5** [3] 115–119 (1979).

5   X. Mao, S. Wang, S. Shimai, and J. Guo, "Transparent polycrystalline alumina ceramics with orientated optical axes," *J. Am. Ceram. Soc.*, **91** [10] 3431–3433 (2008).

6   H. Yi, X. Mao, G. Zhou, S. Chen, X. Zou, S. Wang, and S. Shimai, "Crystal plane evolution of grain oriented alumina ceramics with high transparency," *Ceram. Int.*, **38** [7] 5557–5561 (2012).

7   R. Apetz and M.P.B. Van Bruggen, "Transparent alumina; A light-scattering model," *J. Am. Ceram. Soc.*, **86** [3] 480–486 (2003).

8   P. Liu, H. Yi, G. Zhou, J. Zhang, and S. Wang, "HIP and pressureless sintering of transparent alumina shaped by magnetic field assisted slip casting," *Opt. Mater. Express*, **5** [2] 441–46 (2015).

9   R.L. Walton, M.D. Vaudin, A.K. Hofer, E.R. Kupp, R.J. Meyer, and G.L. Messing, "Tailoring particle alignment and grain orientation during tape casting and templated grain growth," *J. Am. Ceram. Soc.*, **102** [5] 2405–2414 (2019).

10   M.M. Seabaugh, G.L. Messing, and M.D. Vaudin, "Texture Development and Microstructure Evolution in Liquid-Phase-Sintered α-Alumina Ceramics Prepared by Templated Grain Growth," *J. Am. Ceram. Soc.*, **83** [12] 3109–3116 (2000).

11   M.M. Seabaugh, M.D. Vaudin, J.P. Cline, and G.L. Messing, "Comparison of Texture Analysis Techniques for Highly Oriented α-Al2O3," *J. Am. Ceram. Soc.*, **83** [8] 2049–2054 (2000).

[12]   D. Kovar, B.H. King, R.W. Trice, and J.W. Halloran, "Fibrous Monolithic Ceramics," *J. Am. Ceram. Soc.*, **80** [10] 2471–2487 (1997).

[13]   R.W. Trice and J.W. Halloran, "Investigation of the Physical and Mechanical Properties of Hot-Pressed Boron Nitride/Oxide Ceramic Composites," *J. Am. Ceram. Soc.*, **82** [9] 2563–2565 (1999).

[14]   A.H. Heuer, D.J. Sellers, and W.H. Rhodes, "Hot-Working of Aluminum Oxide: I, Primary Recrystallization and Texture," *J. Am. Ceram. Soc.*, **52** [9] 468–474 (1969).

[15]   X. Wu and I. Chen, "Exaggerated Texture and Grain Growth in a Supperplastic SiAlON," *J. Am. Ceram. Soc.*, **75** [10] 2733–2741 (1992).

[16]   T. Takenaka, H. Noda, A. Yoneda, and K. Sakata, "Grain orientation effects on superconducting properties of hot-forged oxide ceramics," *Ferroelectrics*, **102** [1] 329–336 (1990).

[17]   J.S. Reed, *Introduction to the principles of ceramic processing*. Wiley, New York, 1988.

[18]   D. Brandon, D. Chen, and H. Chan, "Control of texture in monolithic alumina," *Mater. Sci. Eng. A*, **195** [C] 189–196 (1995).

[19]   M. Jabbari, R. Bulatova, A.I.Y. Tok, C.R.H. Bahl, E. Mitsoulis, and J.H. Hattel, "Ceramic tape casting: A review of current methods and trends with emphasis on rheological behaviour and flow analysis," *Mater. Sci. Eng. B Solid-State Mater. Adv. Technol.*, **212** 39–61 (2016).

[20]   H. Watanabe, T. Kimura, and T. Yamaguchi, "Particle Orientation During Tape Casting in the Fabrication of Grain-Oriented Bismuth Titanate," *J. Am. Ceram. Soc.*, **72** [2] 289–293 (1989).

[21]   S.Y. Lienard, D. Kovar, R.J. Moon, K.J. Bowman, and J.W. Halloran, "Texture development in Si 3 N 4 /BN fibrous monolithic ceramics," **3** [52] 3365–3371 (n.d.).

[22]   L. Zhang, J. Vleugels, and O. Van Der Biest, "Fabrication of textured alumina by orienting template particles during electrophoretic deposition," *J. Eur. Ceram. Soc.*, **30** 1195–1202 (2010).

[23]   S. Behr, U. Vainio, M. Müller, A. Schreyer, and G.A. Schneider, "Large-scale parallel alignment of platelet-shaped particles through gravitational sedimentation," *Nat. Publ. Gr.*, (2015).

24   T.S. Suzuki, T. Uchikoshi, and Y. Sakka, "Control of texture in alumina by colloidal processing in a strong magnetic field," *Sci. Technol. Adv. Mater.*, (2006).

25   E. Suvaci, M.M. Seabaugh, and G.L. Messing, "Reaction-based Processing of Textured Alumina by Templated Grain Growth," *J. Eur. Ceram. Soc.*, **19** [13–14] 2465–2474 (1999).

26   M.D. Snel, J. van Hoolst, A.M. de Wilde, M. Mertens, F. Snijkers, and J. Luyten, "Influence of tape cast parameters on texture formation in alumina by templated grain growth," *J. Eur. Ceram. Soc.*, **29** [13] 2757–2763 (2009).

27   R.J. Pavlacka and G.L. Messing, "Processing and mechanical response of highly textured Al2O3," *J. Eur. Ceram. Soc.*, **30** [14] 2917–2925 (2010).

28   J.A. Horn, S.C. Zhang, U. Selvaraj, G.L. Messing, and S. Trolier-McKinstry, "Templated grain growth of textured bismuth titanate," *J. Am. Ceram. Soc.*, **82** [4] 921–926 (1999).

29   M.D. Vaudin, M.W. Rupich, M. Jowett, G.N. Riley, and J.F. Bingert, "A method for crystallographic texture investigations using standard x-ray equipment," *J. Mater. Res.*, **13** [10] 2910–2919 (1998).

30   M.D. Vaudin, "Measurement of Axisymmetric Crystallographic Texture | NIST," *Spec. Publ. (NIST SP)*, (2009).

31   Y.T. Chou, Y.T. Ko, and M.F. Yan, "Fluid Flow Model for Ceramic Tape Casting," *J. Am. Ceram. Soc.*, **70** [10] C-280-C-282 (1987).

32   N.G. McCrum, C.P. Buckley, and C.B. Bucknall, *Principles of Polymer Engineering*, 2nd ed. Oxford Universtiy Press, New York, 1997.

33   A.P. Singh and A.D. Rey, "Computer simulation of dynamics and morphology of discotic mesophases in extensional flows," *Liq. Cryst.*, **18** [2] 219–230 (1995).

34   M.S.N. Oliveira, M.A. Alves, F.T. Pinho, and G.H. McKinley, "Viscous flow through microfabricated hyperbolic contractions," *Exp. Fluids*, **43** [2–3] 437–451 (2007).

35   G.B. Jeffery, "The Motion of Ellipsoidal Particles Immersed in a Viscous Fluid," *Proc. R. Soc. A Math. Phys. Eng. Sci.*, **102** [715] 161–179 (1922).

36   C.L. Tucker and S.G. Advani, "Processing of Short-Fiber Systems;" pp. 151–164 in *Flow Rheol. Polym. Compos. Manuf.* Edited by B. Pipes. Elisevier, 1994.

37   F. Folgar and C.L. Tucker, "Orientation Behavior of Fibers in Concentrated Suspensions," *J. Reinf. Plast. Compos.*, **3** [2] 98–119 (1984).

38   P.M. Raj, S.M. Dunn, and W.R. Cannon, "Measurement of Particle Orientation in Tape Cast Ceramic Microstructures," **10** [I] 33–51 (1998).

39   Z. Fu and A. Roosen, "Shrinkage of tape cast products during binder burnout," *J. Am. Ceram. Soc.*, **98** [1] 20–29 (2015).

40   D.S. Park and C.W. Kim, "Modification of tape casting for aligning the whiskers," *J. Mater. Sci.*, **34** [23] 5827–5832 (1999).

41   H.J. Kim, M.J.M. Krane, K.P. Trumble, and K.J. Bowman, "Analytical fluid flow models for tape casting," *J. Am. Ceram. Soc.*, **89** [9] 2769–2775 (2006).

42   Z. Luo, Z. Lv, D. Jiang, J. Zhang, Z. Chen, and Z. Huang, "Aqueous tape casting of boron carbide ceramic," *Ceram. Int.*, **39** [2] 2123–2126 (2013).

43   M.N. Rahaman, *Ceramic processing and sintering, second edition*. CRC Press, 2017.

44   A. Wonisch, P. Polfer, T. Kraft, A. Dellert, A. Heunisch, and A. Roosen, "A comprehensive simulation scheme for tape casting: From flow behavior to anisotropy development," *J. Am. Ceram. Soc.*, **94** [7] 2053–2060 (2011).

45   A.M. Knapp and J.W. Halloran, "Characterization of Thermoplastic Blends as Binders for Ceramics," *J. Am. Ceram. Soc.*, **89** [10] 3010–3018 (2006).

46   P. Zhou, P. Hu, X. Zhang, and W. Han, "Laminated ZrB2-SiC ceramic with improved strength and toughness," *Scr. Mater.*, **64** [3] 276–279 (2011).

47   Y.-H. Koh, H.-W. Kim, H.-E. Kim, and J.W. Halloran, "Thermal shock resistance of fibrous monolithic Si3N4/BN ceramics," *J. Eur. Ceram. Soc.*, **24** [8] 2339–2347 (2004).

48   W.G. Fahrenholtz, G.E. Hilmas, A.L. Chamberlain, and J.W. Zimmermann, "Processing and characterization of ZrB2-based ultra-high temperature monolithic and fibrous monolithic ceramics," *J. Mater. Sci.*, **39** [19] 5951–5957 (2004).

49   R.W. Trice and E.B. Pickens, "Alternatives to hot-pressing silicon nitride-boron nitride fibrous monolith composites;" in *Innov. Process. Synth. Ceram. Glas. Compos. VII*. 2012.

50   G. Hilmas, A. Brady, U. Abdali, G. Zywicki, and J. Halloran, "Fibrous monoliths: non-brittle fracture from powder-processed ceramics," *Mater. Sci. Eng. A*, **195** [C] 263–268 (1995).

51   X. Xu and G.E. Hilmas, "The rheological behavior of ceramic/polymer mixtures for coextrusion processing," *J. Mater. Sci.*, **42** [4] 1381–1387 (2007).

52 Y.H. Koh, J.W. Halloran, G. Kiziltas, D. Psychoudakis, and J. Volakis, "Thermoplastic green machining for textured dielectric substrate for broadband miniature antenna," *J. Am. Ceram. Soc.*, **88** [2] 297–302 (2005).

53 A.M. Knapp and J.W. Halloran, "Binder Removal from Ceramic-Filled Thermoplastic Blends," *J. Am. Ceram. Soc.*, **89** [9] 2776–2781 (2006).

54 D. Kovar, M.D. Thouless, and J.W. Halloran, "Crack Deflection and Propagation in Layered Silicon Nitride/Boron Nitride Ceramics," *J. Am. Ceram. Soc.*, **81** [4] 1004–1112 (2005).

55 S.Y. Lienard, D. Kovar, R.J. Moon, K.J. Bowman, and J.W. Halloran, "Texture development in Si3N4/BN fibrous monolithic ceramics," *J. Mater. Sci.*, **35** [13] 3365–3371 (2000).

56 M. Okamoto, P.H. Nam, P. Maiti, T. Kotaka, T. Nakayama, M. Takada, M. Ohshima, A. Usuki, *et al.*, "Biaxial Flow-Induced Alignment of Silicate Layers in Polypropylene/Clay Nanocomposite Foam," *Nano Lett.*, **1** [9] 503–505 (2001).

57 A. Karnis, H.L. Goldsmith, and S.G. Mason, "The kinetics of flowing dispersions. I. Concentrated suspensions of rigid particles," *J. Colloid Interface Sci.*, **22** [6] 531–553 (1966).

58 A.P. Schlup, W.J. Costakis, W. Rheinheimer, R.W. Trice, and J.P. Youngblood, "Hot-Pressing Platelet Alumina to Transparency," *J. Am. Ceram. Soc.*, jace.16932 (2019).

59 B. Susmita, V. Sahar, K. Dongxu, and A. Bandyopadhyay, "Additive Manufacturing of Ceramics;" pp. 143–184 in *Addit. Manuf.* CRC Press, 2015.

60 J.N. Stuecker, J. Cesarano, and D.A. Hirschfeld, "Control of the viscous behavior of highly concentrated mullite suspensions for robocasting," *J. Mater. Process. Technol.*, **142** [2] 318–325 (2003).

61 B.H. King, S.L. Morissette, H. Denham, J. Cesarano, and D. Dimos, "Influence of rheology on deposition behavior of ceramic pastes in direct fabrication systems," *Solid Free. Fabr. Proceedings, August*, 391–398 (1998).

62 J.A. Lewis and G.M. Gratson, *Direct writing in three dimensions*, *Mater. Today*, **7** [7] 32–39 (2004).

63 J. Cesarano, *A Review of Robocasting Technology*, *MRS Proc.*, **542** (1998).

64 J.A. Lewis, J.E. Smay, J. Stuecker, and J. Cesarano, "Direct Ink Writing of Three-Dimensional Ceramic Structures," *J. Am. Ceram. Soc.*, **89** [12] 3599–3609 (2006).

65 L. Rueschhoff, W. Costakis, M. Michie, J. Youngblood, and R. Trice, "Additive Manufacturing of Dense Ceramic Parts via Direct Ink Writing of Aqueous Alumina Suspensions," *Int. J. Appl. Ceram. Technol.*, **13** [5] 821–830 (2016).

66 W.J. Costakis, L.M. Rueschhoff, A.I. Diaz-Cano, J.P. Youngblood, and R.W. Trice, "Additive manufacturing of boron carbide via continuous filament direct ink writing of aqueous ceramic suspensions," *J. Eur. Ceram. Soc.*, **36** [14] 3249–3256 (2016).

67 J. Cesarano and I.A. Aksay, "Processing of Highly Concentrated Aqueous alpha-Alumina Suspensions Stabilized with Polyelectrolytes," *J. Am. Ceram. Soc.*, **71** [12] 1062–1067 (1988).

68 G. Franchin, L. Wahl, and P. Colombo, "Direct ink writing of ceramic matrix composite structures," *J. Am. Ceram. Soc.*, **100** [10] 4397–4401 (2017).

69 B.G. Compton and J.A. Lewis, "3D-printing of lightweight cellular composites," *Adv. Mater.*, **26** [34] 5930–5935 (2014).

70 M. Acosta, V.L. Wiesner, C.J. Martinez, R.W. Trice, and J.P. Youngblood, "Effect of Polyvinylpyrrolidone Additions on the Rheology of Aqueous, Highly Loaded Alumina Suspensions," *J. Am. Ceram. Soc.*, **96** [5] 1372–1382 (2013).

71 V.L. Wiesner, "Fabricating Complex-Shaped Components by Room-Temperature Injection Molding of Aqueous Ceramic Suspension Gels;" Purdue University, 2013.

72 R.W. Trice and J.W. Halloran, "Influence of microstructure and temperature on the interfacial fracture energy of silicon nitride/boron nitride fibrous monolithic ceramics," *J. Am. Ceram. Soc.*, **82** [9] 2502–2508 (1999).

73 R.W. Trice and J.W. Halloran, "Effect of Sintering Aid Composition on the Processing of Si3N4/BN Fibrous Monolithic Ceramics," *J. Am. Ceram. Soc.*, **82** [11] 2943–2947 (1999).

74 M.M.H. Kuroda and C.E. Scott, "Blade geometry effects on initial dispersion of chopped glass fibers," *Polym. Compos.*, **23** [5] 828–838 (2002).

75 J.E. Goodrich and R.S. Porter, "A rheological interpretation of torque-rheometer data," *Polym. Eng. Sci.*, **7** [1] 45–51 (1967).

76 D.R. Beeaff and G.E. Hilmas, "Rheological behavior of coextruded multilayer architectures," *J. Mater. Sci.*, **37** [6] 1259–1264 (2002).

77   M. Bousmina, A. Ait-Kadi, and J.B. Faisant, "Determination of shear rate and viscosity from batch mixer data," *J. Rheol. (N. Y. N. Y).*, **43** [2] 415–433 (2002).

78   L.L. Blyler and J.H. Daane, "An analysis of Brabender torque rheometer data," *Polym. Eng. Sci.*, **7** [3] 178–181 (1967).

79   A. Marquez, J. Quijano, and M. Gaulin, "A calibration technique to evaluate the power-law parameters of polymer melts using a torque-rheometer," *Polym. Eng. Sci.*, **36** [20] 2556–2563 (1996).

80   C.R. Santi, E. Hage, C.A. Correa, and J. Vlachopoulos, "Torque viscometry of molten polymers and composites," *Appl. Rheol.*, **19** [1] (2009).

81   W.H. Herschel and R. Bulkley, "Measurement of consistency as applied to rubber-benzene solutions," *Proc ASTM Part II*, **26** [82] 621–629 (1926).

82   M.D. Vaudin, *TexturePlus / NIST*, *Natl. Inst. Stand. Technol. Ceram. Div. Gaithersburg, MD*, (2001).

83   Y. Chang, S. Poterala, D. Yener, and G.L. Messing, "Fabrication of highly textured fine-grained α-alumina by templated grain growth of nanoscale precursors," *J. Am. Ceram. Soc.*, **96** [5] 1390–1397 (2013).

84   A. Krell, P. Blank, H. Ma, T. Hutzler, M.P.B. Van Bruggen, and R. Apetz, "Transparent sintered corundum with high hardness and strength," *J. Am. Ceram. Soc.*, **86** [1] 12–18 (2003).

85   A. Pringuet, T. Takahashi, S. Baba, Y. Kamo, Z. Kato, K. Uematsu, S. Tanaka, and K. Lu, "Fabrication of Transparent Grain-Oriented Polycrystalline Alumina by Colloidal Processing," *J. Am. Ceram. Soc.*, **99** [10] 3217–3219 (2016).

86   "Designation: C693 − 93 (Reapproved 2013) Standard Test Method for Density of Glass by Buoyancy 1," (n.d.).

87   R.J. Young, *Introduction to polymers*, 2nd ed. CRC Press, Boca Raton: London, 1991.

88   M. Gilbert, "Relation of Structure to Thermal and Mechanical Properties;" pp. 59–73 in *Brydson's Plast. Mater. Eighth Ed.* Butterworth-Heinemann, 2016.

89   I.M. Krieger and T.J. Dougherty, "A Mechanism for Non-Newtonian Flow in Suspensions of Rigid Spheres," *Trans. Soc. Rheol.*, **3** [1] 137–152 (1959).

90   Malvern, *Investigating the Impact of Particle Characteristics on Suspension Rheology*. 2017.

91 B.D. Lubachevsky and F.H. Stillinger, "Geometric properties of random disk packings," *J. Stat. Phys.*, **60** [5–6] 561–583 (1990).

92 R.L. Coble, "Diffusion Models for Hot Pressing with Surface Energy and Pressure Effects as Driving Forces," *J. Appl. Phys.*, **41** [12] 4798–4807 (1970).

93 A. M'Barki, L. Bocquet, and A. Stevenson, "Linking Rheology and Printability for Dense and Strong Ceramics by Direct Ink Writing," *Sci. Rep.*, **7** [1] 6017 (2017).

94 J.E. Smay, J. Cesarano, and J.A. Lewis, "Colloidal Inks for Directed Assembly of 3-D Periodic Structures," *Langmuir*, **18** [14] 5429–5437 (2002).

95 T.F. Tadros, *Rheology of Dispersions: Principles and Applications*. 2010.

96 H.B. Denham, J. Cesarano, B.H. King, and P. Calvert, "Mechanical behavior of robocast alumina," *Solid Free. Fabr. Proceedings, August*, 589–596 (1998).

97 V.L. Wiesner, L.M. Rueschhoff, A.I. Diaz-Cano, R.W. Trice, and J.P. Youngblood, "Producing dense zirconium diboride components by room-temperature injection molding of aqueous ceramic suspensions," *Ceram. Int.*, **42** [2] 2750–2760 (2016).

98 M. Subbanna and S.. Malghan, "Shear yield stress of flocculated alumina–zirconia mixed suspensions," *Chem. Eng. Sci.*, **53** [17] 3073–3079 (1998).

99 S.L. Morissette, J.A. Lewis, J. Cesarano, D.B. Dimos, and T. Baer, "Solid Freeform Fabrication of Aqueous Alumina-Poly(vinyl alcohol) Gelcasting Suspensions," *J. Am. Ceram. Soc.*, **83** [10] 2409–2416 (2004).

100 S. Liu and J.H. Masliyah, "Suspensions: Fundamentals and Applications in the Petroleum Industry;" pp. 107–176 in *Rheol. Suspens.* 2009.

101 G.M. Channell and C.F. Zukoski, "Shear and compressive rheology of aggregated alumina suspensions," *AIChE J.*, **43** [7] 1700–1708 (1997).

102 J.I. Cesarano, T.A. Baer, and P. Calvert, *Recent developments in freeform fabrication of dense ceramics from slurry deposition*. Albuquerque, NM, and Livermore, CA (United States), 1997.

103 T.G. Mezger, *The rheology handbook : for users of rotational and oscillatory rheometers*. Vincentz Network, 2006.

104 Anton Paar GmbH, *Amplitude sweeps*, *https://wiki.anton-paar.com/en/amplitude-sweeps/*, (n.d.).

105   W.J. Costakis, A. Schlup, J.P. Youngblood, and R.W. Trice, "Aligning α-alumina platelets via uniaxial pressing of ceramic-filled polymer blends for improved sintered transparency," *J. Am. Ceram. Soc.*, **103** [6] 3500–3512 (2020).

106   Y. Sakka, T.S. Suzuki, and T. Uchikoshi, "Fabrication and some properties of textured alumina-related compounds by colloidal processing in high-magnetic field and sintering," *J. Eur. Ceram. Soc.*, (2008).

107   T. Uchikoshi, T.S. Suzuki, and Y. Sakka, "Crystalline orientation of alumina ceramics prepared by electrophoretic deposition under a high magnetic field;" pp. 8074–8078 in *J. Mater. Sci.* 2006.

108   L. Zhang, J. Vleugels, and O. Van Der Biest, "Slip casting of alumina suspensions in a strong magnetic field," *J. Am. Ceram. Soc.*, (2010).

109   P. Calvert, T.L. Lin, and H. Martin, "Extrusion freeform fabrication of chopped-fibre reinforced composites," *High Perform. Polym.*, **9** [4] 449–456 (1997).

110   J. Peng, T.L. Lin, and P. Calvert, "Orientation effects in freeformed short-fiber composites," *Compos. Part A Appl. Sci. Manuf.*, **30** [2] 133–138 (1999).

111   B.N. Kim, K. Hiraga, K. Morita, and H. Yoshida, "Effects of heating rate on microstructure and transparency of spark-plasma-sintered alumina," *J. Eur. Ceram. Soc.*, **29** [2] 323–327 (2009).

112   B.N. Kim, K. Hiraga, K. Morita, and H. Yoshida, "Spark plasma sintering of transparent alumina," *Scr. Mater.*, (2007).

113   B.N. Kim, K. Hiraga, K. Morita, H. Yoshida, T. Miyazaki, and Y. Kagawa, "Microstructure and optical properties of transparent alumina," *Acta Mater.*, **57** [5] 1319–1326 (2009).

114   W.H. Rhodes, D.J. Sellers, and T. Vasilos, "Hot-Working of Aluminum Oxide: 11, Optical Properties," *J. Am. Ceram. Soc.*, **58** [1–2] 31–34 (1974).

115   W.H. Rhodes, D.J. Sellers, A.H. Heuer, and T. Vasilof, *Development And Evaluation Of Transparent Aluminum Oxide*. 1967.

116   P. Sellers, D J, L. Rhodes, W H, and W. Vasilos, T, "United States Patent, Method of Preparing Transparent Alumina," [19] (1975).

VITA

William (Willy) James Costakis Jr. was born Hammond, IN and raised in Merrillville, IN where he attended Merrillville high school. Upon graduation, He attended Wabash College, where he obtained a Bachelor of Arts with a major focus in Physics and a minor focus in Mathematics. While at Wabash College, he held a Resident Assistant position and a Physics Tutor position. He was actively involved in the community through organizing tutoring programs for local children. Furthermore, he was the president of the Wabash College Rugby club for one and a half years. After graduating from Wabash College, he decided to continue his undergraduate studies at Purdue University's College of Engineering in the School of Materials Science and Engineering. During his second semester, he started work on the additive manufacturing of aqueous-based ceramics suspensions under the guidance of Prof. Rodney Trice and Prof. Jeffrey Youngblood. Following this project, he was awarded a Summer Undergraduate Research Apprenticeship Program position from the Undergraduate Army Educational Outreach Program and Army Research Office. In this program, he was able to work on the additive manufacturing of boron carbide suspensions which lead to his 1st first author publication. While at Purdue, he joined the Materials Advantage chapter and held the position of Safety officer for 1 year. After graduation, he decided to continue his education and joined the Materials Engineering Graduate Program at Purdue University. In the early years of his graduate program, he was involved in the founding and continuation of the Purdue Climbing Club. During this time, he has held the positions of treasurer, vice-president and president. Also, he was actively involved in the Material Engineering and Science Graduate Student Association by holding the position of Outreach Co-chair. Additionally, he was involved with a ceramics professional society, The American Ceramic Society (ACerS), through the participation in congressional visits, conference participation, and professional workshop attendance. He was actively involved by serving on both the Programing and External Partner Committees in the ACerS President's Council of Student Advisors (PCSA) from 2016 to 2018. Furthermore, he was involved in the organizing and planning of the ACerS Winter Workshop at the International Conference and Exposition on Advanced Ceramics and Composites from 2018 to 2020, where he worked with a team of young professionals and to invite distinguished researchers from different fields of ceramic research to give seminars. During the summer of 2017, he was awarded an ORISE fellowship with the Army Research Laboratory to work under the

direction of Dr. Lionel Vargas-Gonzalez. He has given 7 conference presentations, one invited seminar at a government laboratory, and has five publications with five additional publications in progress stemming from his graduate research. After graduation, Willy will join the Air Force Research Lab in Dayton, OH as an NRC Postdoctoral Fellow.

PUBLICATIONS

<u>PUBLISHED ARTICLES</u>

S.M. El Awad Azrak, W.J. Costakis, R.J. Moon, G.T. Schueneman, J.P. Youngblood, Continuous Processing of Cellulose Nanofibril (CNF) Sheets Through Conventional Single-Screw Extrusion, (*submitted for review*).

W.J. Costakis, A. Schlup, J.P. Youngblood, R.W. Trice, Aligning α-alumina platelets via uniaxial pressing of ceramic-filled polymer blends for improved sintered transparency, J. Am. Ceram. Soc. (2020) jace.17044. doi:10.1111/jace.17044.

A.P. Schlup, W.J. Costakis, W. Rheinheimer, R.W. Trice, J.P. Youngblood, Hot-Pressing Platelet Alumina to Transparency, J. Am. Ceram. Soc. (2019) jace.16932. doi:10.1111/jace.16932.

W.J. Costakis, L.M. Rueschhoff, A.I. Diaz-Cano, J.P. Youngblood, R.W. Trice, Additive manufacturing of boron carbide via continuous filament direct ink writing of aqueous ceramic suspensions, J. Eur. Ceram. Soc. 36 (2016) 3249–3256. doi:10.1016/j.jeurceramsoc.2016.06.002.

L. Rueschhoff, W. Costakis, M. Michie, J. Youngblood, R. Trice, Additive Manufacturing of Dense Ceramic Parts via Direct Ink Writing of Aqueous Alumina Suspensions, Int. J. Appl. Ceram. Technol. 13 (2016) 821–830. doi:10.1111/ijac.12557.

<u>IN PREPARATION</u>

W.J. Costakis, A.P. Schlup, C. Meisel, J.P. Youngblood, R.W. Trice, Aligning α-Alumina Platelets via Direct Ink Writing for Sintered Transparency, (In Preparation).

W.J. Costakis, A.P. Schlup, J.P. Youngblood, R.W. Trice, Hot-pressing of equiaxed and platelet alumina powders to transparency, (In Preparation).

A.P. Schlup, W.J. Costakis, J.P. Youngblood, R.W. Trice, "Density Gradients in Transparent Pre-Aligned Platelet Alumina Processed via Hot-Pressing" (In Preparation).

A.P. Schlup, W.J. Costakis, J.P. Youngblood, R.W. Trice, "Mechanical Properties of Transparent Alumina Produces via Hot-Pressing Pre-Aligned Platelet Alumina" (In Preparation).

A.P. Schlup, W.J. Costakis, J.P. Youngblood, R.W. Trice, "Modifications to the Rayleigh-Gans-Debye Model for Crystallographically-Aligned Transparent Alumina" (In Preparation).